INSTITUTO
UNIVERSITÁRIO
DE LISBOA

Transmission of PAM4 signals in amplified inter-datacenters connections with direct-detection and multicore fibers limited by inter-core crosstalk

Rafael Alexandre Domingues Dias

Master in Telecommunications and Computer Engineering

Supervisor
Prof. Doctor João Lopes Rebola, Assistant Professor
Iscte–Instituto Universitário de Lisboa

Co-supervisor
Prof. Doctor Adolfo da Visitação Tregeira Cartaxo, Full Professor
Iscte–Instituto Universitário de Lisboa

December, 2020

TECNOLOGIAS
E ARQUITETURA

Transmission of PAM4 signals in amplified inter-datacenters connections with direct-detection and multicore fibers limited by inter-core crosstalk

Rafael Alexandre Domingues Dias

Master in Telecommunications and Computer Engineering

Supervisor

Prof. Doctor João Lopes Rebola, Assistant Professor

Iscte–Instituto Universitário de Lisboa

Co-supervisor

Prof. Doctor Adolfo da Visitação Tregeira Cartaxo, Full Professor

Iscte–Instituto Universitário de Lisboa

December, 2020

Acknowledgements

I express my utmost gratitude to my supervisors Professor Doctor João Lopes Rebola and Professor Doctor Adolfo da Visitação Tregeira Cartaxo, for all the support, guidance, knowledge and advises, that enabled me to do this dissertation. Also, I want to recognize Instituto de Telecomunicações (IT)-IUL and Iscte-Instituto Universitário de Lisboa, for providing me their resources.

I also thank my employer for always providing me flexibility to attend my academic duties.

Also, gratitude goes to all my friends who directly or indirectly helped me complete this dissertation.

Additionally, I want to deeply thank my girlfriend Marta Dias, for all the love, kindness and support.

Last, but not the least, I want to thank my family, I am greatly indebted for all the love, care, tolerance, education and support they have provided me, which made me strive and succeed.

Resumo

Neste trabalho é proposta a utilização de modulação com 4 níveis de amplitude (PAM4) e de fibras multinúcleo (MCFs) para suportar ligações entre centros de dados com capacidade muito elevada. As limitações impostas pela diafonia entre núcleos (ICXT) no desempenho de ligações PAM4 a 112 Gb/s suportadas por MCFs com modulação de intensidade e deteção direta são analisadas através de simulação númerica. Consideram-se ligações até 80 km com amplificação óptica e compensação óptica total da dispersão cromática.

Nessas ligações, para um núcleo interferente e um produto entre atrasos de propagação entre núcleos e ritmo de símbolo (SSRPs) elevado, o nível máximo aceitável de ICXT para alcançar uma probabilidade de indisponibilidade (OP) de 10^{-4} é -13.9 dB. Para SSRPs reduzidos, é observada uma redução do nível de ICXT de aproximadamente 8.1 dB para alcançar a mesma OP. Devido à compensação total de dispersão, a OP não é significativamente afetada com o aumento do comprimento da MCF, de 10 km, onde o ruído elétrico contribui significativamente para a degradação do desempenho, até 80 km, onde o batimento de ruído sinal-emissão espontânea amplificada é dominante. Para uma OP=10^{-4}, o nível máximo aceitável de ICXT varia 1.4 dB com o aumento do comprimento da MCF. Para múltiplos núcleos interferentes, duplicando o número de núcleos, o nível máximo aceitável de ICXT por núcleo interferente para alcançar uma OP=10^{-4} diminui aproximadamente 3 dB. Mostra-se também que um único núcleo com SSRP reduzido é suficiente para introduzir uma forte redução no nível máximo aceitável de ICXT.

Palavras-chave: diafonia entre núcleos, fibra multinúcleo, indisponibilidade, ligações entre centros de dados, PAM4, taxa de erro de bit.

Abstract

In this work, we propose the use of four-level pulse amplitude modulation (PAM4) and multicore fibers (MCFs) to support very high capacity inter-datacenter links. The limitations imposed by inter-core crosstalk (ICXT) on the performance of 112 Gb/s up to 80 km-long optically amplified PAM4 inter-datacenter links supported by MCFs with intensity-modulation and direct-detection and full chromatic dispersion compensation in the optical domain are analyzed through numerical simulation.

We show that, in those PAM4 inter-datacenter links, for one interfering core and high skew-symbol rate product, the maximum acceptable ICXT level to achieve an outage probability (OP) of 10^{-4} is -13.9 dB. For low skew-symbol rate product, the ICXT level decreases about 8.1 dB to achieve the same OP. Due to using full dispersion compensation, the OP is not much affected by increasing the MCF length, from 10 km, where electrical noise significantly contributes to the performance degradation, to 80 km, where signal-amplified spontaneous emission beat noise is dominant. For an OP of 10^{-4}, the maximum acceptable ICXT level shows only a 1.4 dB variation with the MCF length increase. Also, when doubling the number of interfering cores, the maximum ICXT level per interfering core to reach an OP of 10^{-4} decreases around 3 dB. For several interfering cores, having a single core with low skew-symbol rate products is enough to induce a severe reduction of the maximum acceptable ICXT level.

Keywords: bit error rate, inter-core crosstalk, inter-datacenter connections, multicore fiber, outage probability, PAM4.

Contents

List of Figures

List of Tables

List of Acronyms

ASE	**A**mplified **S**pontaneous **E**mission
BER	**B**it **E**rror **R**ate
B2B	**B**ack-**t**o-**B**ack
CD	**C**hromatic **D**ispersion
CDC	**C**hromatic **D**ispersion **C**ompensation
DCF	**D**ispersion **C**ompensating **F**iber
DCM	**D**iscrete **C**hanges **M**odel
DD	**D**irect **D**etection
DEMUX	**D**emultiplexer
DSP	**D**igital **S**ignal **P**rocessing
EDFA	**E**rbium-**D**oped **F**iber **A**mplifier
FEC	**F**orward **E**rror **C**orrection
FMF	**F**ew-**M**ode **F**iber
FWM	**F**our-**W**ave **M**ixing
ICXT	**I**ntercore **C**rosstalk
IM	**I**ntensity **M**odulation
IM-DD	**I**ntensity **M**odulation **D**irect **D**etection
ISI	**I**nter**S**ymbol **I**nterference
LR	**L**ong **R**each
MCF	**M**ulti **C**ore **F**iber
MMF	**M**ulti **M**ode **F**iber
MC	**M**onte **C**arlo
MUX	**M**ultiplexer
MC-EDFA	**M**ulti **C**ore **E**rbium **D**oped **F**iber **A**mplifier
NEP	**N**oise **E**quivalent **P**ower
NRZ	**N**on **R**eturn-to-**Z**ero
OOK	**O**n-**O**ff **K**eying

OP	**O**utage **P**robability
OSNR	**O**ptical **S**ignal-to-**N**oise **R**atio
PAM	**P**ulse **A**mplitude **M**odulation
PAM4	**P**ulse **A**mplitude **M**odulation with **4** levels
PAM8	**P**ulse **A**mplitude **M**odulation with **8** levels
PMP	**P**hase **M**atching **P**oint
RPS	**R**andom **P**hase **S**hift
SCF	**S**ingle **C**ore **F**iber
SDM	**S**pace **D**ivision **M**ultiplexing
SM	**S**ingle **M**ode
SMF	**S**ingle **M**ode **F**iber
SR	**S**hort **R**each
SSMF	**S**tandard **S**ingle **M**ode **F**iber
SC-EDFA	**S**ingle **C**ore **E**rbium **D**oped **F**iber **A**mplifier
SC-SMF	**S**ingle **C**ore **S**ingle **M**ode **F**iber
SM-MCF	**S**ingle **M**ode **M**ulti **C**ore **F**iber
SSRP	**S**kew-**S**ymbol **R**ate **P**roduct
WDM	**W**avelength **D**ivision **M**ultiplexing
XT	**C**ross**T**alk

List of Symbols

a_k	Transmitted PAM4 symbol
A	Normalized amplitude level corresponding to symbol '2'
$B_{e,n}$	Noise equivalent bandwidth of the receiver electrical filter
$B_{e,RX}$	Receiver electrical filter bandwidth at -3 dB
$B_{e,TX}$	Transmitter electrical filter bandwidth at -3 dB
B_o	Optical filter bandwidth at -3 dB
$B_{o,n}$	Noise equivalent bandwidth of the optical filter
B_n	n-th order Bessel polynomial
$\overline{\beta}_l$	Average of the propagation constants of polarizations **x** and **y** in core l
$\overline{\beta}_m$	Average of the propagation constants of polarizations **x** and **y** in core m
$\overline{\beta}_n$	Average of the propagation constants of polarizations **x** and **y** in core n
$\overline{\beta}_{0,l}$	Propagation constant at the carrier wavelength in core l
$\overline{\beta}_{1,l}$	Inverse of the group velocity in core l
$\overline{\beta}_{2,l}$	Group velocity dispersion in core l
$\overline{\beta}_{3,l}$	High order dispersion in core l
C	Normalized amplitude level corresponding to symbol '1'
$\mathbf{c_F(t)}$	PAM4 signal at the output of the interfered core n
$c_{F,x}(t)$	PAM4 signal at the output of the interfered core n in polarization **x**
$c_{F,y}(t)$	PAM4 signal at the output of the interfered core n in polarization **y**
$\mathbf{c_m(t)}$	PAM4 signal at the input of the interfering core m
$c_{m,x}(t)$	PAM4 signal at the input of the core interfering m in polarization **x**
$c_{m,y}(t)$	PAM4 signal at the input of the interfering core m in polarization **y**
$\mathbf{c_n(t)}$	PAM4 signal at the input of the interfered core n
$c_{n,x}(t)$	PAM4 signal at the input of the interfered core n in polarization **x**
$c_{n,y}(t)$	PAM4 signal at the input of the interfered core n in polarization **y**
$c_{PIN}(t)$	Signal at the output of the PIN photo-detector
$\mathbf{c_{XT}(t)}$	ICXT signal at the output of the interfering core m
$c_{XT,x}(t)$	ICXT signal at the output of the interfering core m in polarization **x**

$c_{XT,y}(t)$	ICXT signal at the output of the interfering core m in polarization **y**
$D_{\lambda,l}$	Dispersion parameter of core l
$D_{\lambda,n}$	Dispersion parameter of core n
$D_{\lambda,DCF}$	Dispersion parameter of the DCF
$\mathcal{F}^{-1}\{\ \}$	Inverse Fourier transform
f_o	Optical filter central frequency
$F_{a,b}(\omega)$	ICXT transfer function in polarization directions **a** and **b**
$F_{x,x}(\omega)$	ICXT transfer function from polarization direction **x** to **x**
$F_{x,y}(\omega)$	ICXT transfer function from polarization direction **x** to **y**
$F_{y,x}(\omega)$	ICXT transfer function from polarization direction **y** to **x**
$F_{y,y}(\omega)$	ICXT transfer function from polarization direction **y** to **y**
F_i	Optimized decision threshold with i=1,2,3
F_i	Normalized decision threshold with i=1,2,3
F_n	EDFA noise figure
h	Planck constant
$H_F(\omega)$	Linear propagation transfer function of the fiber
$H_{bessel}(\omega)$	Bessel filter transfer function
$H_{e,RX}(\omega)$	Amplitude transfer function of the receiver electrical filter
I_{ASE}	Average current due to the ASE noise per polarization mode
$i_{i,k}$	Current at the input of the decision circuit with i=0,1,2,3 and $k \in \{1,...,4^{N_{reg}}\}$
i_L	Optical filter insertion loss in linear units
$\overline{K}_{nm}$	Average inter-core coupling coefficient of both polarization directions
L	MCF length
n	Electrical or optical filter order
N	Number of generated PAM4 symbols in each MCF realization
n_{eff}	Effective refractive of core l
N_{reg}	Number of the bits of the offset register
N_c	Number of interfering cores
N_o	Number of occurrences of BER above the BER limit
N_p	Number of PMPs

N_r	Number of simulated realizations
N_s	Number of samples per symbol
P_{av}	Average power of the PAM4 optical signal at the optical transmitter output
P_i	Theoretical power corresponding to the i-th transmitted symbol
q	Electron charge
$Q_n(s)$	n-th order polynomial factor
r	Extinction ratio
R_s	Symbol rate
R_λ	PIN responsivity
S_{mn}	MCF skew parameter
d_{mn}	Walkoff between cores m and n
T_s	Symbol period
X_c	ICXT level at the MCF output
z_k	Longitudinal coordinate corresponding to the k-th PMP
t_k	Sampling time instant
ξ_m	Variable between 0 and 1 that controls the power distribution between polarizations in core m
ξ_n	Variable between 0 and 1 that controls the power distribution between polarizations in core n
η	Photo-detector efficiency
λ	Carrier wavelength
α_{DCF}	DCF attenuation coefficient
α_n	MCF attenuation coefficient of core n
α_m	MCF attenuation coefficient of core m
ν_0	Optical frequency of the transmitted PAM4 signal
S_λ	Slope of the dispersion at the carrier wavelength
S_{ASE}	ASE noise power spectral density per polarization mode
σ_c^2	Power of the electrical noise
$\sigma_{i,k}$	Noise standard deviation of the current at the input of the decision circuit with i=0,1,2,3

$\sigma^2_{n,k,ASE}$	Power of the detected ASE noise for the k-th received PAM4 signal at the electrical filter output
$\phi_{nm,k}$	RPS associated with the k-th PMP
ω	Angular frequency
$v_{g,l}$	Group velocity in core l

Chapter 1

Introduction

In this work, the performance evaluation of optically amplified direct detection (DD) pulse amplitude modulation (PAM) with 4 levels links used in inter-datacenters connections supported by multicore fibers (MCFs), which are limited by inter-core crosstalk (ICXT) caused by the interference between signal transmission in different fiber cores is assessed. The performance assessment is obtained mainly using the outage probability (OP) and the maximum acceptable ICXT level to not exceed a given OP. The performance comparison with PAM4 transmission and on-off keying (OOK) transmission in unamplified intra-datacenters connections is also assessed.

1.1 Dissertation motivation

Nowadays, datacenters provide a vital infrastructure to Internet online services and in the last few years, worldwide traffic in optical networks has been increasing dramatically around 30% per year [1], [2]. This growth is fuelled by the progressive development of next-generation 5G mobile broadband technologies, expansion of the Internet of things, and increasing of high-data-rate applications such as streaming video, real-time gaming, cloud computing, and big data analysis [2]. This growth is demanding a higher capacity in datacenters. To accomplish such demands, cloud companies and content providers have built multiple datacenters in different locations which are separated by large distances because this approach offers multiple benefits (increased availability, reduced latency to customers) for distributed applications with a wide range of users such as email, multimedia services, social networks and online storage [3]. Moreover, the most amount of traffic is now exchanged between servers inside the same datacenter and between datacenters [1]. In 2007, the first generation of intra-datacenters technology was based on a single channel that operated at 10 Gb/s and used OOK modulation and DD [4]. In 2010, this technology evolved into a second-generation by having 4 wavelength division multiplexed

(WDM) channels instead of a single channel [4]. In 2014, the third generation was released with the same 4 WDM channels at a bit rate of 25 Gb/s per channel and OOK modulation, operating at an aggregate rate of 100 Gb/s [4]. The third generation was the limit for OOK signals transmission since this strategy could not scale further [5]. Recent research has focused on transmitting a more spectrally efficient modulation format compatible with intensity modulation and DD (IM-DD) to minimize power consumption [5]. Hence, in 2017, a generation of datacenters connections was released employing a more cost-effective and bandwidth-efficient PAM4, with 8 WDM and 50 Gb/s, with the same baud rate at 25 Gbaud/s, allowing an aggregate rate of 400 Gb/s [4], [5]. By enabling such data rates, PAM4 format is expected to help deliver the aggregated data rates of 800 Gb/s and 1.6 Tb/s in datacenter connections by enabling 50 and 100 Gb/s per wavelength in future connections [4], [5]. Nevertheless, PAM4 systems have to assure optical signal-to-noise ratio (OSNR) power margin constraints in optically amplified and unamplified systems, respectively.

Typically, datacenter links can be classified as intra-datacenter or as inter-datacenter connections. Intra-datacenter links can reach up to 10 km, are typically unamplified and usually operate around 1310 nm to minimize chromatic dispersion (CD). Inter-datacenter links can reach up to 100 km and use optical amplification, operating around 1550 nm to leverage erbium-doped fiber amplifiers (EDFAs). In these links, CD becomes significant and must be compensated [5]. Datacenters links above 100 m are usually implemented using single-core single-mode fibers (SC-SMF). In [6], it has been shown that SC-SMF transmissions have achieved data rates around 100 Tb/s by relying on optical coherent-detection and digital signal processing (DSP). However, optical DD systems are preferred due to considerably lower cost and complexity comparing to coherent-detection systems [6]. Moreover, increasing capacity per single fiber is not enough, since, in datacenter facilities, space is a limited resource and must be utilized most efficiently. Reducing space and cable occupation can be accomplished by increasing the number of cores in a fiber cross-section or by increasing the number of modes in a fiber core [7]. As space-efficient use is important inside datacenters, reducing fiber per area density is important and therefore, MCFs are seen as a very attractive technology [8]. In this work, homogeneous weakly-coupled MCFs are proposed and studied as the transmission medium for inter-datacenters connections, relying in these fibers. In weakly-coupled MCFs, all cores have the same propagation constant

and have similar properties in comparison to the other cores, resulting that each core may work as an independent transmission channel. All these characteristics, which reduce complexity in comparison with other MCF types, make homogeneous weakly-coupled MCFs an attractive solution for such links [2], [9].

However, the reach and transmission performance with weakly-coupled MCFs is impaired by a physical intrinsic phenomenon known as inter-core crosstalk (ICXT) [10], [11]. This effect limits the short-haul DD system performance and the datecenters link length and can cause service outage [12]. Therefore, it is essential to study the bit error rate (BER) and the outage probability (OP) in PAM4 IM-DD transmissions supported by MCFs [10], [11]. The impact of ICXT on the transmission depends on various MCF characteristics. Therefore, an exhaustive and careful characterization of the ICXT impact on the inter-datacenter link performance is essential for development of techniques to suppress and mitigate its effect [6], [13]. This work aims to study inter-datacenter links where distances can reach up to 80 km. For this purpose, the link must be optically amplified to compensate fiber losses and CD must also be taken into account and mitigated.

1.2 Dissertation objectives

In this work, the major objective is to study the transmission of PAM4 signals in optically amplified inter-datacenters connections with DD and homogeneous weakly-coupled MCFs impaired by ICXT. The main objectives of this work are:

- Study and characterization of inter-datacenter systems with amplification, DD and PAM4 transmission.

- Study of the dual-polarization discrete changes model (DCM) to characterize the ICXT in weakly-coupled homogeneous MCFs.

- Study and implementation of an amplification block and a CD compensation block to enable inter-datacenter links with lengths up to 80 km.

- Evaluation of the maximum acceptable ICXT level to not exceed a given OP for optically amplified IM-DD communication systems with PAM4 modulation in homogeneous weakly-coupled MCFs.

1.3 Dissertation organization

This work organization is the following. In Chapter 2, the fundamental concepts for datacenters connections, such as, evolution of datacenters architecture and transmission technologies, transmission over MCFs, the need for amplification using EDFAs in inter-datacenter links and techniques for CD compensation are discussed and presented. In Chapter 3, the studied system equivalent model of the optical PAM4 inter-datacenter link is presented. The model is composed by optical transmitter, dual-polarization DCM of the MCF, CD compensation module, optical preamplifier model and DD optical receiver model. Also in this chapter, the method used to calculate the BER is described and the BER estimation in an optically amplified PAM4 link without ICXT is studied. In Chapter 4, the impact of ICXT on the performance of optically amplified PAM4 IM-DD links is assessed. The assessment is focused on the OP as the main performance metric. The OP is studied for a single interfering core considering several inter-core skews and MCF lengths and for a different number of interfering cores with the same and with distinct inter-core skews. In Chapter 5, the final conclusions are presented.

1.4 Main original contributions

The main original contributions of this work are the following:

• Implementation of a combined efficient technique of simulation and theoretical analysis to assess the performance of an optically amplified PAM4 system with DD, full loss compensation, and CD compensation, supported by MCFs and impaired by ICXT;

• Demonstration that the PAM4 signals in optically amplified inter-datacenters links with DD and homogeneous weakly-coupled MCFs are more tolerant to ICXT in comparison to PAM4 and

OOK signals in unamplified intra-datacenter links with DD and homogeneous weakly-coupled MCFs mainly due to dispersion compensation;

• Assessment of the OP in optically amplified PAM4 systems with full loss compensation, CD compensation, and DD impaired by ICXT, with a single interfering core for several inter-core skews and MCF lengths and different signal extinction ratios;

• Assessment of the OP degradation with the increase of the number of cores with the same and with distinct inter-core skews in MCF-supported PAM4 IM-DD systems with full loss and CD compensation.

Chapter 2

Inter-datacenter connections supported by MCFs: fundamental concepts

In this chapter, the most important concepts concerning this work are presented. Section 2.1 provides a review of the datacenters architecture. Then, in Section 2.2, a review of the signal transmission in datacenter connections is presented. Section 2.3 describes the transmission in optical fibers and, in section 2.4, a more in-depth description is given regarding MCFs. Section 2.5 describes the ICXT impairment in MCFs transmission. Section 2.6, provides a brief description about amplification in MCFs supported systems and, in section 2.7, some concepts about dispersion compensation are explained. Section 2.8, shows the pre-forward error correction (FEC) BERs typically used in PAM4 DD systems. In section 2.9 a review, regarding works that have analyzed the transmission of PAM4 signals over MCFs is presented.

2.1 Traffic and datacenter architectures evolution

Over the past few years, datacenters have an increasingly important role in information technology. Service providers have used datacenters as the solution to provide communication, network services, and storage big data information to the increasing number of network users and devices. Moreover, cloud technology has been emerging and it is projected that by 2021 more than 95% of datacenter traffic will be cloud traffic [1]. This led to the development of large-scale public cloud datacenters known as hyper-scale datacenters [1]. As shown in Fig. 2.1, from 2016 to 2021, the number of hyper-scale datacenters is expected to double, reaching a value of 628, that will represent in the future, 53% of the operating datacenters [1]. Globally, datacenter IP traffic has been increasing over the last few years, which justifies the increasing

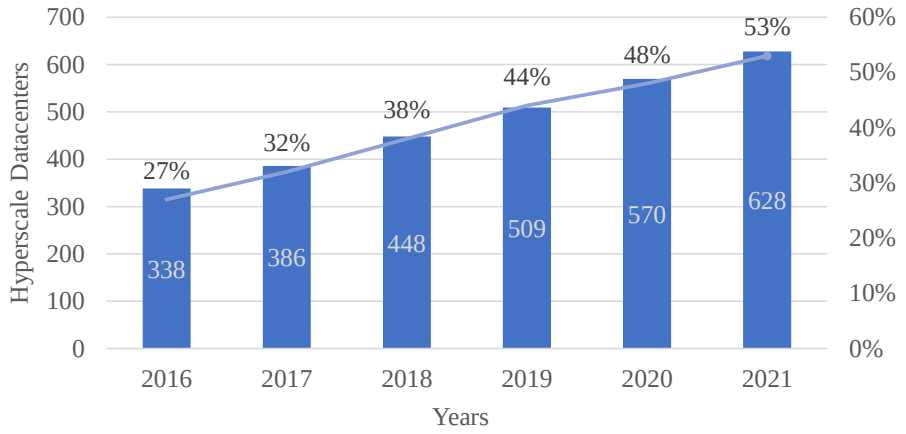

FIGURE 2.1: Worldwide hyper-scale datacenter increase [1].

number of hyper-scale datacenters. This traffic can be classified into three types: i) traffic from datacenter to the user, which flows through the Internet; ii) traffic from datacenter to datacenter; iii) traffic within datacenters, which remains in the datacenter, excluding traffic that remains within a given server rack. Fig. 2.2 shows the expected evolution of each data traffic type in the next years. Traffic from datacenter to the user is forecasted to have an increase of 25.2% of the compound annual growth rate. Datacenter to datacenter traffic is forecasted to have an increase representing the higher percetange of the compound annual growth rate, with 32.7%, while traffic within the datacenter is forecasted to have an increase of 23.4% of the compound annual growth rate [1]. The continuing increase of traffic raised efficiency issues and led to different

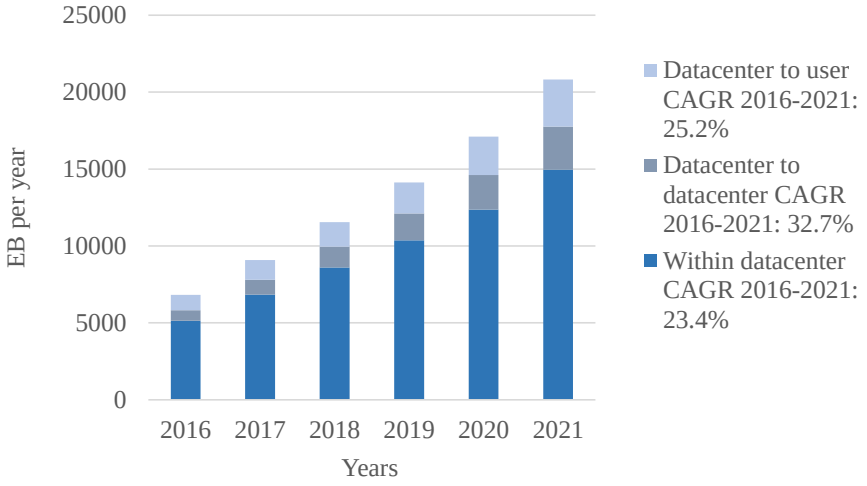

FIGURE 2.2: Worldwide datacenter traffic type development [1].

approaches to how traffic was transmitted in datacenters. Hence, traditional north-south traffic evolved to east-west traffic. North-south traffic is known to be traffic to the user that flows from the datacenter to the Internet. East-west traffic is traffic between servers within and between datacenters. The east-west traffic implementation raised awareness for datacenters technology to expand and be enhanced to support it instead of the traditional north-south. In 2021, north-south traffic will account 15% of total traffic while east-west traffic is expected to account 85% [1].

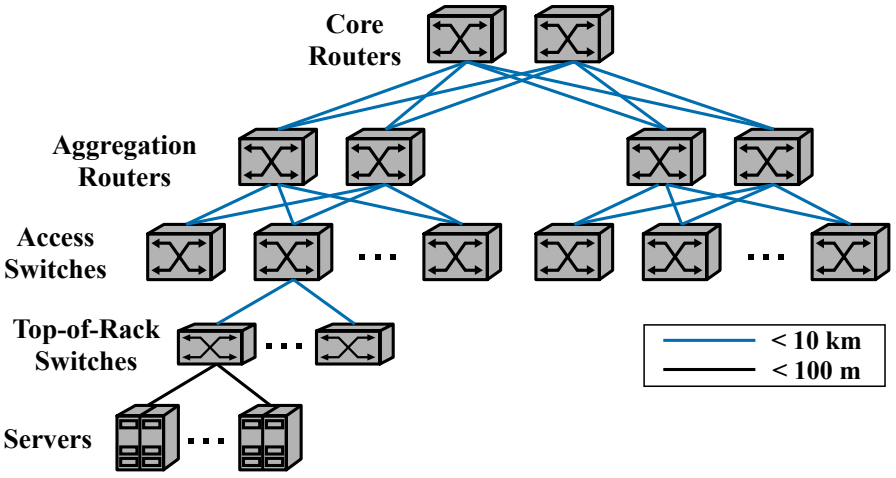

FIGURE 2.3: Datacenter conventional structure, based on [5].

In Fig. 2.3, a conventional datacenter structure with three levels is illustrated. The conventional structure has top-of-rack switches connecting servers to access switches, which are connected to two aggregation routers for redundancy and, finally, these aggregation routers are connected to the core routers, also with redundancy. The conventional structure is efficient to handle north-south traffic. However, it is not particularly suitable to handle east-west traffic, since traffic between servers in the same datacenter must do a round trip between the bottom and the top level, traversing several components and increasing latency [5], [14]. Therefore, this datacenter structure is not suitable for links above 10 km.

Fig. 2.4 shows the two-level structure developed to support east-west traffic more efficiently. In this structure, top-of-rack switches connect servers to leaf switches, which, in turn, are now connected to all spine switches. This major change increases connections redundancy inside the datacenter. This structure can be expanded by simply inserting a new spine or leaf switch. Moreover, it assures a higher resilience to failures, because leaf switches are connected to all spine switches which results in a minor performance degradation if a spine switch fails. Also, in

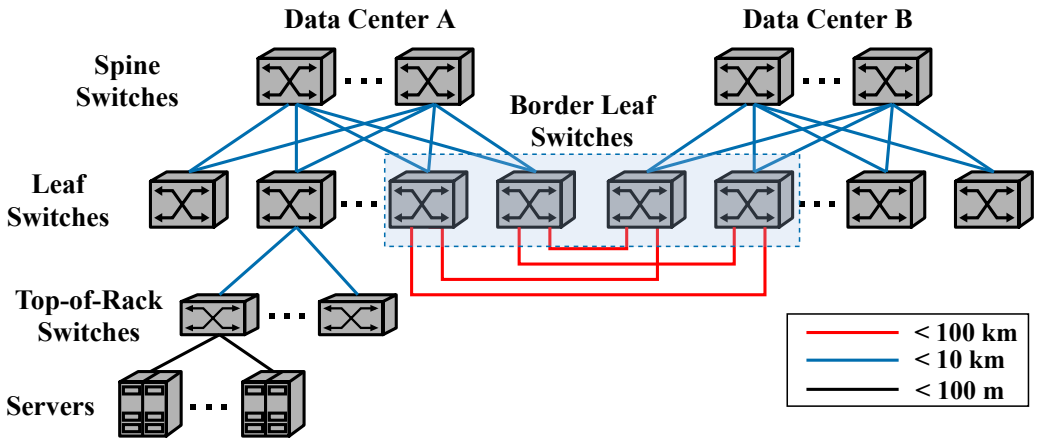

FIGURE 2.4: Datacenter current structure, based on [5].

inter-datacenter connections, which may reach 100 km, the connection between datacenters is ensured by connecting border leaf switches of different datacenters [5]. To support the desired higher data rates and these longer distances, the datacenter connections above 100 m are mainly supported by optical fibers.

2.2 Technology evolution in datacenter links

Datacenter connections are constantly under evolution to keep up with the requirements of handling huge amounts of traffic at increasingly higher capacities. Moreover, datacenter communication systems have design priorities such as low complexity, low cost, and power consumption. Hence, datacenter connections are usually based in IM-DD links, which imposes the use of intensity-modulated signals such as OOK and PAM [5].

In Fig. 2.5, the evolution of intra-datacenter technology is shown by scaling the capacity in three axis solution: increasing the symbol rate per lane, increasing the number of bits per symbol or increasing the number of parallel lanes (WDM channels) [15].

OOK is typically the most used modulation format in IM-DD links, because of its simplicity. The strategy of increasing the symbol rate axis is usually the most cost-effective way to increase the data rate because it increases the available capacity without replicating any electrical or optical components. However, scaling in symbol rate requires using larger bandwidth,

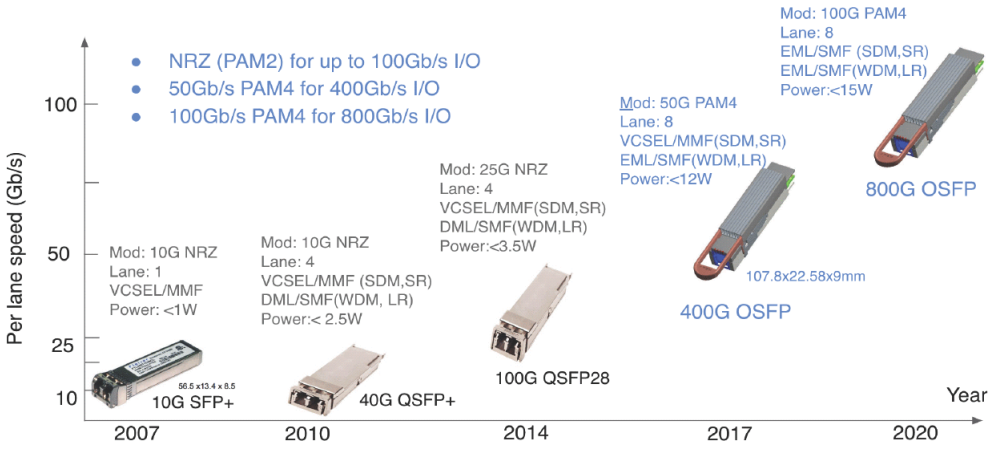

FIGURE 2.5: Intra-datacenter optics technology evolution. VCSEL: vertical cavity surface emitting laser; MMF: multimode fiber, SMF: single mode fiber; EML: externally modulated laser, SDM: space division muitiplexing; WDM: wavelength division multiplexing, SR: short reach, LR: long reach, taken from [4].

which is a limited resource due to available components bandwidth [15]. This strategy was used on OOK (in Fig. 2.5, mentioned as NRZ) signals from 2007 to 2014. However, OOK transmissions impose significant limitations when scaling the data rate due to its low spectral efficiency [5]. In order to surpass the limitation imposed by OOK modulation, PAM4 signal transmission has been introduced for datacenter communications in 2017 [4], [14]. The PAM4 modulation format is characterized by having four amplitude levels, having symbols composed by a combination of two bits which reduces the signal bandwidth by half and doubles spectral efficiency in comparison to OOK signals, which only used 1 bit per symbol. Therefore, PAM4 is expected to be an economical and efficient enabler of 100G and 400G single-channel transmission in intra and inter-datacenter connections [4], [5], as shown in Fig. 2.5. Using the more bandwidth-efficient modulation PAM4 allows achieving higher data rates without requiring higher bandwidth components. However, this is achieved at the expense of signal-to-noise ratio and higher inter-symbol interference (ISI) [15]. In 2020, PAM4 transmissions are expected to enable an aggregated data rate of 800 Gb/s in intra-datacenter connections [4], [5], by using 100G single-channel transmission, using 8 lanes (channels).

Space division multiplexing (SDM) is a very effective strategy to increase the aggregated data rate and can be achieved by increasing the number of parallel lanes, which can be done in three domains: i) space, ii) polarization, or iii) frequency. However, this solution increases

the number of electrical and optical components in proportion to the number of lanes, hence, increasing the system cost. In addition, for distances over a few hundred meters, scaling in space is undesirable due to higher fiber cost and volume [15]. Hence, over the last few years, MCFs have been one of the most appealing technologies to surpass these limitations while increasing the link capacity.

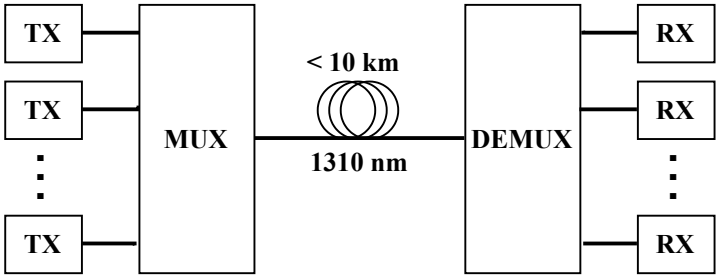

FIGURE 2.6: Intra-datacenter links. TX: transmitter, MUX: multiplexer, DEMUX: demultiplexer, RX: receiver, based on [4].

Datacenter connections can be classified as intra-datacenter links or as inter-datacenter links, with architectures illustrated in Figs. 2.6 and 2.7, respectively. Fig. 2.6 shows the typical model of an intra-datacenter link, which can reach up to 10 km and usually operates at a wavelength around 1310 nm, in order to minimize CD. Intra-datacenter links are usually unamplified which leads to low power margins [5], [16]. Hence, in such connections, PIN photodetectors can be replaced by avalanche photodiodes to increase receiver sensitivity and the corresponding system margin [5].

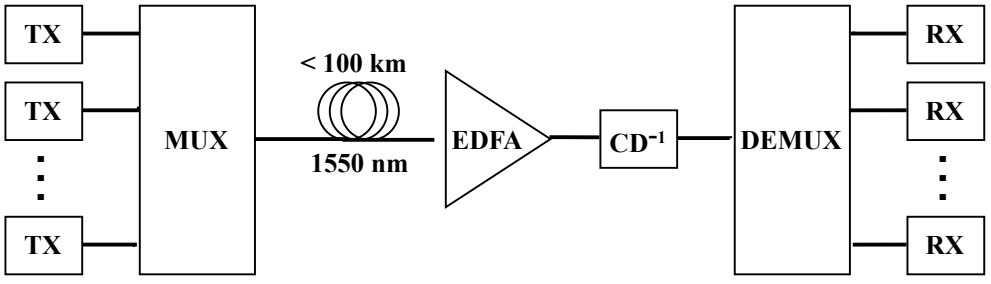

FIGURE 2.7: Inter-datacenter link. TX: transmitter, MUX: multiplexer, EDFA: erbium-doped fiber amplifier, CD^{-1}: chromatic dispersion compensation module, DEMUX: demultiplexer, RX: receiver, based on [4].

Fig. 2.7 shows the system model of an inter-datacenter link, which can reach up to 100 km and usually operate around 1550 nm in order to enable amplification, using EDFAs that operate

around this wavelength. In these links, due to the higher distances and higher wavelength, CD becomes significant and must be reduced by using dispersion compensation techniques, such as dispersion compensating fibers (DCFs), tunable fiber Bragg gratings, or by replacing standard SMFs by dispersion-shifted fibers [5], [16].

2.3 Optical fibers

Currently, intra and inter-datacenter transmission is mainly supported by optical fibers. Optical fibers allow light transmission with low loss over very long distances with a large available signal bandwidth. Optical fibers are made of silica and are composed by a core in which the light is guided, embedded in an outer cladding with a slightly lower refractive, so that, the light is guided through total internal reflection inside the core.

Optical fibers can be classified into two types: single-mode fibers (SMF) and multi-mode fibers (MMF). The core diameter in SMFs is typically around 10 μm, while MMFs core has more doping material density, resulting in a core diameter of about 50 μm [17]. Moreover, MMF transmission is significantly affected by intermodal dispersion and fiber losses. By having lower power attenuation and smaller pulse spreading due to dispersion, SMFs can provide significantly higher data rates and longer distances in comparison with MMFs [18]. Transmission in SMFs can achieve bit rates of about 100 Tb/s in very long distances, being the most commonly used fiber [18].

Transmission over optical fibers is impaired by several effects, such as dispersion, attenuation and non-linear effects. The attenuation limits the magnitude of the optical power transmitted in the fiber and it is introduced by the absorption, extrinsic and intrinsic effects [17]. The absorption effect appears due to a strong wavelength dependence of the attenuation coefficient of fused silica glass. Extrinsic effects are due to impurities in the fabrication process. Intrinsic effects are mainly caused by the Rayleigh scattering effect. The attenuation coefficient in standard single-mode fibers (SSMFs) is typically 0.5 dB/km at 1310 nm and 0.2 dB/km at 1550 nm [17].

The dispersion in SMFs is mainly characterized into two types: polarization-mode dispersion and CD. The polarization-mode dispersion is caused by the birefringence of the fiber

that results from slight differences between the refractive indices concerning the polarization directions of the degenerated modes that propagate along the fiber [17]. This effect changes along the fiber length, varies with time and enlarges the optical pulses differently in the two polarization directions. CD results mainly from material and waveguide dispersion. The material dispersion arises from the dependence on the refractive index of the silica with the wavelength, while waveguide dispersion is a consequence of refractive index differences in the fiber design parameters. CD results in optical pulse broadening as a result of several wavelengths traveling at different velocities along the fiber [17]. In links using SSMF, CD can typically be compensated by introducing a DCF after the SMF. Alternatively, there is the possibility to substitute the SSMF with a dispersion-shifted fiber, where the zero-dispersion wavelength is shifted to 1550 nm [17].

Finally, the non-linear effects are a consequence of the physical medium properties variation, caused by the response of the dielectric to light, producing a non-linear behaviour. Non-linear effects in the optical fiber result from two mechanisms, the Kerr effect and inelastic scattering [17], [19]. The Kerr effect results from refractive index changes caused by high power signals transmission in the fiber. The Kerr effect induces signal degradation caused by: i) self-phase modulation, ii) cross-phase modulation and iii) four-wave mixing (FWM). Self-phase modulation produces frequency chirp on the optical pulses. The frequency chirp of an optical pulse is characterized as the time dependence of the optical signal instantaneous frequency. The combination of chirp and CD, affects the signal frequencies differently along fiber propagation and leads to an increase of ISI at the receiver, which limits the transmission distance [17]. Cross-phase modulation is similar to self-phase modulation but generalized for WDM transmission by having one wavelength affecting the phase of other wavelengths through the Kerr effect. The FMW effect creates additional wavelengths propagating in the fiber, which can interfere with wavelengths already existing in the fiber leading to crosstalk (XT) [19]. The inelastic scattering originates the Brillouin and Raman scattering, being associated with acoustic waves and optical waves, respectively [17], [19]. The stimulated Brillouin scaterring occours only in the backward propagation direction, whereas stimulated Raman scaterring can occur in both directions. Although stimulated Brillouin scaterring does not induce crosstalk when all channels propagate in the forward direction, it limits the channel power because

part of the channel power can be transferred to a backward-propagating Stokes wave [17]. However, stimulated Brillouin scaterring can be easily avoided because the channel spacing must match almost exactly the Brillioun shift (about 10 GHz in the 1.55 μm region) for stimulated Brillouin scaterring to occur [17]. The stimulated Raman scaterring can significantly affect the performance of WDM systems due to the transfer of signal power from channels with lower wavelengths to channels with higher wavelengths. However, the stimulated Raman scaterring power penalty can be reduced simply by decreasing the channel spacing or by having sufficient dispersion, so that signals travel at different velocities, reducing the chances of overlapping between pulses propagating at different wavelengths [20].

2.4 Multicore fibers

Recently, SC-SMF transmissions have accomplished capacities around 100 Tb/s [6]. Nevertheless, the reached data rate of 100 Tb/s has been identified as the fundamental limit of standard SC-SMF, and this rate is not expected to fulfill the world wide growing capacity demand, resulting in a data capacity crunch [6]. A possible solution to support cost-efficient network capacity scaling is through the use of SDM, which consists of incorporating multiple spatial paths in the transmission. SDM solution can be implemented with three different approaches. The first approach is to use multiple different modes in a single fiber, such as in few-mode fibers (FMFs) or MMFs. The second approach is to use MCFs and the third approach is to use multiple parallel (bundled) SC-SMFs [2], [6], [7]. For this purpose, MCFs are seen as an appealing technology to surpass the capacity limitations encountered in SC-SMFs [6]. Moreover, MCFs have accomplished capacities ten times higher than SC-SMFs for similar distances, reaching a capacity-distance product of 10 Pbps·km [6]. MCFs have multiple cores inside the same cladding and are characterized by multiple parameters such as core diameter, core pitch, and outer cladding thickness, as schematically depicted in Fig. 2.8 for a seven core MCF, in opposition to a single core fiber (SCF).

The core pitch is the distance between neighboring cores and the outer cladding thickness is the minimum distance between the center of the outer cores and the cladding-coating interface [21]. The value of these parameters differ accordingly to the MCF type and the number

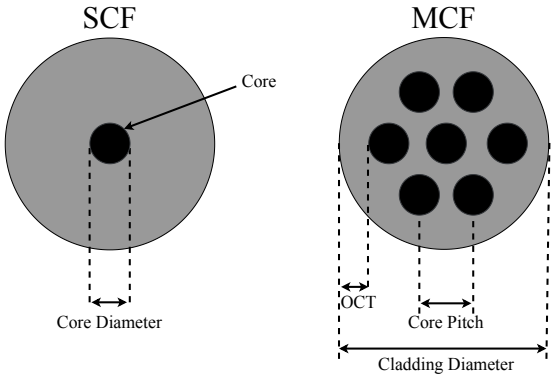

FIGURE 2.8: Single-core fiber and multicore fiber cross-section illustration.

of cores. Recent fabrication studies have demonstrated a single-mode MCF with 37 cores, cladding diameter of 248 μm, core pitch of 29 μm and outer cladding thickness of 39 μm [22] and a 39-core 3-mode fiber with 3 rings, having a core pitch between 39.7 and 41 μm and outer cladding thickness of 29 μm [23].

Regarding signal-coupling, MCFs can be classified into two types: i) weakly-coupled or ii) strongly-coupled MCFs [6]. In weakly-coupled MCFs, each core works as a single channel with low inter-core interference. Their core pitch is typically higher than 30 μm and the coupling coefficient is typically lower than 0.01 m^{-1} to ensure a crosstalk level lower than -30 dB [6]. In strongly-coupled MCFs, the core pitch is usually lower than 30 μm and the coupling coefficient is higher than 0.1 m^{-1}. As the distance between cores is reduced, the inter-core interference is increased, however, core density and consequently transmission capacity are improved. Transmissions over strongly-coupled MCFs require digital signal processing (DSP) to reduce this crosstalk impact. Hence, transmission over strongly-coupled MCFs demands receivers with higher complexity [6].

MCFs can also be classified in three types regarding the core characteristics: i) homogeneous, ii) quasi-homogeneous, or iii) heterogeneous. Homogeneous MCFs are characterized by having cores with similar properties, such as geometry, refractive index, and propagation constants [2], [9]. Quase-homogeneous fibers are characterized by exhibiting disparities in the fiber structure that occur during their fabrication process, resulting in slight variations in propagation constants of the different cores [9], [24]. Heterogeneous fibers have intrinsic index differences between adjacent cores and different core geometry, resulting in different propagation constants

between cores. Hence, heterogeneous fibers require the use of DSP at the receiver in order to compensate the differences between propagation delays of the signals in the different cores due to the different propagation constants of the cores. Therefore, heterogeneous fibers based links are more complex to implement than homogeneous fibers links [2].

In this work, homogeneous weakly-coupled SM-MCFs are going to be considered in order to ensure lower complexity and simplicity at the receiver, since these are key drivers in datacenter connections. Moreover, SM-MCFs are an easier migration path from existing SMF based networks [25]. However, these fibers are impaired by ICXT, which results in performance degradation and fiber length limitation in links supported by SM-MCFs.

2.5 Inter-core crosstalk in multicore fibers

Homogeneous weakly-coupled MCFs have been reported as an attractive medium for signal transmission. However, homogeneous fibers suffer from a type of interference known as ICXT, which affects signal transmission quality. Moreover, in [26], it is shown that the variation of ICXT power leads to the requirement of higher OSNR margins in order to ensure system performance. Hence, the ICXT characterization and ways of suppressing it have been investigated in several works. In [6], the reduction of the coupling coefficient between cores is proposed as a solution using trench-assisted MCFs and hole-assisted MCFs. This strategy accomplishes to suppress crosstalk due to the existence of low index trench layers. Another proposed solution is to use heterogeneous MCFs since these fibers reduce core coupling by having all cores with a different propagation constant. Alternatively, propagation-direction interleaving techniques can be used. In this case, adjacent cores are assigned in opposite transmissions directions, hence, reducing the ICXT impact on the performance [6].

The ICXT effect is reasonably well studied in the literature [27], [28], [29] and, due to the random evolution of ICXT over time, ICXT-impaired systems may experience: (i) random variations of the bit error rate (BER) over short time periods [12], [30], and (ii) system outage over long time periods due to high ICXT levels [12]. Studies have shown that ICXT has a significant dependence on the used wavelength and MCF parameters, such as fiber bending,

twist, and fiber length [21], [31]. In the literature, there are several proposals of analytical models that take into account the ICXT field generation, which depends on several parameters of the MCF. Several works have shown that the ICXT results mostly from the discrete contribution of points along the longitudinal propagation direction of the MCF, known as phase matching points (PMPs) [28]. The PMPs, where the difference between the effective refractive index of the interfering and interfered cores is zero, manifest randomly along the fiber [32]. Each contribution is weighted by an independent random phase shift (RPS) and the corresponding propagation delay [26]. Random variations of the twist rate, bending radius, or other fiber conditions are modeled by the RPSs. In addition, it is shown that the ICXT power variations can be attributed to perturbations such as bends, twists, and structural fluctuations of the fiber that impact the PMPs [13]. In [13], a single polarization DCM scheme was proposed to characterize the ICXT and its dependence on the fiber properties. In subsequent works, the dependence on the modulation frequency and on the differences between the dispersion parameters of the cores was included in the DCM [27], [28]. In [32], a DCM with a dual-polarization scheme, for weakly-coupled MCFs has been proposed. In this work, the dual-polarization DCM was assumed to characterize the ICXT induced by the different MCF interfering cores in a single interfered core. This model is described with more detail in Chapter 3.

2.6 Optical amplification in inter-datacenter links supported by MCFs

Inter-datacenter connections can reach up to 100 km. Hence, EDFAs operating at 1550 nm must be used to compensate the optical link losses. A possible solution regarding links supported by SCFs is to use the mature technology of single-core EDFA (SC-EDFA) [33]. However, links supported by MCFs with such a solution would lead to high power consumption and become costly since they would require a SC-EDFA for each core. Hence, to support amplification in MCFs, multi-core-EDFAs (MC-EDFAs) have been studied in the literature to reduce power consumption, the number of required components, and overall cost in comparison to multiple SC-EDFAs and have demonstrated promising features such as supporting high data capacity

and allowing standard cladding diameter of 125 μm [34]. However, MC-EDFAs induce ICXT on the transmitted signals, a situation that never occurs in SC-EDFAs [33]. In [35], the total crosstalk from 6 outer cores of a MC-EDFA is estimated to be -46.5 dB at the center core.

MC-EDFAs can be classified into two types according to the pumping schemes: core-pumped and cladding-pumped. Both amplifier types have been investigated and reported in the literature [36]. Core-pumped MC-EDFAs have a core-pumping scheme which is based on multiple conventional single-core components, such as single-mode pump laser diodes which are used to pump each of the cores, and may not result in expected cost advantage by integration [37]. Cladding-pumping MC-EDFAs have a cladding-pumping scheme in which all cores are simultaneously pumped using a single high-power multi-mode laser diode [38]. However, for cladding-pumping MC-EDFAs, each core pump power can not be adjusted independently from other pump power cores, which can lead to unwanted gain changes in other cores. A solution for this issue is a hybrid-pumping scheme that employs both cladding and core pumping [36]. Hybrid-pumped MC-EDFAs gain controllability can be compared to that of a conventional SC-EDFA, implying that a conventional design scheme is applicable in designing a gain-controlled hybrid-pumped MC-EDFA [36].

2.7 Dispersion compensation in inter-datacenter connections

With the introduction of amplification in the link, the problem of transmission loss in inter-datacenter links is reduced. However, CD becomes a serious problem that limits capacity in such links [39]. In IM-DD systems, the effect of CD combined with photodetection induces a non-linear operation on the signal, and, simple receiver-side electronic equalization is usually not effective [5]. The CD compensation can also be performed in the optical domain, with optical technologies, such DCFs or tunable fiber Bragg gratings. Moreover, when power consumption is a primary concern, fibers with smaller CD or optical CD compensation should be used, since electronic compensation leads to high power consumption [5].

2.7.1 Optical dispersion compensation

A possible solution for dispersion compensation is using standard fibers exhibiting near-zero dispersion near 1550 nm, as dispersion-shifted fibers. The 1550 nm window provides better options and long-distance transmission due to the lower attenuation and higher bandwidth than the 1310 nm window and enables the use of simple and cost-effective WDM technologies [39]. However, dispersion-shifted fibers are much sensitive to FWM and they are not efficient for WDM and dense wavelength division multiplexing transmissions. Alternatively, a typical solution at 1550 nm for compensating fiber dispersion is to use DCFs, which are one of the main components of the dispersion compensation modules implemented in typical WDM systems. DCFs are characterized by having a negative dispersion, which allows optical dispersion compensation by setting a pre-defined DCF length. However, DCFs attenuation is typically 0.5 dB/km at 1550 nm, which will increase the transmission loss. Moreover, DCFs insertion loss is typically around 5 dB and DCFs have small mode field diameter resulting in an effective area typically of the order of 20 μm^2, hence, enhancing the non-linear effects in DCFs [39]. Alternative solutions to dispersion-shifted fibers and DCFs have been suggested to reduce insertion losses, nonlinearities, and cost [39]. A possible solution might rely on chirped fiber Bragg gratings, which provide an additional feature: dynamic dispersion compensation, which is not possible with DCF and becomes essential for high-speed WDM systems [40]. However, one fiber Bragg grating can only compensate a single wavelength. Thus, a high number of fiber Bragg gratings (as high as the number of channels) must be used to compensate the dispersion in WDM systems [17]. Hence, besides the technological issue of having a high number of fiber Bragg grating components, the cost also scales with the number of WDM channels.

In this work, a DCF is going to be considered to optically compensate the chromatic dispersion, since it is the most common CDC solution.

2.7.2 Electrical dispersion compensation

CD compensation can also be performed through DSP after photodetection at the optical receiver in the electrical domain. This compensation has the challenging task of reducing the

effect of a combination of signal distortion and noise such as high ISI due to CD, amplified spontaneous emission (ASE) noise, and, in MCFs, ICXT [41]. Inter-datecenter links are impaired by high values of CD. Hence, simple electric dispersion compensation techniques, such as adaptive equalization performed with DSP are not effective [5]. In [41], single-channel 100 Gbit/s transmission based on PAM4 at 56 Gbaud together with DSP based de-mapping is demonstrated.

2.8 FEC in PAM4 systems

Transmission in DD links, using modulations formats with higher-order than OOK typically required the use of FEC [42]. In the literature, several works that transmit PAM4 signals in IM-DD links systems use a pre-FEC BER (the BER before the DSP at the receiver) of 3.8×10^{-3} [16], [43], [44], [45], [46]. Therefore, in this work, we assume FEC and consider a target BER limit of 3.8×10^{-3} in presence of ICXT. We assume also a target BER limit of 3.8×10^{-5} in absence of ICXT, which is two orders of magnitude below the target BER in the presence of ICXT. A similar assumption was considered in [47], [48]. To achieve this BER without ICXT, for λ=1550 nm, the required PAM4 signal power at the output of the optical transmitter for a particular signal extinction ratio must be determined.

2.9 PAM4 signaling over multicore fibers

Recently, the capacity upgrade in datacenter links over MCFs has been proposed through the use of the PAM4 format. In [49], the impact of ICXT on 56 Gbaud PAM4 signal transmission along a 2.5 km MCF over a weakly-coupled and uncoupled 7-core fiber has been studied, and it is concluded that the ICXT depends on the carrier wavelength in a range of 1540-1560 nm. Longer wavelengths lead to worse transmission performance which leads to higher instability in transmissions over weakly-coupled MCFs. The demonstration of a cheaper transmitter configuration in a PAM4 transmission over MCF using directly modulated lasers instead of external modulated lasers, has also been studied [50]. In this study, there is no information

about the characteristics and MCF type used in this experiment. In [31], the transmission of PAM4 signals is demonstrated over 2 km of SM-MCF with 4 cores with 125 μm cladding, which is desirable for a simpler migration from an existing SMF system to a MCF system. In [51], the transmission of 100 Gbps PAM4 transmission is successfully demonstrated over 1 km dispersion-uncompensated and 10 km dispersion-compensated through a SM-MCF with 7 cores, using a direct modulated vertical cavity surface emitting laser and digital equalization techniques. In this experiment, the importance of dispersion compensation is demonstrated.

Chapter 3

Inter-datacenter link description and performance assessment

In this chapter, the system equivalent model for an inter-datacenter link supported by MCFs is presented. The optical transmitter block considering several optical transmitters is described in section 3.2. In section 3.3, the dual-polarization DCM of the MCF used to characterize the ICXT is described. The chromatic dispersion compensation (CDC) module is presented in section 3.4. In section 3.5, the optical preamplifier model is presented. The DD optical receiver (photo-detector and electrical filter) is presented in section 3.6. In section 3.7, the method used to estimate the BER is described, and the study of the BER estimation in an optically amplified PAM4 inter-datacenter without ICXT is performed in section 3.8. In section 3.9, the main conclusions regarding this chapter are presented.

3.1 Inter-datacenter link modeling

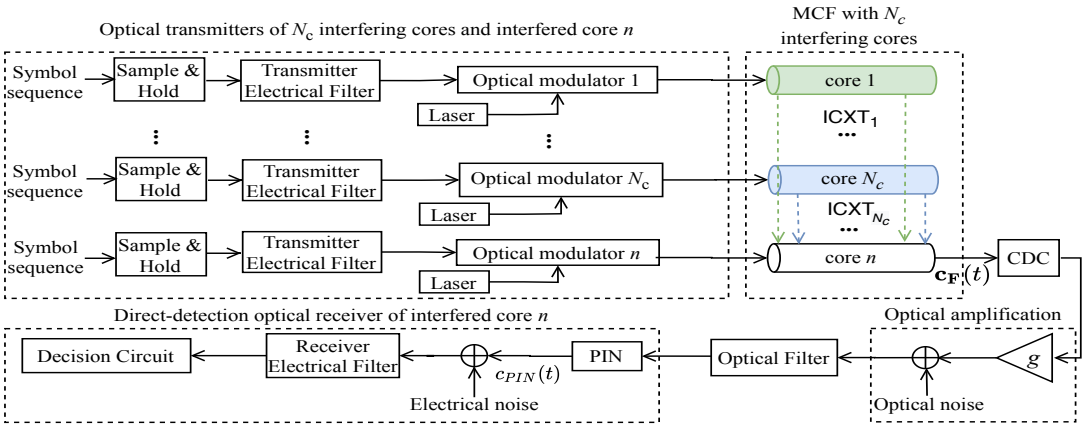

FIGURE 3.1: Equivalent model of the inter-datacenter link supported by MCF. The MCF has one interfered core denoted as n, which represents the core under test, and the interfering cores, each one denoted as m, with m=1,...,N_c.

3.2 PAM4 signal generation at the optical transmitter output

In Fig. 3.1, at the transmitter block, for each optical transmitter concerning to a different fiber core, distinct and independent PAM4 symbol sequences are generated. After symbols generation, the PAM4 symbols with non-ideal extinction ratio are sampled and passed through an electrical filter that models the frequency limitations of the electrical part of the transmitter. After electrical filtering, the PAM4 signal is converted to the optical domain by an optical modulator. Each optical modulator is assumed without chirp and with a finite extinction ratio.

In the simulator, the PAM4 symbols sequence is generated using four-level deBruijn sequences of maximum length $4^{N_{reg}}$, obtained from Galois arithmetic. N_{reg} is the offset register length used to generate the four-level deBruijn sequence.

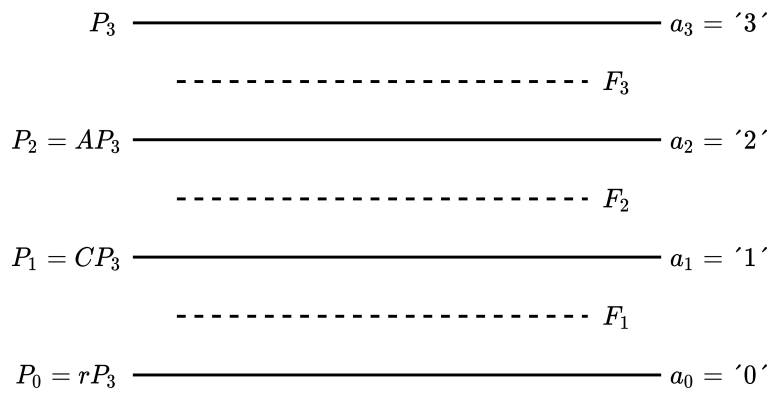

FIGURE 3.2: Representation of the ideal PAM4 power levels with non-ideal extinction ratio at the optical transmitter output and the corresponding ideal decision thresholds.

The PAM4 symbols denoted as a_k (with k=0, 1, 2 and 3), with corresponding power levels P_k, are equally likely to occur [52]. The representation of the ideal power levels of a PAM4 signal for a non-ideal extinction ratio r, is illustrated in Fig. 3.2, where the constants A and C define the PAM4 signal intermediate power levels, P_1 and P_2 [53], and F_s, (with s=1, 2 and 3), are the ideal decision thresholds. The PAM4 signal extinction ratio is defined as [52]

$$r = \frac{P_0}{P_3} \tag{3.1}$$

The average power of the PAM4 optical signal shown in Fig. 3.2 is given by [53]

$$P_{av} = \frac{1 + A + C + r}{4} P_3 \tag{3.2}$$

This work studies an optically amplified inter-datacenter link. In optically amplified links, signal-amplified spontaneous emission (ASE) beat noise typically dominates the performance degradation and leads to different received noise powers proportional to the different intensity levels of the signal [5]. In [53], the optimization of A and C is studied in order to minimize the error probability for optically amplified PAM4 links where signal-ASE beat noise is dominant over electrical noise, in order to minimize the error probability in comparison to a similar system using PAM4 signals with equispaced levels. The values of A and C were not optimized taking ASE-ASE beat noise into account, because it would result in a maximum receiver sensitivity improvement of 0.5 dB [53]. Hence, when taking only signal-ASE beat noise into account, A and C optimal values are given by [53]

$$C = \frac{1 + 4\sqrt{r} + 4r}{9} \tag{3.3}$$

$$A = \frac{4 + 4\sqrt{r} + r}{9} \tag{3.4}$$

After signal generation and sampling, to model the amplitude and phase distortion induced by the filtering and parasitics at the electrical part of the transmitter, the ideal PAM4 signal is filtered by a 3$^{\text{rd}}$ order Bessel filter. The -3 dB bandwidth of this transmitter electrical filter, $B_{e,TX}$, is set the same as the symbol rate, R_s.

In Fig. 3.3 a) and b), an example of the PAM4 transmitted signal for $r = 0$ and $r = 0.1$, respectively, at the input of a fiber core, that could be either an interfering core m or the interfered core n, through the eye-patterns, is shown through the eye-patterns observed at the optical transmitter output. It is possible to observe that the eye-pattern is still completely open with absence of ISI on the quaternary symbols at the optimum sampling instant and has some distortion at the symbol transitions.

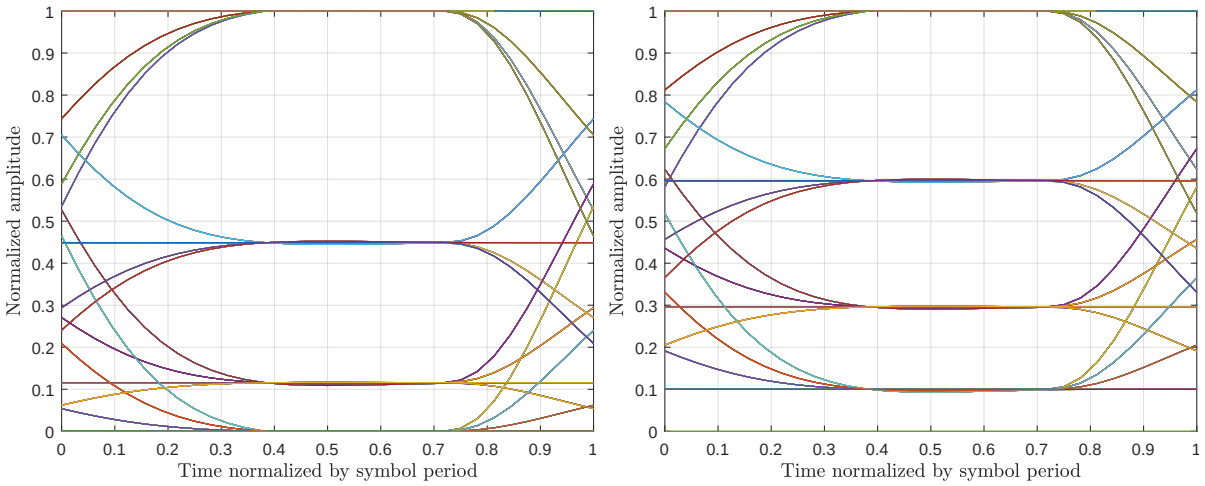

(a) $r = 0$ (b) $r = 0.1$

FIGURE 3.3: Normalized eye-pattern of the PAM4 signal at the optical transmitter output.

3.3 MCF modeling and ICXT generation

In the following, the simulation model known as dual-polarization DCM, used to characterize the ICXT induced by the interfering cores of the MCF, is presented [32]. The dual-polarization DCM characterizes the ICXT induced by the different cores of the MCF on the interfered core, n. This model provides a very good characterization of the ICXT impact, as shown in [32] and in agreement with experimental results [12], [29], [30]. Linear propagation along the MCF is assumed in all cores. The dual-polarization DCM describes the ICXT generation in the two polarization directions **x** and **y**.

For an interfering core m, the power splitting at the input of the MCF is represented as

$$\begin{aligned} c_{m,x}(t) &= c_m(t) \times \sqrt{\xi_m} \\ c_{m,y}(t) &= c_m(t) \times \sqrt{1-\xi_m} \\ \mathbf{c_m}(t) &= c_{m,x}(t)\hat{\mathbf{x}} + c_{m,y}(t)\hat{\mathbf{y}} \end{aligned} \tag{3.5}$$

where the bold notation represents a vector, $\mathbf{c_m(t)}$ is the optical field at the input of an interfering core m (with m=1,...,N_c), $c_{m,x}(t)$ and $c_{m,y}(t)$ are the optical field transmitted in polarizations **x**

and **y**, respectively, the input of that interfering core and ξ_m controls the power splitting between the two polarization directions. The parameter ξ_m can vary between 0 and 1 [32].

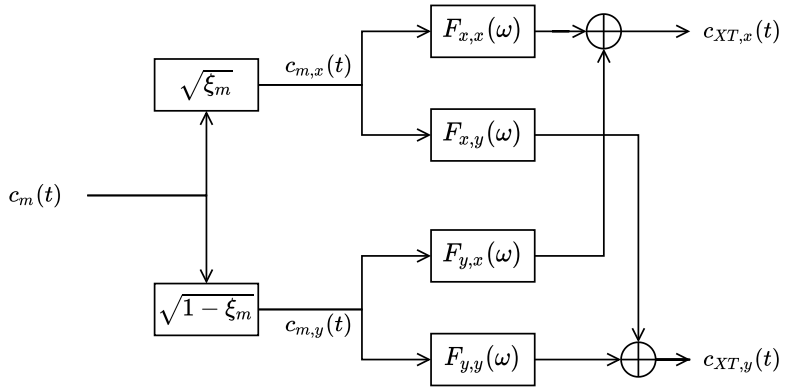

FIGURE 3.4: Dual-polarization DCM for an interfering core m [32].

The transfer functions $F_{a,b}(\omega)$ model the frequency response of the ICXT from polarization a (with $a = x$ or y) at the input of an interfering core m to polarization b (with $b = x$ or y) at the output of the interfered core n. The transfer function $F_{a,b}(\omega)$ is given by [32]

$$F_{a,b}(\omega) = -\frac{j}{\sqrt{2}}\overline{K}_{nm}\exp\left(-j\overline{\beta}_n(\omega)L\right)\cdot\exp\left(-\frac{\alpha_n}{2}L\right)\cdot \sum_{k=1}^{N_p}\exp\left[-j(\overline{\beta}_m(\omega)-\overline{\beta}_n(\omega))z_k\right]\exp\left[-j\phi_{nm,k}^{(a,b)}\right] \quad (3.6)$$

where α_n is the power attenuation coefficient of core n (which is assumed equal to the attenuation coefficient of any of the interfering cores), $\overline{K}_{nm}$ is the average inter-core coupling coefficient, which corresponds to the average of its contribution in the two polarization directions given by $\overline{K}_{nm}$=$(K_{nm}^{(x)} + K_{nm}^{(y)})/2$ [32], ω is the angular frequency, L is the MCF length, N_p is the number of PMPs [28], $\phi_{nm,k}^{(a,b)}$ represents the RPS associated with the k-th PMP, which is modelled by an uniform distribution between 0 and 2π, and $\overline{\beta}_l(\omega)$ is the average of the propagation constants in the two polarization directions in core l (with l=m or n). In each direction, the propagation constant is given by [17]

$$\beta_l(\omega) = \beta_{0,l} + \beta_{1,l}\omega + \frac{\beta_{2,l}}{2}\omega^2 + \frac{\beta_{3,l}}{6}\omega^3 \quad (3.7)$$

where $\beta_{0,l}$ is the propagation constant at the carrier wavelength, $\beta_{1,l}$ is the inverse of the group velocity, $\beta_{2,l}$ is the group velocity dispersion and $\beta_{3,l}$ is the higher order dispersion, for core l.

The skew between an interfering core m and the interfered core n, is given by $S_{mn} = d_{mn}L$, where d_{mn} is the walkoff between cores m and n defined by $d_{mn} = \beta_{1,m} - \beta_{1,n}$ [32]. The propagation constants are given by [17]

$$\beta_{0,l} = \frac{2\pi}{\lambda} n_{eff} \tag{3.8}$$

$$\beta_{1,l} = \frac{1}{v_{g,l}} \tag{3.9}$$

$$\beta_{2,l} = -\frac{\lambda^2 D_{\lambda,l}}{2\pi c} \tag{3.10}$$

$$\beta_{3,l} = \left(\frac{\lambda^2}{2\pi c}\right)^2 S_\lambda + \frac{\lambda^3 D_{\lambda,l}}{2\pi^2 c^2} \tag{3.11}$$

where n_{eff} is the effective refractive of core l at the wavelength λ, $v_{g,l}$ is the group velocity in core l, λ is the carrier wavelength, $D_{\lambda,l}$ is the dispersion at the carrier wavelength of core l and S_λ is the slope of the dispersion parameter at the carrier wavelength in the same core.

The longitudinal coordinate of the k-th PMP, z_k, is randomly distributed between two consecutive PMPs and is given by

$$z_k = \frac{L}{N_p}(r_k + k - 1) \tag{3.12}$$

where r_k $\left(1 \leq k \leq N_p\right)$ are independent random variables with uniform distribution in the interval $[0, 1[$.

The dual-polarization DCM has been derived with the goal of keeping the complexity and time of simulation at reasonable levels. In such model, the evolution of the ICXT impact on the system performance is evaluated in time fractions with a much shorter duration than the ICXT decorrelation time. Those time fractions are separated by time intervals longer than the decorrelation time of ICXT. This means that, from time fraction to time fraction, the ICXT is uncorrelated and, within each time fraction, is totally correlated [32]. For this reason, each time fraction corresponds to an independent set of RPSs, which we name MCF realization. Therefore, the different MCF realizations are obtained by generating randomly different sets of N_p RPSs. In each iteration of the Monte Carlo (MC) simulator, one MCF realization is generated, and the

symbols of the PAM4 signal transmitted in an interfering core m are randomly generated. The transfer functions $F_{x,x}(\omega)$ and $F_{y,x}(\omega)$ model the ICXT generated from polarization **x** and **y** of an interfering core m to the polarization **x** of core n. The transfer functions $F_{x,y}(\omega)$ and $F_{y,y}(\omega)$ model the ICXT generated from both polarizations of an interfering core m to the polarization **y** of core n [32]. For equal powers at the input of the interfered and interfering cores and identical loss in the two cores, the ratio between the mean ICXT power and the mean power of the signal at the output of the interfered core n, named ICXT level, X_c, is related to the parameters of Eq. 3.6 by $X_c = N_p|K_{nm}|^2$ [32].

The power splitting, for core n, is represented by

$$\begin{aligned} c_{n,x}(t) &= c_n(t) \times \sqrt{\xi_n} \\ c_{n,y}(t) &= c_n(t) \times \sqrt{1-\xi_n} \\ \mathbf{c_n}(t) &= c_{n,x}(t)\hat{\mathbf{x}} + c_{n,y}(t)\hat{\mathbf{y}} \end{aligned} \tag{3.13}$$

where $\mathbf{c_n}(\mathbf{t})$, is the interfered optical field, $c_{n,x}(t)$ and $c_{n,y}(t)$ are the optical field transmitted in polarizations **x** and **y** at the input of core n, respectively. The parameter ξ_n controls the power distribution between the two polarization directions and can vary between 0 and 1 [32]. After the power splitting, the PAM4 signal passes through the core n, being this propagation modelled by the linear propagation transfer function $H_F(\omega)$. Hence, the signal at the output of core n without ICXT is given by

$$\begin{aligned} c_{F,x}(t) &= c_{n,x}(t) * \mathcal{F}^{-1}[H_F(\omega)] \\ c_{F,y}(t) &= c_{n,y}(t) * \mathcal{F}^{-1}[H_F(\omega)] \\ \mathbf{c_F}(t) &= c_{F,x}(t)\hat{\mathbf{x}} + c_{F,y}(t)\hat{\mathbf{y}} \end{aligned} \tag{3.14}$$

where $*$ stands for convolution, $\mathcal{F}^{-1}$ stands for the inverse Fourier Transform and $H_F(\omega)$ is given by [17]

$$H_F(\omega) = \exp\left(-j\overline{\beta}_n(\omega)L\right) \cdot \exp\left(-\frac{\alpha_n}{2}L\right) \tag{3.15}$$

The signals that interfer with the signal at the output of the core n, $c_{XT,x}(t)$ and $c_{XT,y}(t)$, are given by [32]

$$\begin{aligned} c_{XT,x}(t) &= c_{m,x}(t) * \mathcal{F}^{-1}[F_{xx}(\omega)] + c_{m,y}(t) * \mathcal{F}^{-1}[F_{yx}(\omega)] \\ c_{XT,y}(t) &= c_{m,x}(t) * \mathcal{F}^{-1}[F_{xy}(\omega)] + c_{m,y}(t) * \mathcal{F}^{-1}[F_{yy}(\omega)] \\ \mathbf{c_{XT}}(t) &= c_{XT,x}(t)\hat{\mathbf{x}} + c_{XT,y}(t)\hat{\mathbf{y}} \end{aligned} \tag{3.16}$$

3.4 Chromatic dispersion compensation modeling

In order to compensate the dispersion introduced along the transmission through core n, at the output of the MCF, a DCF is used to fully compensate the distortion due to chromatic dispersion on the signal impaired by ICXT. The DCF is modelled considering linear propagation transmission, with α_{DCF} characterizing the DCF attenuation coefficient. In this work, the DCF length is designed to fully compensate the accumulated dispersion induced by the MCF at the operating wavelength. Therefore, the estimated DCF length is given by [17]

$$L_{DCF} = \frac{-D_{\lambda,n}L}{D_{\lambda,DCF}} \tag{3.17}$$

where $D_{\lambda,n}$ is the dispersion parameter of core n and $D_{\lambda,DCF}$ is the DCF dispersion parameter.

3.5 EDFA modeling

After passing through the CDC module, the PAM4 signal arrives at the EDFA input, which is followed by an optical filter. In this work, the EDFA flat power gain, g, is set to fully compensate the losses introduced by the SM-MCF and DCF. The amplifier gain, in dB, to achieve a fully loss compensated link is given by [17]

$$G = \alpha_n L + \alpha_{DCF} L_{DCF} \tag{3.18}$$

3.5.1 ASE noise

The ASE noise is modelled as additive white Gaussian noise with power spectral density, per polarization mode, given by [17]

$$S_{ASE} = \frac{F_n}{2}(g-1)h\nu_0 \tag{3.19}$$

where $h\nu_0$ is the photon energy and F_n is the amplifier noise figure.

3.5.2 Optical filter

Before passing through the photo-detector, the signal with ICXT and ASE noise passes through an optical filter. The optical filter is used to reduce the power of the optical noise without introducing much ISI [17]. The optical filter is modelled by a 4^{th} order super Gaussian filter. The transfer function of the i-th order super Gaussian filter is given by [54]

$$H_o(f) = \frac{1}{\sqrt{i_L}} \exp\left[-\left(\frac{2\,|f-f_o|}{B_o}\right)^{2i} \ln\sqrt{2}\right] \tag{3.20}$$

where f_o is the optical filter central frequency, i_L is the insertion loss in linear units, and B_o is the optical filter bandwidth at -3 dB.

The ASE noise power at the amplifier output, per polarization mode, is given by

$$P_{ASE} = S_{ASE} B_{o,n} \tag{3.21}$$

where $B_{o,n}$ is the noise equivalent bandwidth of the optical filter. For a super Gaussian optical filters with sufficiently high order ($n \geq 3$), the amplitude transfer function tends to a rectangular shape, and, hence, $B_{o,n} \approx B_o$ [17].

3.6 Optical receiver for the interfered core

After passing through the MCF, the optical amplifier and the CDC module, the PAM4 signal impaired by ICXT and ASE noise arrives at the DD optical receiver input, which includes a PIN photo-detector, an electrical filter and a decision circuit.

3.6.1 PIN photo-detector

PIN photodiodes convert light into electricity through the photoelectric effect. The signal at the output of the PIN photo-detector, $c_{PIN}(t)$, is given by [17]

$$\begin{aligned} c_{PIN}(t) &= R_\lambda[|c_{XT,x}(t) + c_{F,x}(t)|^2 + |c_{XT,y}(t) + c_{F,y}(t)|^2] \\ &= R_\lambda[|c_{XT,x}(t)|^2 + |c_{F,x}(t)|^2 + 2 \cdot \mathrm{Re}[c_{XT,x}(t) \cdot c_{F,x}(t)] + \\ &\qquad |c_{XT,y}(t)|^2 + |c_{F,y}(t)|^2 + 2 \cdot \mathrm{Re}[c_{XT,y}(t) \cdot c_{F,y}(t)]] \end{aligned} \tag{3.22}$$

where $|c_{F,x}(t)|^2$ and $|c_{F,y}(t)|^2$ represent the detected signal, $|c_{XT,x}(t)|^2$ and $|c_{XT,y}(t)|^2$ correspond to the ICXT-ICXT beating, $2 \cdot \mathrm{Re}\left[|c_{XT,x}(t) \cdot c_{F,x}(t)|\right]$ and $2 \cdot \mathrm{Re}\left[|c_{XT,y}(t) \cdot c_{F,y}(t)\right|]$ are the signal-ICXT beating and Re [ ] stands for the real part of a complex number. The PIN responsivity, R_λ, is given by [17]

$$R_\lambda = \frac{\eta q}{h\nu_0} \quad [\mathrm{A/W}] \tag{3.23}$$

where η is the photo-detector efficiency, q is the electron charge (q=1.602×10^{-19} C), h is the Planck constant (h=6.602×10^{-34} J·s) and ν_0 is the optical frequency of the incident optical power.

After detecting the received signal, the average current due to the ASE noise, per polarization mode, is given by [53]

$$I_{ASE} = R_\lambda S_{ASE} B_{o,n} \tag{3.24}$$

3.6.2 Electrical noise

The electrical noise is modeled by a Gaussian distribution. The power of the electrical noise is given by [17]

$$\sigma_c^2 = R_\lambda^2 NEP^2 B_{e,n} \tag{3.25}$$

where NEP is the noise equivalent power, defined as the minimum optical power necessary to generate a photocurrent equal to the noise current of the photo-detector [17]. The bandwidth $B_{e,n}$ is the noise equivalent bandwidth of the receiver electrical filter, given by

$$B_{e,n} = \int_0^{+\infty} \frac{|H_{e,RX}(f)|^2}{|H_{e,RX}(0)|} df \tag{3.26}$$

where $H_{e,RX}(f)$ is the amplitude transfer function of the electrical filter.

3.6.3 Electrical filter

After passing through the photo-detector, the signal with ICXT, ASE and electrical noise passes through an electrical filter. The electrical filter is used to reduce the noise power without introducing much ISI on the signal [17]. In this work, the electrical filter of the optical receiver is modelled as 3$^{\text{rd}}$ order Bessel filter, whose n-th order amplitude transfer function is given by [55]

$$|H_{bessel}(s)| = \frac{1}{Q_n(s)} \tag{3.27}$$

with

$$s = j \cdot \frac{2f}{B_{e,RX}} \tag{3.28}$$

where $B_{e,RX}$ is the receiver electrical filter bandwidth at -3-dB and $Q_n(s)$ is the n-th order polynomial factor and can be obtained from [55]

$$|Q_{n+1}(s)| = Q_n(s) + \frac{s^2}{4n^2 - 1} Q_{n-1}(s) \tag{3.29}$$

with

$$|Q_n(s)| = s^n B_n \left(\frac{1}{s}\right) \tag{3.30}$$

where B_n is the n-th order Bessel polynomial [55].

The power of the detected ASE noise for the k-th received PAM4 signal at the electrical filter output, is given by [53]

$$\sigma^2_{n,k,ASE} = 4R_\lambda B_{e,n} S_{ASE} \left(R_\lambda \cdot gP_k + I_{ASE}\right) \tag{3.31}$$

where P_k is the symbol level corresponding to the received a_k symbol taken from the eye-pattern. In Eq. (3.31), the first sum term represents the signal-ASE beat noise and the second term represents the ASE-ASE beat noise. The current I_{ASE} is set to zero when ASE-ASE beat noise is not taken into account.

3.7 Bit error rate estimation

The BER is calculated by the semi-analytical method known as the exhaustive Gaussian approach, which, for a PAM4 received signal, is given by [53]

$$BER = \frac{1}{2 \cdot 4^{N_{reg}}} \left\{ \sum_{\substack{j=1 \\ a_k=0}}^{4^{N_{reg}}} Q\left(\frac{F_1 - i_{0,j}}{\sigma_{0,j}}\right) + \sum_{\substack{j=1 \\ a_k=1}}^{4^{N_{reg}}} \left[Q\left(\frac{i_{1,j} - F_1}{\sigma_{1,j}}\right) + Q\left(\frac{F_2 - i_{1,j}}{\sigma_{1,j}}\right) \right] + \right.$$
$$\left. \sum_{\substack{j=1 \\ a_k=2}}^{4^{N_{reg}}} \left[Q\left(\frac{i_{2,j} - F_2}{\sigma_{2,j}}\right) + Q\left(\frac{F_3 - i_{2,j}}{\sigma_{2,j}}\right) \right] + \sum_{\substack{j=1 \\ a_k=3}}^{4^{N_{reg}}} Q\left(\frac{i_{3,j} - F_3}{\sigma_{3,j}}\right) \right\} \tag{3.32}$$

where $i_{0,j}$, $i_{1,j}$, $i_{2,j}$ and $i_{3,j}$ correspond to the means of the currents at the input of the decision circuit for the symbols a_k at the time sampling instants, $t_j = t_o + T_s(j-1)$, with j=1,...,$4^{N_{reg}}$ and T_s the symbol period; t_o is extracted from the received eye-pattern at the decision circuit input and $\sigma_{0,j}$, $\sigma_{1,j}$, $\sigma_{2,j}$ and $\sigma_{3,j}$ are the noise standard deviations for the different time sampling instants [52]. The $Q(x)$ function is given by [56]

$$Q(x) = \int_x^\infty \frac{1}{\sqrt{2\pi}} e^{-\frac{\xi^2}{2}} d\xi \tag{3.33}$$

In the simulation of the PAM4 signal, since the corresponding eye diagram has four power levels, it is not trivial to find the optimum sampling instant. Hence, in this work, the selection of the optimum sampling time instant t_j, i.e., the sampling instant that leads to the lower BER, is obtained by testing multiple sampling instants around the three sampling instants where each different eye is larger and only the lowest achieved BER is considered.

The decision thresholds F_1, F_2 and F_3 are optimized in each time-fraction by applying the bisection method to minimize the BER [57]. The effect of ICXT and ISI resulting from the filtering is taken into account by the waveform distortion at these t_j sampling time instants and, in Eq. 3.32, this effect is included in the mean currents $i_{k,j}$. The effect of electrical noise, signal-ASE, and ASE-ASE beat noises are taken into account semi-analytically in the standard deviations of the received symbols, $\sigma_{k,j}$. The consideration of the impact of all noise types in a semi-analytical way allows a much faster BER computation (though accurate enough [58]) in each time fraction.

3.8 Study of the optically amplified PAM4 link without ICXT

In this section, the study of the BER in the optically amplified optical link shown in Fig. 3.1 is presented, taking signal-ASE, ASE-ASE beat noises and electrical noise into account, and neglecting ICXT.

The system validation for a non-optically amplified and for the optically amplified links, taking signal-ASE and ASE-ASE beat noises into account is made in Appendix A by comparison with the results obtained theoretically through the formulas proposed in [53]. The parameters used in the study are presented in Table 3.1.

TABLE 3.1: Simulation parameters in a back-to-back situation.

Simulation parameter	Value
Symbol rate	R_s = 56 Gbaud
Number of samples per symbol	N_s =32
Number of generated PAM4 symbols in each realization	$N = 4^4$
PIN responsivity	R_λ=1 A/W
Carrier wavelength	λ = 1550 nm
Noise equivalent power	NEP=10^{-12} W/$\sqrt{\text{Hz}}$
TX electrical filter bandwidth	$B_{e,TX} = R_s$
Optical filter order	n=4
EDFA gain	G=30 dB
EDFA noise figure	F_n=4.77 dB

3.8.1 Optical and electrical filter bandwidths optimization

In this subsection, the optimum optical and receiver electrical filter -3 dB bandwidths that maximize the receiver sensitivity in a back-to-back (B2B) configuration are assessed for a reference target BER of 3.8×10^{-5}.

After analysing Fig. 3.5, it is possible to identify that the optimal optical and electrical -3 dB bandwidths pair is about $1.6\times R_s$ and $0.95\times R_s$, for $r = 0$ and $2.4\times R_s$ and $0.75\times R_s$, for $r = 0.1$. For both extinction ratios, it is possible to identify that the optical -3 dB bandwidth enlargement above the optimum value has a small effect on the sensitivity degradation, due to the slow increase of the ASE-ASE beat noise power. For a B_o narrower than the optimum, the receiver sensitivity degradation is mainly due to closing of the eye diagram due to strong ISI. It is also possible to identify an enhanced degradation of the the receiver sensitivities for lower electrical filter bandwidths, mainly for $r = 0$, due to the higher ISI in the eye of the PAM4 signal with optimized levels, caused by the narrower electrical filtering.

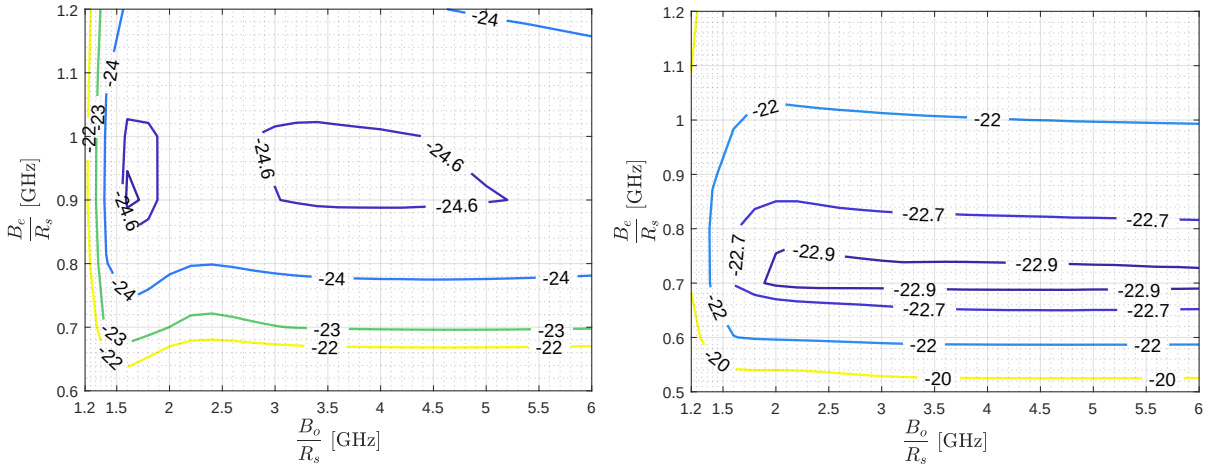

(a) $r = 0$ (b) $r = 0.1$

FIGURE 3.5: Dependence of the receiver sensitivity on the optical and electrical receiver electrical filter -3 dB bandwidths, B_o and $B_{e,RX}$, for a) $r = 0$ and b) $r = 0.1$, obtained by simulation for a target BER of 3.8×10^{-5}, for an optically amplified link in a B2B configuration with optimized PAM4 power levels, considering both signal-ASE and ASE-ASE beat noises.

From Fig. 3.5 and in order to find a pair of -3 dB bandwidths that can be used for both extinction ratios, while not enhancing too much the sensitivity degradation in relation to the optimum sensitivity, we select the optimal bandwidths pair of B_o=1.6×R_s and $B_{e,RX}$=0.85×R_s where a sensitivity degradation of only 0.1 dB and 0.15 dB, respectively, for $r = 0$ and $r = 0.1$, is found. Moreover, this pair is selected having in mind the possible implementation of WDM transmission in each core of the MCF, where a minimum of 100 GHz of channel spacing (as defined in ITU-T G.694.1 [59]) must be used to guarantee the transmission of 56 Gbaud PAM4 signals. However, as the optimum optical bandwidth of 1.6×R_s = 89.6 GHz, is close to the 100 GHz WDM channel spacing, additional degradation due to intercarrier XT between WDM carriers might arise. However, the analysis of intercarrier crosstalk is out of scope of this work. In all subsequent results, this optimal bandwidths pair is used, in the simulations. For the selected pair of -3 dB bandwidths, from changing $r = 0$ to $r = 0.1$, there is a degradation of around 2 dB on the receiver sensitivity.

3.8.2 Chromatic dispersion compensation

In this subsection, the impact of fiber dispersion on the performance of the optically amplified 112 Gbit/s PAM4 link is evaluated and the importance of optical dispersion compensation for

such high bit rates is demonstrated. The average signal power at the transmitter output required as a function of the length of the SM-MCF, having full dispersion compensation and full loss compensation to reach the target BER of 3.8×10^{-5} is assessed.

In this study, the maximum gain of the EDFA was defined as 30 dB, since this value enables a maximum SM-MCF length of 105.3 km, which slightly exceeds the target distances of 80 up to 100 km. The parameters used in the simulation are presented in Table 3.2.

TABLE 3.2: Simulation parameters for dispersion compensation of the optical link.

Simulation parameter	Value
SM-MCF maximum length	$L_{SM-MCF,max}$ = 105.3 km
SM-MCF CD parameter	$D_{\lambda,n}$ = 17 ps/(nm·km)
SM-MCF attenuation coefficient	α_n=0.2 dB/km
DCF chromatic dispersion parameter	$D_{\lambda,DCF}$=-100 ps/(nm·km)
DCF attenuation coefficient	α_{DCF}=0.5 dB/km
Target BER	3.8×10^{-5}
RX electrical filter bandwidth	$B_{e,RX} = 0.85 \times R_s$
RX optical filter bandwidth	$B_o = 1.6 \times R_s$

Fig. 3.6 shows the simulated SM-MCF and DCF lengths, regarding an optically amplified link with optimized PAM4 power levels, dispersion compensation and full loss compensation, for $r = 0$ and $r = 0.1$, respectively, as a function of the required transmitted signal power to achieve a target BER of 3.8×10^{-5}.

Fig. 3.6 shows that the transmitted signal power necessary to maintain the target BER increases almost linearly with the MCF length for both extinction ratios. At the total length of the MCF, the required transmitted signal power is 5.31 dBm and 7.49 dBm, respectively, for $r = 0$ and $r = 0.1$, which in comparison with the B2B situation, gives an increase of the signal power of 27.8 dB and 31.2 dB. Although not shown in this work, it was verified by simulation that without optical dispersion compensation, the eye-pattern is completely closed after 1.5 km and 1 km, respectively, $r = 0$ and $r = 0.1$, which confirms the importance of using DCFs or other dispersion compensation techniques to support the high data rate PAM4 signal transmission in longer inter-datacenter connections.

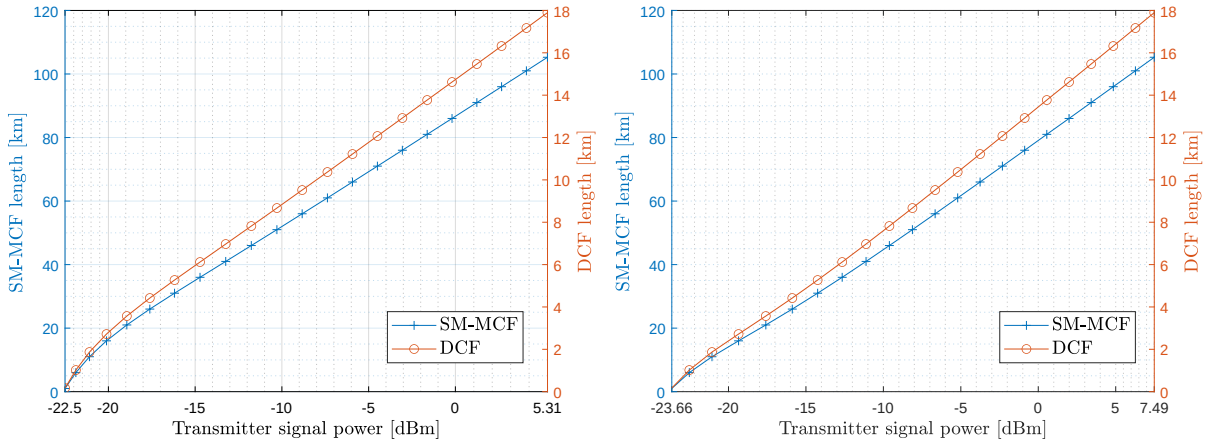

(a) $r = 0$ (b) $r = 0.1$

FIGURE 3.6: SM-MCF and DCF lengths as a function of the transmitter signal power, for a) $r = 0$ and b) $r = 0.1$, obtained by simulation for a target BER of 3.8×10^{-5}, for an optically amplified link with optimized PAM4 power levels, dispersion compensation and full loss compensation; $B_{e,RX}$=0.85×R_s and B_o=1.6×R_s.

Fig. 3.7 shows the electrical noise power, the ASE-ASE beat noise power and signal-ASE beat noise power for the symbols '0', '1', '2' and '3', L=10 km, L=40 km and L=80 km, for a) $r = 0$ and b) $r = 0.1$, at the sampling time instants t_k. From Fig. 3.7, it is possible to observe that for L=10 km and both extinction ratios, the electrical noise impacts the system performance, since its power is in the same order of the magnitude of the signal-ASE noise power for the symbols '1', '2' and '3', and clearly higher than the ASE-ASE noise power. Moreover, for $r = 0$, the electrical noise power is higher than the signal-ASE noise power of the '0' symbol, while for $r = 0.1$, it has a similar value. As the SM-MCF length increases, the ASE-ASE and signal-ASE noise powers start to increase due to the optical amplifier gain increase. For L=80 km and both extinction ratios, as shown in Fig. 3.7 e) and f), the electrical noise power contribution to the performance degradation is completely negligible and the ASE-ASE noise power is in the same order of magnitude of the signal-ASE noise power of the '0' symbol.

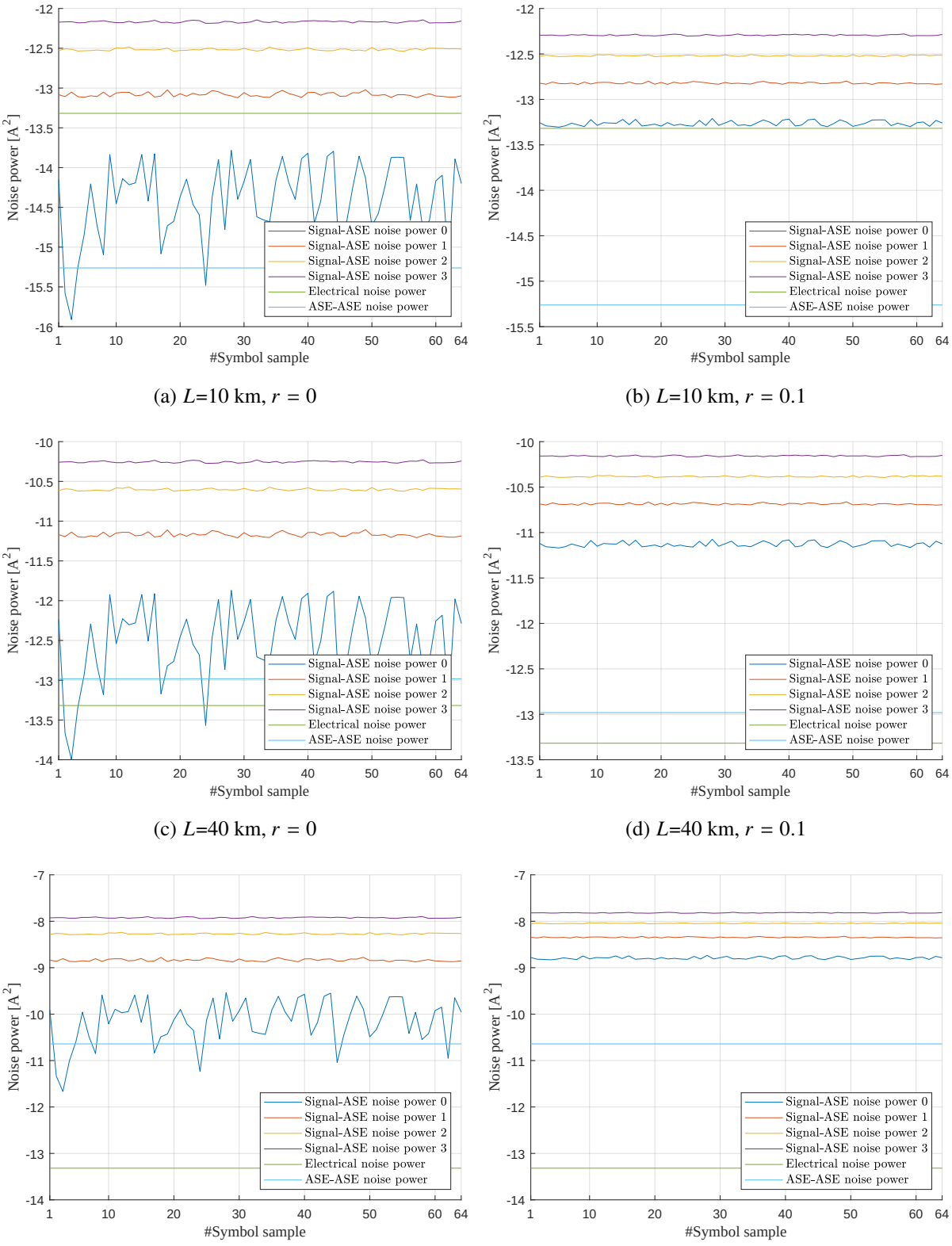

(a) L=10 km, r = 0

(b) L=10 km, r = 0.1

(c) L=40 km, r = 0

(d) L=40 km, r = 0.1

(e) L=80 km, r = 0

(f) L=80 km, r = 0.1

FIGURE 3.7: Noise powers at the decision circuit input, at the sampling time instants, for an optically amplified link with optimized PAM4 power levels, for L=10 km, L=40 km and L=80 km. The electrical noise power, the ASE-ASE noise power and the signal-ASE noise power for the symbols, '0', '1', '2' and '3' are represented.

3.9 Conclusions

In this chapter, the model of an optically amplified IM-DD inter-datacenter system was presented. The optical transmitter, the dual-polarization DCM model used to characterize the ICXT, the DCF used to compensate the chromatic dispersion, the EDFA to compensate the link losses and the DD optical receiver have been characterized. The BER estimation method was described with detail.

After presenting the system equivalent model, the electrical and optical filter bandwidths were studied in order to minimize the necessary transmitter signal power to achieve the target BER of 3.8×10^{-5} in B2B, and the achieved optimal bandwidths pair was B_o=1.6×R_s and $B_{e,RX}$=0.85×R_s. The impact of fiber dispersion introduced by increasing the SM-MCF length was studied and showed that the system would not be feasible for distances over 1.5 km without dispersion compensation. The impact of having full dispersion compensation was, then, studied and showed that optical dispersion compensation allows reaching much longer optically amplified link distances achieving the typical distances found in inter-datacenter connections. Assuming a maximum EDFA power gain of 30 dB and full dispersion compensation, the maximum SM-MCF length achieved was 105.3 km followed by a 17.9 km DCF.

The study of the ICXT impact on the transmission performance of PAM4 signals supported by MCFs is left for Chapter 4.

Chapter 4

Numerical results and discussion

In this chapter, the ICXT impact on the transmission performance of the optically amplified IM-DD inter-datacenter link with the equivalent model described in Chapter 3, is assessed and discussed. The system simulation parameters used throughout this work are presented in section 4.1. In section 4.2, the impact of ICXT on the BER and received eye-patterns is studied and analysed. In section 4.3, the OP of the PAM4 inter-datacenter link with IM-DD is investigated by varying the MCF length, skew-symbol rate product and PAM4 signal extinction ratio, for one interfering core, and, then, the OP is assessed by increasing the number of interfering cores. In section 4.4, the conclusions regarding the numerical results are presented.

4.1 System and simulation parameters

The simulation parameters used to study the optically amplified inter-datacenter link are presented in: Table 3.1, where a B2B optimized system without ICXT was studied, and except for the gain of the preamplifier which is set for perfect link loss compensation; Table 3.2, where the impact of fiber dispersion and CDC was studied; and Table 4.1, which presents the relevant parameters required to study the ICXT. The high number of PMPs is chosen to characterize the ICXT statistics rigorously [28]. Two different skew-symbol rate products (SSRPs) are analysed: i) $|S_{mn} \cdot R_s|$=1000 or $|S_{mn} \cdot R_s| \gg 1$, where the PAM4 signal symbol rate is much higher than the ICXT decorrelation bandwidth [29] and the ICXT creates amplitude levels in the received eye-pattern that seem to exhibit a "noise"-like behavior [60], and ii) $|S_{mn} \cdot R_s|$=0.01 or $|S_{mn} \cdot R_s| \ll 1$, where the PAM4 signal symbol rate is much lower than the ICXT decorrelation bandwidth [29] and well-defined amplitude levels in the eye-patterns are created due to ICXT [60].

TABLE 4.1: Simulation and system parameters.

Simulation parameter	Value
SM-MCF length	L = 10, 20, 30, 40, 50, 60, 70, 80 km
Number of PMPs	N_p = 1000
Skew-symbol rate product	$\|S_{mn}\cdot R_s\|$=1000, $\|S_{mn}\cdot R_s\|$=0.01
BER limit	3.8×10^{-3}
Target BER in the absence of ICXT	3.8×10^{-5}
Number of interfering cores with PAM4 signaling	N_c= 1, 2, 4

4.2 Impact of ICXT on the BER and received eye-pattern

In this section, the number of MCF realizations required to achieve a stabilized average BER estimate is assessed. The average BER is calculated after generating each MCF realization by averaging the BERs per MCF realization previously calculated.

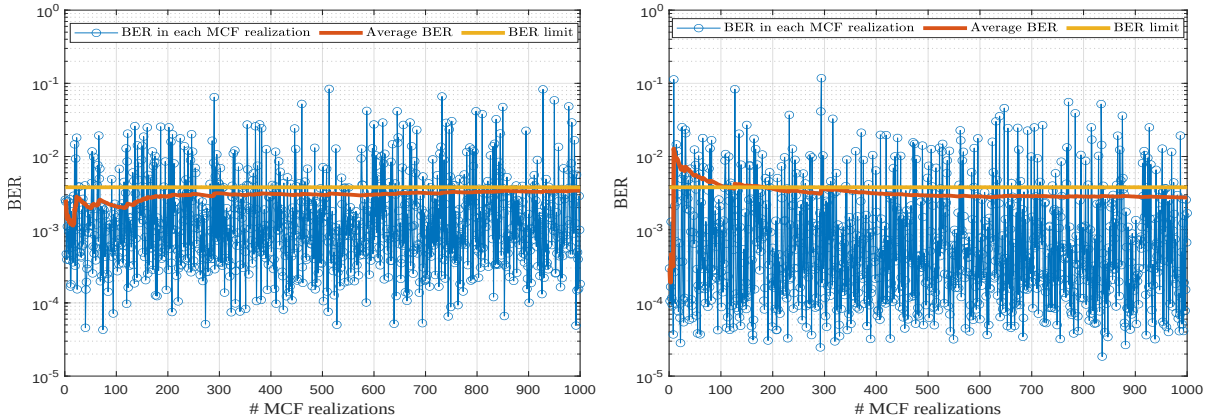

(a) $|S_{mn}\cdot R_s|$=1000, $X_c = -14$ dB (b) $|S_{mn}\cdot R_s|$=0.01, $X_c = -16$ dB

FIGURE 4.1: BER and average BER estimations per MCF realization, for an ICXT level of -14 dB and -16 dB, for $r = 0$.

Fig. 4.1 shows the BERs and average BER estimations per MCF realization, for high and low SSRP, an ICXT level of -14 dB and -16 dB and $r = 0$. Fig. 4.2 shows the BERs and average BER estimations per MCF realization, for high and low SSRP, for an ICXT level of -20 dB and $r = 0$.

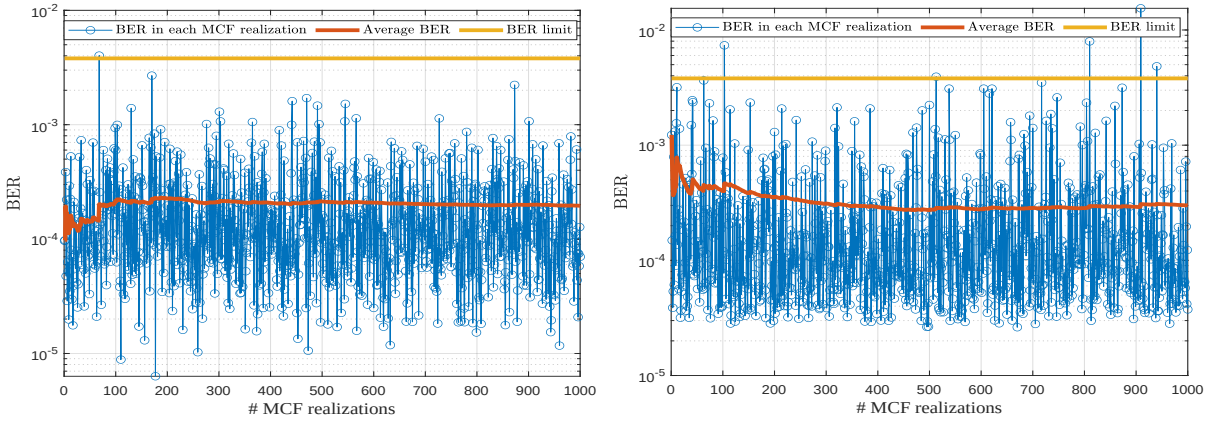

(a) $|S_{mn} \cdot R_s|$=1000 (b) $|S_{mn} \cdot R_s|$=0.01

FIGURE 4.2: BER and average BER estimations per MCF realization, for an ICXT level of -20 dB and $r = 0$.

Fig. 4.1 corresponds to a case where the ICXT level leads to an average BER near the BER limit, while in Fig. 4.2, the influence of ICXT on the performance is smaller and leads to lower average BERs. In Figs. 4.1 a) and b), after 1000 MCF realizations, the average BER is stabilized at 3.4×10^{-3} and 2.7×10^{-3}, respectively. In Fig. 4.2 a) and b), for the same number of MCF realizations, stabilized BERs of 1.95×10^{-4} and 3×10^{-4}, respectively, are achieved. Simulating 1000 MCF realizations is enough to achieve a stabilized value of the average BER, similarly to what has been concluded in [47], for OOK systems.

TABLE 4.2: Stabilized average BERs, number of simulated BERs above the BER limit and OP estimates after 1000 MCF realizations, for $r = 0$.

Fig.	Average BER	BERs above the BER limit	OP
4.1 a)	2.1×10^{-3}	187	0.187
4.1 b)	2.5×10^{-3}	145	0.145
4.2 a)	8.64×10^{-5}	1	0.001
4.2 b)	1.38×10^{-4}	5	0.005

In Table 4.2 the average BERs and OP estimates after 1000 MCF realizations, for $r = 0$, from Fig. 4.1 and Fig. 4.2 are presented. Fig. 4.1 shows that, with low SSRP and an ICXT level of -16 dB, the OP is about 0.187, while for high SSRP and an ICXT level of -14 dB, the estimated OP is around 0.145. From Table 4.2, we conclude that, with ICXT levels of -14 dB

and -16 dB, there are more occurrences of system outage, in comparison to an ICXT level of -20 dB. In Fig. 4.2 a), for low SSRP, the BER limit is exceeded more times in comparison to Fig. 4.2 b), for high SSRP. Hence, it can be infered that for high SSRP, the performance of the PAM4 inter-datacenter link is less impaired by ICXT, than for low SSRP. Moreover, in Fig. 4.1 a), a 2 dB higher ICXT level required to achieve an OP similar to the one found for low SSRP. Similar conclusions regarding the average BER have been obtained for links with 20 km, for OOK signalling on the interfered and interfering cores [47] and for PAM4 signalling in the interfered core and OOK signalling in the interfering core [11].

The results shown in Fig. 4.1 indicate that, for these ICXT levels, the average BER is kept below the BER limit. However, the BER in each MCF realization surpasses the BER limit several times, which leads to system outage. The OPs estimated in Fig. 4.1 are considerably above the typically required OP (below 10^{-4}) in optical communication systems. This demonstrates that, in these inter-datacenter links supported by MCFs: i) the OP is a more important performance metric than the average BER, and ii) it is crucial to study the OP.

The impact of the ICXT on the performance is also observable in the received eye-patterns. Fig. 4.3 shows the received eye-patterns at the decision circuit input for $r = 0$, high SSRP and an ICXT level of -14 dB, for a) the best BER (4.29×10^{-5}) and b) the worst BER (8.30×10^{-2}) per MCF realization shown in Fig. 4.1 a). Fig. 4.4 shows the received eye-patterns for $r = 0$, low SSRP and an ICXT level of -16 dB, for a) the best BER (1.85×10^{-5}) and b) the worst BER (1.175×10^{-1}) per MCF realization shown in Fig. 4.1 b). These eye patterns do not take the effect of noise (electrical or optical) into account in order to highlight the ICXT impact on the received eye-patterns.

In Fig. 4.3 b) and Fig. 4.4 b), for the worst BER, due to the severe degradation caused by ICXT, the eye is fully closed. For the best BER, Fig. 4.4 a) exhibits much more "well-defined" amplitude levels caused by ICXT than in the eye-pattern shown in Fig. 4.3 a). These "well-defined" amplitude levels are mainly in symbol transitions. There are two main reasons for this behavior: firstly, the ICXT level is 2 dB lower in Fig. 4.4 a), for low SSRP. Secondly, while low SSRP has a around one symbol in the interfering core contributing to ICXT, high SSRP has around 1000 symbols contributions. A similar behavior was observed for OOK

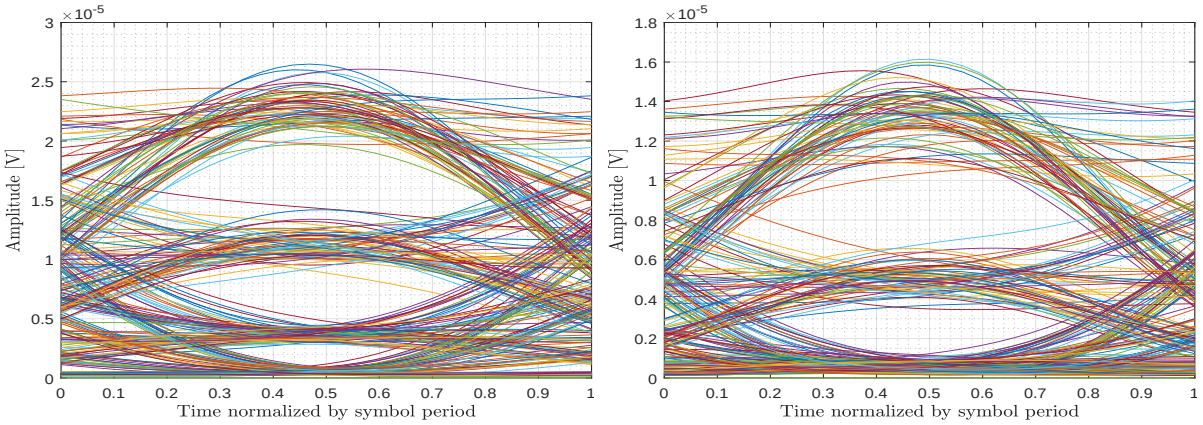

(a) BER=4.29×10^{-5} (b) BER=8.30×10^{-2}

FIGURE 4.3: Eye-patterns at the decision circuit input for high SSRP, an ICXT level of -14 dB and $r = 0$, for the best and worst BERs per MCF realization shown in Fig. 4.1 (a).

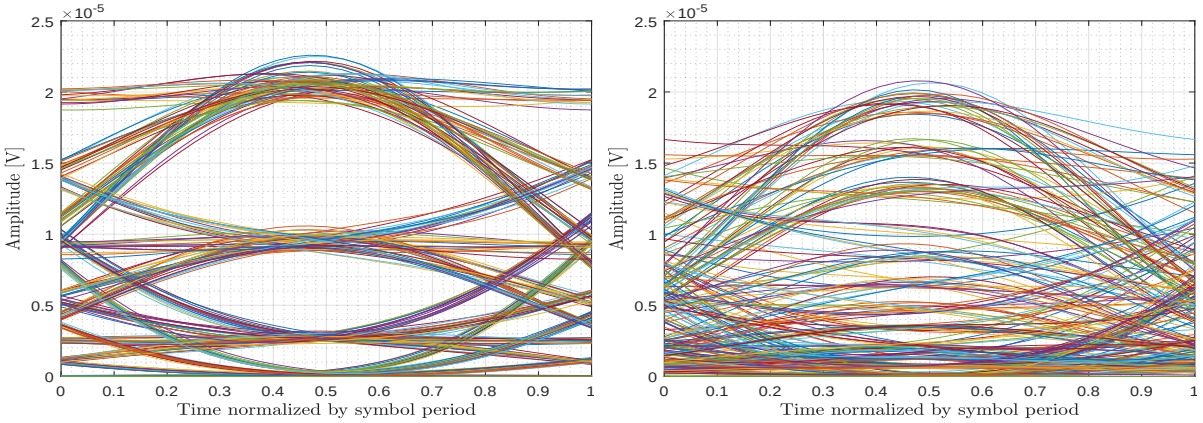

(a) BER=1.85×10^{-5} (b) BER=1.175×10^{-1}

FIGURE 4.4: Eye-patterns at the decision circuit input for low SSRP, an ICXT level of -16 dB and $r = 0$, for the best and worst BERs per MCF realization shown in Fig. 4.1 (b).

systems [47], [48], [61] and PAM4 signals transmission impaired by ICXT induced by OOK signals in the interfered core [11].

Fig. 4.5 shows the BER and average BER estimations per MCF realization, for $r = 0.1$, for a) $X_c = -12$ dB, $|S_{mn} \cdot R_s|$=1000 and b) $X_c = -14$ dB, $|S_{mn} \cdot R_s|$=0.01. Fig. 4.6 shows the BER and average BER estimations per MCF realization, for an ICXT level of -20 dB and $r = 0.1$, for a) $|S_{mn} \cdot R_s|$=1000 and b) $|S_{mn} \cdot R_s|$=0.01.

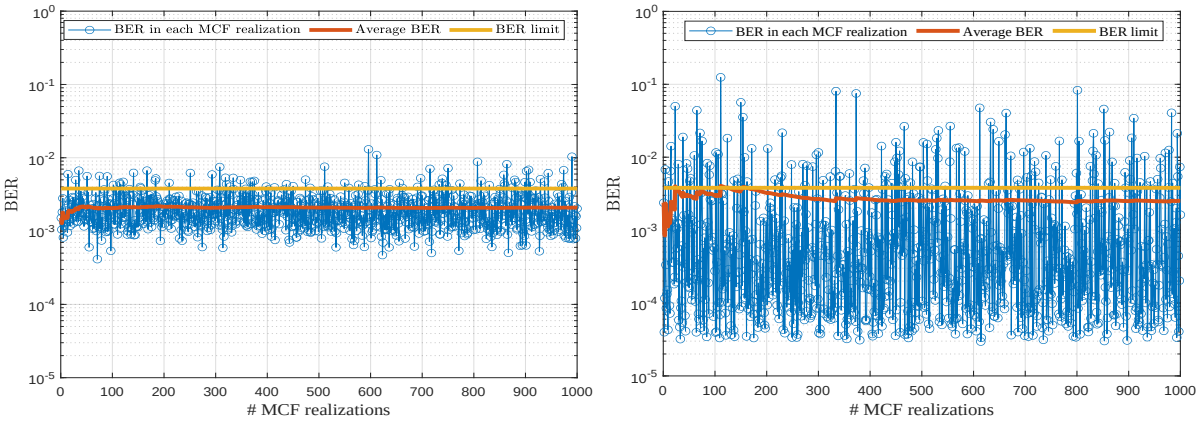

(a) $|S_{mn} \cdot R_s|$=1000, $X_c = -12$ dB (b) $|S_{mn} \cdot R_s|$=0.01, $X_c = -14$ dB

FIGURE 4.5: BER and average BER estimations per MCF realization, for $r = 0.1$.

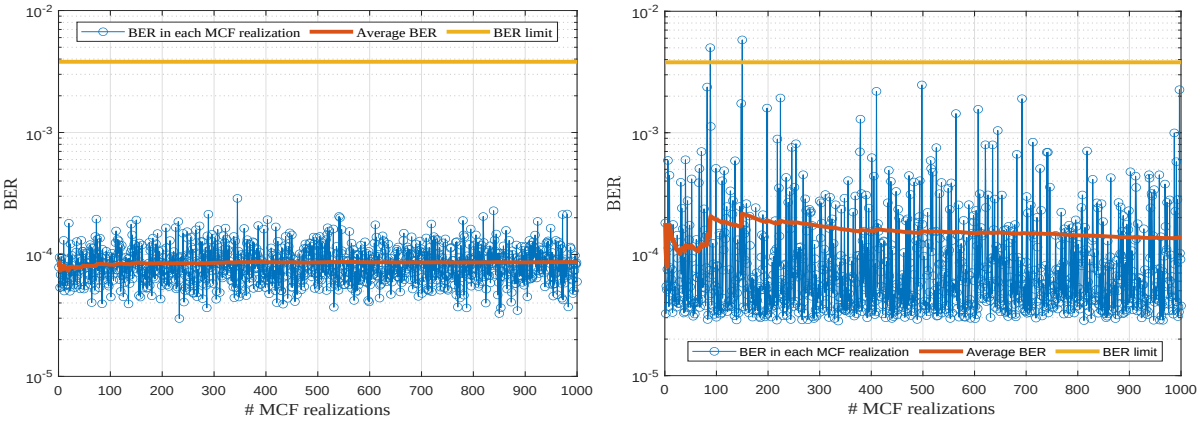

(a) $|S_{mn} \cdot R_s|$=1000 (b) $|S_{mn} \cdot R_s|$=0.01

FIGURE 4.6: BER and average BER estimations per MCF realization, for an ICXT level of -20 dB and $r = 0.1$.

TABLE 4.3: Stabilized average BERs, number of simulated BERs above the BER limit and OP estimates after 1000 MCF realizations, for $r = 0.1$.

Fig.	Average BER	BERs above the BER limit	OP
4.5 a)	2.1×10^{-3}	75	0.075
4.5 b)	2.5×10^{-3}	145	0.145
4.6 a)	8.64×10^{-5}	0	0
4.6 b)	1.38×10^{-4}	2	0.002

In Table 4.3, the average BERs and OP estimates after 1000 MCF realizations, for $r = 0.1$,

extracted from Fig. 4.5 and Fig. 4.6 are presented. In Fig. 4.5, the ICXT impact is lower, resulting in BERs more distant from the BER limit in comparison to the BERs observed in Fig. 4.2, especially in Fig. 4.6 a), where the BER limit is never exceeded, meaning that there is no outage. It is also possible to observe that, for $r = 0.1$, the BER variance is lower in comparison to $r = 0$, which might justify the lowest OP, since it is more unlikely to have BERs above the BER limit throughout the MCF realizations, for $r = 0.1$. This indicates that, the ICXT degrades less the average BER and received eye-patterns for $r = 0.1$ than for $r = 0$. Similar results regarding the influence of the extinction ratio on the ICXT impact on the performance have been observed in OOK systems [47].

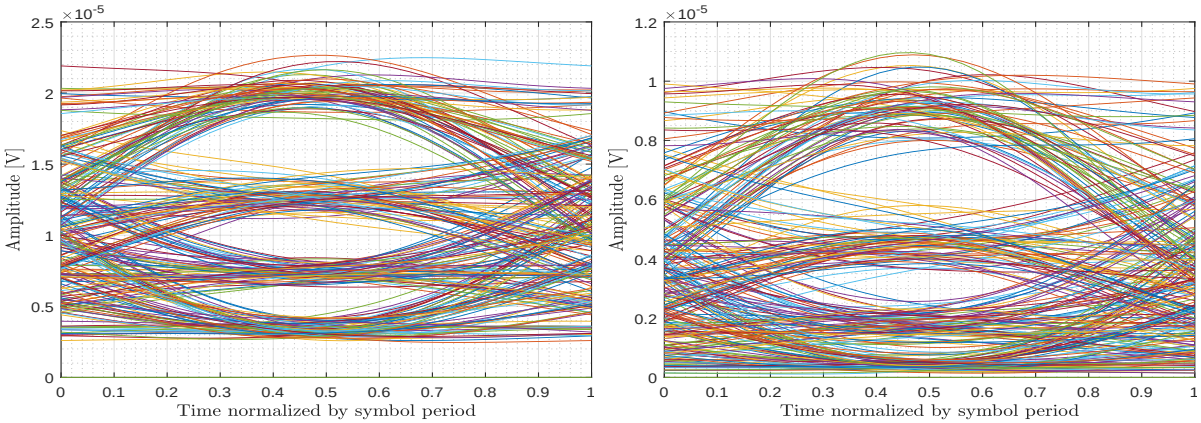

(a) BER=4.13×10^{-4} (b) BER=1.30×10^{-2}

FIGURE 4.7: Eye-patterns at the decision circuit input for high SSRP, an ICXT level of -12 dB and $r = 0.1$, for the best and worst BERs per MCF realization shown in Fig. 4.5 (a).

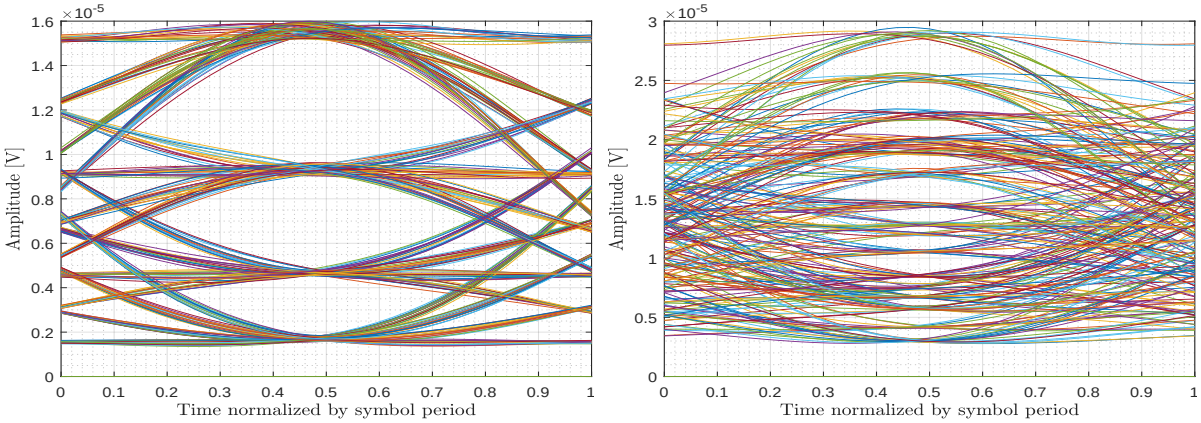

(a) BER=2.96×10^{-5} (b) BER=1.124×10^{-1}

FIGURE 4.8: Eye-patterns at the decision circuit input for low SSRP, an ICXT level of -14 dB and $r = 0.1$, for the best and worst BERs per MCF realization in Fig. 4.5 (b).

Fig. 4.7 shows the eye-patterns obtained for high SSRP, an ICXT level of -12 dB and $r = 0.1$, for a) the best BER (4.13×10^{-4}) per MCF realization and for b) the worst BER (1.30×10^{-2}) per MCF realization in Fig. 4.5 a). Fig. 4.8 shows the eye-patterns at the decision input circuit, obtained for low SSRP, an ICXT level of -14 dB and $r = 0.1$, for a) the best BER (2.96×10^{-5}) per MCF realization and for b) the worst BER (1.124×10^{-1}) per MCF realization in Fig. 4.5 b). Regardless of the extinction ratio, for high SSRP, the eye-patterns that lead to the best BERs have lower eye openings in comparison to the eye-patterns obtained for the best BERs, for low SSRP. There are two main reasons for this behavior: firstly, the ICXT level is 2 dB higher for high SSRP. Secondly, for high SSRP, the eye-patterns have much less "well-defined" amplitude levels due to ICXT in comparison to the eye-pattern found for low SSRP.

Studies regarding the power penalty due to ICXT are neglected in this work, since it was identified in other works that the power penalty metric is ineffective for the assessment of the ICXT impact on IM-DD optical systems [48], [61]. Hence, the following sections are concerned with the study of the OP, which has been identified as an essential performance metric in IM-DD optical systems impaired by ICXT [48], [61].

4.3 Outage probability

The OP is the probability of a system becoming unavailable, i.e., the probability of the BER in the presence of ICXT exceeds a given BER limit [10], [62]. In this work, the BER limit is set at 3.8×10^{-3}. In the simulation, the OP is estimated by [47]

$$OP = \frac{N_o}{N_r} \tag{4.1}$$

where N_o is the number of occurrences of BER above the BER limit and N_r is the number of simulated MCF realizations necessary to reach those occurrences. The required OP in optical communication systems is typically designed to be lower than 10^{-4} [62], [63].

4.3.1 Dependence on the MCF realizations

In this subsection, the dependence of the OP estimation on the number of MCF realizations, for low SSRP and high SSRP, for $r = 0$ and $r = 0.1$, and several ICXT levels is assessed.

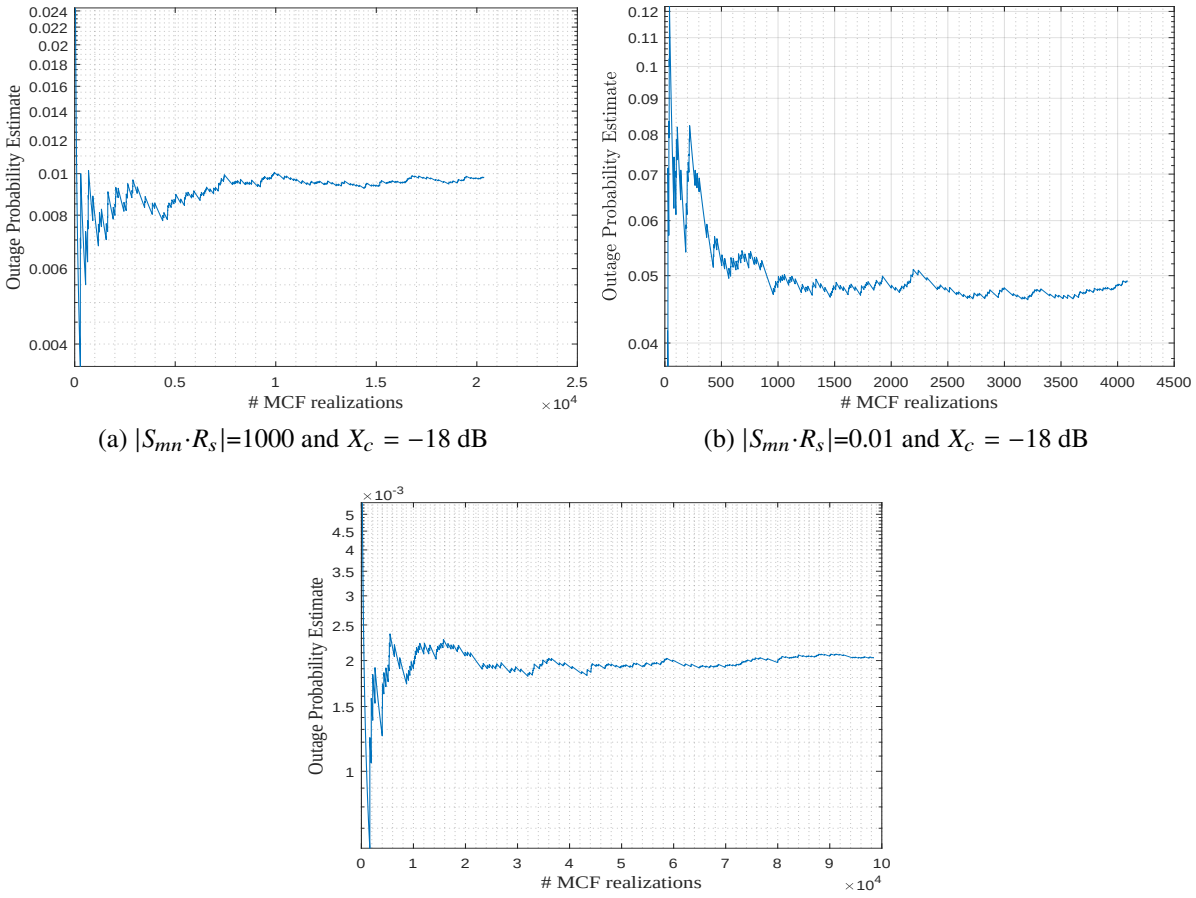

(a) $|S_{mn} \cdot R_s|$=1000 and $X_c = -18$ dB

(b) $|S_{mn} \cdot R_s|$=0.01 and $X_c = -18$ dB

(c) $|S_{mn} \cdot R_s|$=0.01 and $X_c = -22$ dB

FIGURE 4.9: Dependence of the OP estimate on the number of MCF realizations, for $r = 0$.

Fig. 4.9 shows the OP estimate dependence on the number of MCF realizations, for $r = 0$, and a) high SSRP and ICXT level of -18 dB; b) low SSRP and ICXT level of -18 dB and c) low SSRP and ICXT level of -22 dB. In this work, to estimate the OP, the BER is obtained per MCF realization and the simulation is stopped when the number of occurrences of BER above the BER limit reaches 200. In Figs. 4.9 a) and b), it can be seen that for the same ICXT level and extinction ratio, a higher number of MCF realizations is required to reach 200 occurrences of BER above the BER limit, with high SSRP in comparison to low SSRP, since the OP with high SSRP is about $1{\times}10^{-2}$ and is lower than the OP of about $5{\times}10^{-2}$ obtained for low SSRP.

In Figs. 4.9 a) and c), the number of MCF realizations to reach 200 BER occurrences above the BER limit is more than five times higher than in Fig. 4.9 b). In Figs. 4.9 a) and c), the oscillations of the OP estimates tend to diminish and stabilize above 10^{-4} MCF realizations, while in Fig. 4.9 b), the stabilization is reached after about 4000 realizations. Notice that in Fig. 4.9 c), the number of MCF realizations is considerably higher in comparison to Fig. 4.9 a) and b), due to the lower OP (about one order of magnitude) that must be estimated. In Fig. 4.9, it is observable that the required number of MCF realizations to estimate the OP with enough accuracy only depends on the order of magnitude of the OP, similarly to what has been shown in other works, for PAM4 and OOK signalling [10], [47], [48].

In Appendix B, it is concluded that 200 occurrences of BER above the BER limit, are more than enough to achieve a stabilized estimate of outage probability. Thus, in the remainder studies regarding the OP, 200 occurrences are considered. The simulation results presented in this work only reach OPs around 10^{-4} because lower OPs are computationally heavy to achieve using computer simulation. To achieve an OP of 10^{-4} with 200 BER occurrences above the BER limit, around 2 million MCF realizations are required. As the estimation of the BER for one MCF realization takes around 0.6 seconds, around 2 weeks of simulation, in a 16 GB RAM with a 3.2 GHz processor are necessary to reach such low OPs. Similarly, for an OP of 10^{-6}, it would be necessary around 200 weeks. Therefore, to achieve such low OPs, we have performed a cubic interpolation and extrapolation of $\log_{10}(\text{OP})$, similarly to what has been done in [11], [47].

4.3.2 Dependence with one interfering core

In this subsection, we assess the OP for one interfering core, an inter-datacenter link with 10 km, low and high SSRPs and $r = 0$ and $r = 0.1$.

Fig. 4.10 shows the dependence of the OP on the ICXT level, for $r = 0$ and $r = 0.1$, for low SSRP and high SSRP. It is possible to observe that, with high SSRP, a higher crosstalk level is acceptable to achieve the same OP as with low SSRP, regardless of the extinction ratio. Hence, this indicates that, for high SSRP the system is more robust to outage in comparison to low SSRP, similarly to what has been observed in [10], [47], [48] for OOK signalling and also for intra-datacenter links with PAM4 signalling in the interfered core and OOK signalling in

the interfering cores [61]. By comparing $r = 0$ with $r = 0.1$, the lower extinction ratio presents higher OPs for the same crosstalk level, for both SSRPs, similarly to what has been shown in other works [47], [61].

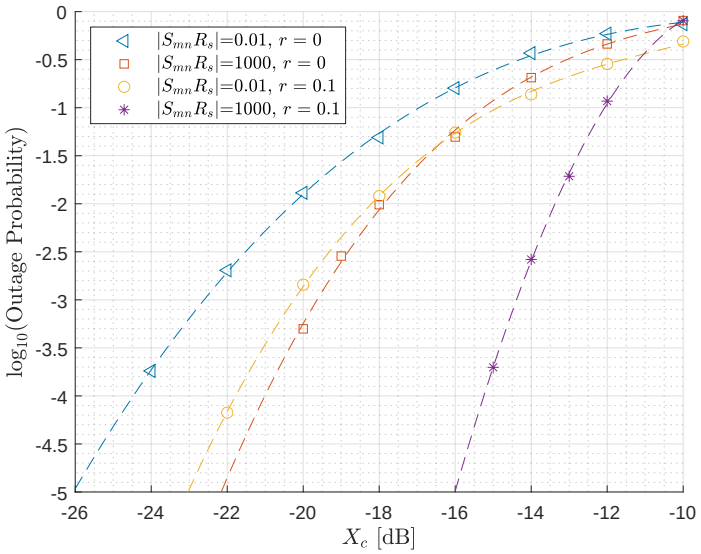

FIGURE 4.10: Dependence of the OP on the ICXT level, extinction ratio and SSRP. The dashed lines represent a cubic interpolation of $\log_{10}$(OP).

The ICXT levels that lead to an OP= 10^{-4} for each inter-core skew and extinction ratio combination, obtained in Fig. 4.10, for one interfering core, are presented in Table 4.4. By comparing with unamplified OOK systems [47], [48], optically amplified PAM4 IM-DD systems with full loss and CDC tolerate a lower acceptable ICXT level to achieve the same OP. The ICXT levels that lead to an OP of 10^{-4} in OOK optical systems with $r = 0$, are around $X_c = -20$ dB for an inter-core skew comparable with high SSRP and $X_c = -23$ dB for an inter-core skew comparable with low SSRP [10], [47]. As can be seen in Table 4.4, in inter-datacenter links with PAM4 signaling, the ICXT level that leads to the same OP is $X_c = -21$ dB, for high SSRP and $X_c = -24.5$ dB for low SSRP, which are 1 dB and 1.5 dB lower, respectively, than in OOK systems. For an intra-datacenter link with PAM4 signalling in the interfered core and OOK signalling in the interfering cores [61], for low SSRP and high SSRP and $r = 0$, the ICXT levels of -31.5 dB and -28 dB, respectively, lead to an OP of 10^{-4}. For $r = 0.1$ and low and high SSRPs, the ICXT levels that lead to the same OP are -31.8 dB and -26.5 dB, respectively. In this case, the intra-datacenter link is very short (only 2 km) and the enhanced distortion of the 112 Gbit/s PAM4 signal caused by the chromatic dispersion is not compensated contrarily to

the case of the PAM4 system with the OP results shown in Fig. 4.10. Hence, even in the absence of ICXT, the received eye-pattern is much more closed and the system margin to any additional degradation is much lower. This may explain the reduced tolerance to ICXT of the system studied in [61], which for $r = 0$ and $r = 0.1$ exhibits, respectively, maximum acceptable ICXT levels exceeding 7 dB and 10 dB lower in comparison to the ICXT levels observed in Fig. 4.10.

TABLE 4.4: ICXT level to achieve an OP of 10^{-4}, with one interfering core.

$\lvert S_{mn}R_s \rvert$	r	X_c [dB]
0.01	0	-24.5
0.01	0.1	-21.9
1000	0	-21
1000	0.1	-15.3

4.3.3 Dependence on the SM-MCF length

In this subsection, we analyse the dependence of the OP on the SM-MCF length, and consequently, on the noise type dominance, i.e., electrical noise dominance or ASE noise dominance, for low SSRP and high SSRP, $r = 0.1$, and several ICXT levels.

The DCF length is also extended with respect to the SM-MCF length in order to achieve a perfect CDC. In this study, we aim to analyse the effect of the ICXT on these environments. Therefore, the ICXT level is set constant for each fiber length, i.e., the ICXT level is considered independent from the SM-MCF length.

Fig. 4.11 shows the OP dependence on the ICXT level, for a) $|S_{mn} \cdot R_s|$=0.01 and b) $|S_{mn} \cdot R_s|$=1000, for $r = 0.1$ and L=10 km, L=40 km and L=80 km. In Fig. 4.11 a), it is possible to observe that for low SSRP, the crosstalk level required to achieve the same OP=10^{-4} increases slightly, less than 0.5 dB, with the SM-MCF length increase.

In Fig. 4.11, for high SSRP, longer SM-MCF lengths lead to an increased tolerance to ICXT, while for low SSRP, the ICXT tolerance is not significantly affected by the SM-MCF length. This means that, for high SSRP, the difference between the dominance of signal-ASE

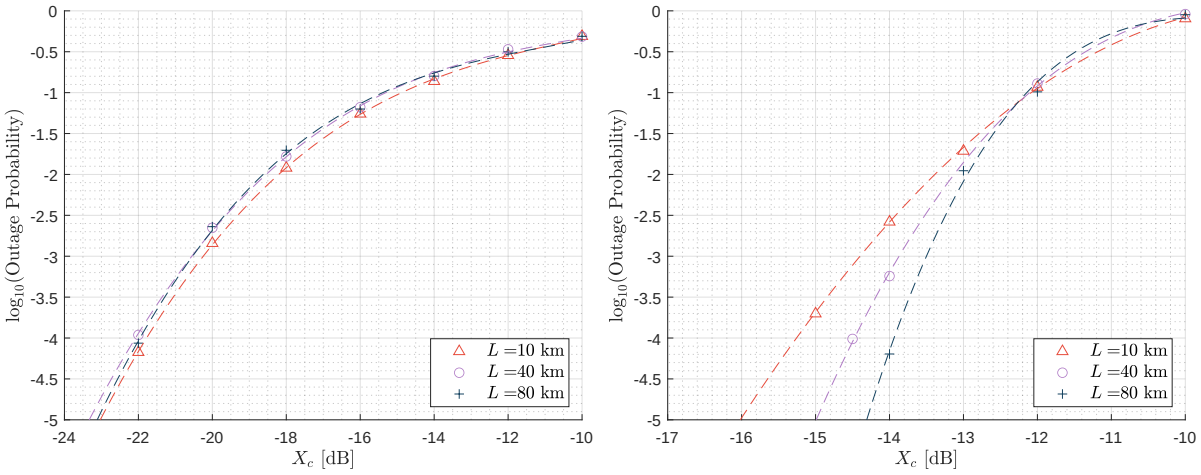

(a) $|S_{mn} \cdot R_s| = 0.01$ (b) $|S_{mn} \cdot R_s| = 1000$

FIGURE 4.11: Dependence of the OP on the ICXT level, for low and high SSRPs and $r = 0.1$. The dashed lines represent a cubic interpolation of $\log_{10}$(OP).

beat noise on the performance, for 80 km, and the enhanced contribution of electrical noise to the performance, for 10 km, may influence the tolerance to ICXT. For low SSRP, the tolerated ICXT level is not particularly affected by the different noise regimes.

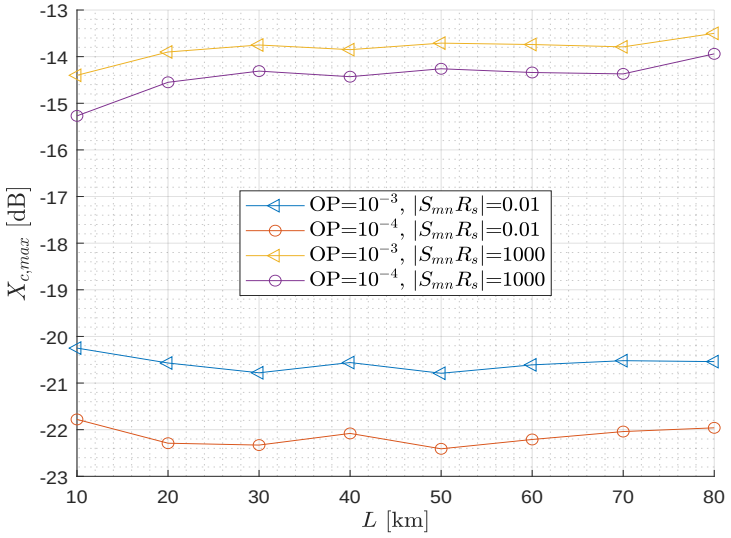

FIGURE 4.12: Dependence of the maximum acceptable ICXT level required to achieve the OP=10^{-3} and OP=10^{-4} on the SM-MCF length, for different SSRPs and $r = 0.1$.

Fig. 4.12 shows the dependence of the maximum acceptable ICXT level required to achieve the OP=10^{-3} and OP=10^{-4} on the SM-MCF length, for low SSRP and high SSRP, for $r = 0.1$, and for SM-MCF lengths from 10 km to 80 km. In Fig. 4.12, only for the SM-MCF lengths of 10, 40 and 80 km, the OPs obtained by simulation reach values between 10^{-3} and 10^{-4}, as shown

in Fig. 4.11. For the other SM-MCF lengths, the simulation has been performed only to get OPs that reach around $10^{-2.5}$. The OPs of 10^{-3} and 10^{-4} have been estimated by extrapolation after the interpolation of the simulation results. Fig. 4.12 confirms the conclusions taken from Fig. 4.11 for other SM-MCF lengths.

In Fig. 4.12, for low SSRP, the ICXT level required to achieve an OP=10^{-4} increases slightly less than 0.5 dB, with the SM-MCF length increase. For high SSRP, the maximum acceptable ICXT level required to achieve the OP=10^{-4} increases with the MCF length increase, showing a 0.8 dB and 1.4 dB enhancement from 40 km and 80 km, respectively, to 10 km. For 80 km and to achieve an OP of 10^{-4}, the maximum acceptable ICXT level is around 8.1 dB higher for high SSRP in comparison to low SSRP. The way dispersion from the MCF and DCF affects the ICXT mechanism for the different link lengths might provide some explanation for these results. Even though, for an OP of 10^{-4}, the maximum acceptable ICXT level shows only a variation not exceeding 1.4 dB with the increase of the MCF length.

4.3.4 Dependence on the inter-core skew

The impact of ICXT on the performance of OOK and intra-datacenter PAM4 communication systems with IM-DD has been shown to be very dependent on the SSRP [26], [61]. In this section, the dependence of the OP on the SSRP is assessed with more detail, for a SM-MCF length of 80 km, $r = 0.1$ and one interfering core.

Fig. 4.13 shows the OP dependence on the SSRP, for various ICXT levels. For SSRP $\ll 0.1$, the ICXT is highly correlated along the signal bandwidth [26], [29], only one PAM4 symbol is contributing to ICXT, and the ICXT behaves as static coupling [29]. Hence, the ICXT effect is enhanced and the highest OP is reached for all ICXT levels studied. For SSRP $\gg 100$, the ICXT is decorrelated along the signal bandwidth [29] and several PAM4 symbols are contributing to ICXT, leading to a similar "noise"-like behaviour [29]. Hence, a significant decrease of the OP is observed [10], [47], reaching a minimum for very high SSRP. For intermediate values of SSRP, a transition between the two ICXT behaviours is observed, similarly to what has been reported in [10], when studying the variance of the short-term average ICXT power. In Fig. 4.13, it is also possible to observe that, for an ICXT level of -12 dB, increasing the SSRP results in an OP

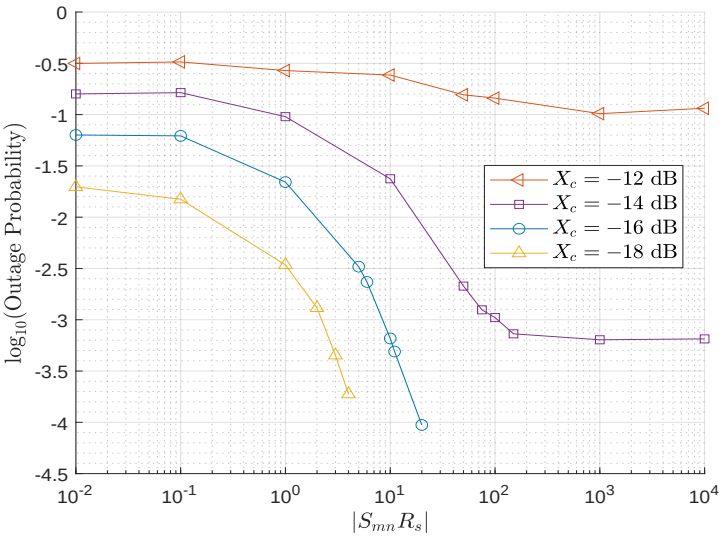

FIGURE 4.13: Dependence of the OP on the SSRP for $r = 0.1$, L=80 km and one interfering core, and X_c=-12 dB, -14 dB, -16 dB and -18 dB.

improvement of less that one order magnitude, while for lower ICXT levels, the OP improves various orders of magnitude with the SSRP increase. These results show that, for high SSRP, the OP has less improvements when the link is impaired by higher ICXT levels, similarly to what has been concluded in [10], for an OOK system.

4.3.5 Dependence on the number of interfering cores

All preceding studies concerning the OP have only considered one interfering core with PAM4 signalling. However, in a MCF, the ICXT may result from the contributions of various interfering cores [13]. In a weakly-coupled MCF, there are typically under 8 interfering cores with a significant contribution to the ICXT on one particular interfered core, which are typically the neighbouring cores to the interfered core [64]. In this subsection, the OP is assessed for 1, 2 and 4 interfering cores, for L=80 km, where signal-ASE beat noise is dominant over electrical noise, for $r = 0$ and $r = 0.1$, for $|S_{mn} \cdot R_s|$=0.01 and $|S_{mn} \cdot R_s|$=1000. In the Matlab simulator, each interfering core signal is generated independently from the other interfering cores using Eq. 3.6.

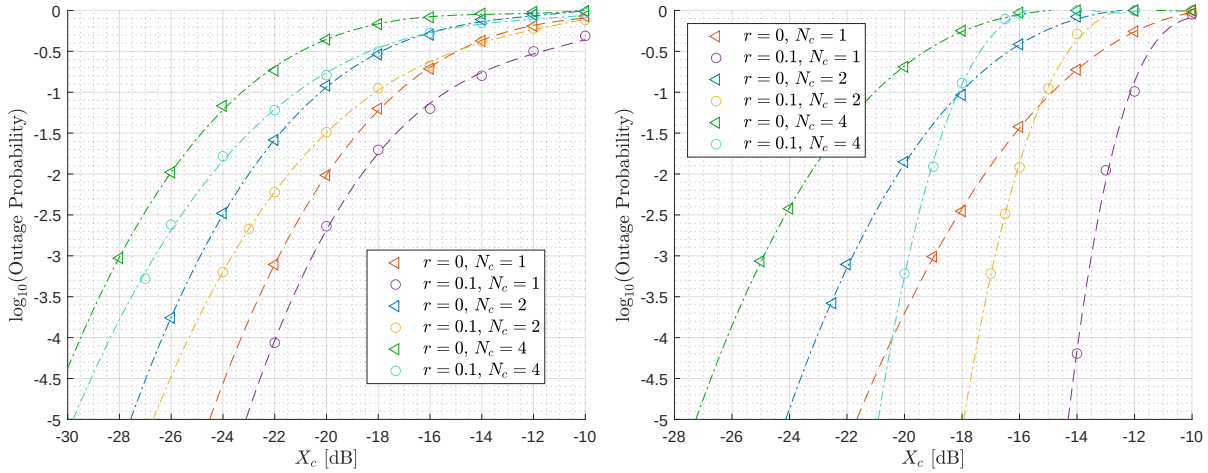

(a) $|S_{mn} \cdot R_s| = 0.01$ (b) $|S_{mn} \cdot R_s| = 1000$

FIGURE 4.14: Dependence of the OP on the ICXT level per interfering core, SSRP and extinction ratio, for 1, 2 and 4 interfering cores with PAM4 signalling. The dashed lines represent a cubic interpolation of $\log_{10}$(OP).

Fig. 4.14 shows the dependence of the OP on the ICXT level per interfering core, extinction ratio and SSRP, for N_c=1, N_c=2 and N_c=4. It is possible to observe that, for both SSRPs, increasing the number of interfering cores from 1 to 2 and 4 results in an increase of the OP for all presented ICXT levels, regardless of the extinction ratio, due to the higher number of interfering terms contributing to ICXT. Fig. 4.14 shows an above 6 dB enhanced tolerance to ICXT, for systems with high SSRP, when comparing $r = 0.1$ with $r = 0$, for all the different cases of interfering cores. For low SSRP, the ICXT tolerance is not so significantly affected by the extinction ratio variation. Furthermore, Fig. 4.14 indicates that, the OP degradation with the increasing number of cores is similar, for both SSRPs.

The ICXT levels that lead to an OP=10^{-4}, for each inter-core skew and extinction ratio combination, extracted from Fig. 4.14, for N_c=1, N_c=2 and N_c=4, are presented in Table 4.5. In Table 4.5, it is possible to observe that, doubling the number of cores, i. e., from 1 to 2 and from 2 to 4, for $r = 0$ and $r = 0.1$, and to achieve an OP of 10^{-4}, an ICXT level reduction between 2.9 dB and 3.5 dB is observed, which is not much dependent on the extinction ratio or on the SSRP regime. For an intra-datacenter link with PAM4 signalling in the interfered core and OOK signalling in the interfering cores [61], for high SSRP, for $r = 0$, the ICXT levels reduce around 3.8 dB, from 1 to 2 and from 2 to 4 interfering cores, in order to achieve the same

OP, which is not much different from our results. However, for $r = 0.1$, from 1 to 2 interfering cores, the ICXT levels to achieve the same OP practically do not exhibit degradation, which is counterintuitive, while from 2 to 4 interfering cores, the maximum acceptable ICXT level reduces 3.5 dB [61].

TABLE 4.5: Maximum acceptable ICXT level (dB) required per interfering core to achieve the OP=10^{-4}, with a L=80 km.

$\lvert S_{mn}R_s \rvert$	r	N_c=1	N_c=2	N_c=4
0.01	0	-23.3	-26.5	-29.5
0.01	0.1	-22	-25.4	-28.7
1000	0	-20.2	-23.2	-26.1
1000	0.1	-13.9	-17.4	-20.3

4.3.6 Dependence on the inter-core skew of multiple interfering cores

In subsection 4.3.5, all the interfering cores had the same inter-core skew. In this subsection, the OP is assessed for L=80 km, for $r = 0$ and $r = 0.1$, for 2 interfering cores, in which, one core has low SSRP and the other core has high SSRP, which may be thought as a heterogeneous fiber situation. Weakly-coupled MCFs with cores with substantially different skews can be found in practice [29], [65].

Fig. 4.15 shows the dependence of the OP on the ICXT level, for L=80 km, for 2 interfering cores, with the same SSRP and with different SSRP, for a) $r = 0$ and b) $r = 0.1$. It is possible to observe that, having 2 interfering cores with different SSRP, leads to an intermediate situation, in comparison to having both cores with low SSRP or high SSRP. When using different SSRP for each core, the maximum acceptable ICXT level required to achieve the OP=10^{-4}, is 2 dB higher and 1.5 dB lower, for $r = 0$, and 2.5 dB higher and 5.3 dB lower, for $r = 0.1$, in comparison to having both cores with low SSRP or high SSRP, respectively. Fig. 4.15 shows that, especially for $r = 0.1$, the effect of having only one core with low SSRP is enough to induce a severe degradation of the maximum acceptable ICXT level for a specific OP, even if the other interfering cores have a small contribution to the maximum acceptable ICXT level, as in the case of high SSRP.

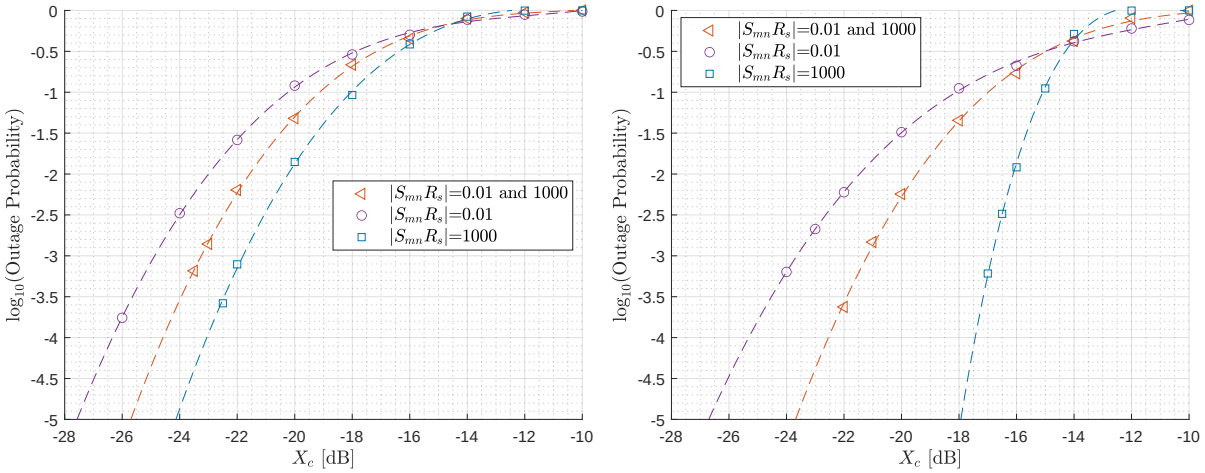

(a) $r = 0$ (b) $r = 0.1$

FIGURE 4.15: Dependence of the OP on the ICXT level per interfering core and extinction ratio, for L=80 km, 2 interfering cores, with the same SSRP and with different SSRP. The dashed lines represent a cubic interpolation of $\log_{10}$(OP).

4.4 Conclusions

Throughout this chapter, the impact of ICXT on an optically amplified IM-DD inter-datacenter system with full loss and dispersion compensation has been studied through MC simulation by assessing the average BER, eye-pattern degradation and OP.

We have shown that, 1000 MCF realizations are more than enough to achieve stabilized average BERs and that the OP is an essential metric to study IM-DD systems supported by MCFs and impaired by ICXT. It has been shown that, for $r = 0.1$, the ICXT degrades less the average BER and received eye-patterns than for $r = 0$.

The OP of the optically amplified PAM4 IM-DD system has been assessed more in-depth. It has been shown that the number of MCF realizations required to estimate the OP with sufficient accuracy depends mainly on the order of magnitude of the OP. For one interfering core and an OP of 10^{-4}, the maximum acceptable ICXT level is around 3.1 dB and 8.1 dB higher for high SSRP in comparison to low SSRP, for $r = 0$ and $r = 0.1$, respectively. These results allow concluding that for high SSRP, the system is more tolerant to the ICXT than for low SSRP. Also, it has been shown that, for high SSRP, a non-ideal extinction ratio tolerates a higher ICXT level of about 6 dB in comparison with null extinction ratio, while, for low SSRP, the ICXT

tolerance is not significantly affected by the extinction ratio variation. Comparing to links with 20 km, for OOK signalling on the interfered and interfering cores [47], for high and low SSRPs, a lower ICXT level around 1 dB and 1.5 dB, respectively, is tolerated. Also, comparing to an 112 Gb/s intra-datacenter 2 km link with PAM4 signalling in the interfered core and OOK signalling in the interfering cores, for high SSRP, a lower ICXT level of less than 10.5 dB is required to achieve the OP of 10^{-4} in comparison to the PAM4 system analyzed in this work. The OP has also been studied considering the variation of the MCF length with the ICXT level independent from the MCF length, from 10 km, where electrical noise significantly contributes to the performance degradation, to 80 km, where signal-ASE beat noise is dominant, and the maximum acceptable ICXT level for an OP=10^{-4}, varies only 1.4 and 0.2 dB, respectively, for high SSRP and low SSRP.

The OP dependence was studied also for multiple interfering cores. It has been shown that, by doubling the number of interfering cores, the maximum acceptable ICXT level per interfering core to reach the same OP decreases nearly 3 dB and 3.5 dB, for $r = 0$ and $r = 0.1$, respectively. Also, having two interfering cores with different SSRP, leads to an intermediate situation regarding the maximum acceptable ICXT level to achieve an OP of 10^{-4}, in comparison to having both cores with high SSRP or low SSRP. For $r = 0$, the maximum acceptable ICXT level is 2 dB higher and 1.5 dB lower, in comparison to having both cores with low SSRP or high SSRP, respectively. For $r = 0.1$, the maximum acceptable ICXT level is 2.5 dB higher and 5.3 dB lower, in comparison to having both cores with low SSRP or high SSRP, respectively. Therefore, having one core with low SSRP is enough to induce a severe degradation of the maximum acceptable ICXT level for a specific OP, even if the other interfering cores have a small contribution to ICXT, as in the case of high SSRP.

Chapter 5

Conclusions and future work

In this chapter, the final conclusions and some suggestions for future work are presented.

5.1 Final conclusions

The impact of ICXT on the transmission performance of PAM4 signals in optically amplified IM-DD inter-datacenter links with full CD and loss compensation has been assessed by numerical simulation. In chapter 2, a literature review of the most important concepts related to this work has been presented: datacenters architecture and signal transmission, optical fibers (namely, multicore fibers and ICXT), and a review of works that studied PAM4 transmission in MCFs.

In chapter 3, the system equivalent model of the optically amplified PAM4 inter-datacenter link developed to study the ICXT impairment has been presented. This system equivalent model is composed by: the optical transmitter, the dual-polarization DCM that characterizes the ICXT, the DCF used to fully compensate the chromatic dispersion, the EDFA used to fully compensate the link losses, the optical filter, the DD optical receiver composed by a PIN photo-detector and an electrical filter. The method for average BER assessment using MC simulation combined with a semi-analytical technique has been also described. The validation of the BER assessment in the absence of ICXT has been performed by achieving a good agreement between the BER estimated analytically with the BER estimated through Matlab simulation, in a B2B configuration, including both signal-ASE and ASE-ASE beat noises.

In chapter 4, the impact of ICXT on the performance of the optically amplified IM-DD inter-datacenter system has been studied and discussed.

We have shown that 1000 MCF realizations are more than enough to obtain stabilized average BERs and that is essential to study the OP in IM-DD systems supported by MCFs impaired by ICXT. It has also been shown that for $r = 0.1$, the ICXT degrades less the average BER and received eye-patterns than for $r = 0$.

The OP of the optically amplified PAM4 IM-DD inter-datacenter link with full loss and CDC system has been assessed more in-depth. It has been concluded that 200 occurrences of BER above the BER limit, are more than enough to achieve an OP of the optical link with very small fluctuations.

The OP for one interfering core has been assessed. It has been shown that, for one interfering core and an OP of 10^{-4}, the maximum acceptable ICXT level is around 3.1 dB and 8.1 dB higher for high SSRP in comparison to low SSRP, for $r = 0$ and $r = 0.1$, respectively. We have also shown that, by comparison with results presented in other works in the literature, fully loss and dispersion compensated PAM4 systems with DD are less affected by ICXT in comparison to unamplified 20 km IM-DD systems with OOK signalling in both interfered and interfering cores and 2 km unamplified systems with PAM4 in the interfered core and OOK signalling in the interfering core. It has also been shown that, with full dispersion compensation and with the ICXT level independent from the MCF length, the maximum acceptable ICXT level for an OP of 10^{-4}, varies only 1.4 and 0.2 dB, respectively, for high SSRP and low SSRP, for a SM-MCF length varying from 10 to 80 km.

The dependence of the OP on the number of interfering cores was also assessed. It has been shown that, regardless of the extinction ratio, by doubling the number of interfering cores, the maximum acceptable ICXT level per interfering core to reach the same OP decreases around 3 dB. This ICXT level dependence on the number of interfering cores is similar to the one found in an 2 km unamplified intra-datacenter link with PAM4 signalling in the interfered core and OOK signalling in the interfering cores [61]. Finally, we have shown that, in case of multiple interfering cores, having a single core with low SSRP is enough to induce a severe reduction of the maximum acceptable ICXT level.

5.2 Future work

In the following, some future work proposals are presented:

• Assess the performance of the PAM4 system by considering electronic equalization of CD after the optical receiver instead of optical dispersion compensation;

• Proposal and analysis of ICXT mitigation techniques, for example, relying on artificial intelligence techniques [66], to reduce the impact of ICXT on the performance of datacenters interconnects;

• Study, more in-depth, the influence of electrical noise and ASE noise dominance, on the ICXT impairment and its effect on the transmission performance degradation;

• Investigation of higher-order PAM signals transmission to increase datacenter links capacity.

Appendices

Appendix A

Optically amplified link system model validation

This appendix shows the validation of the system model for a non-optically amplified and for an optically amplified link considering signal-ASE and ASE-ASE beat noises, and by neglecting signal distortion. Two different links are used for validation. Firstly, a non-optically amplified link with PAM4 signal equispaced levels is used for validation. Secondly, an optically amplified link considering two different possibilities for the transmitted PAM4 signal, one with equispaced power levels and other with optimized power levels is also validated. Validations are first performed in a back-to-back (B2B) configuration. To perform these validations, without signal distortion and ICXT, it is necessary to have an agreement between the simulated and theoretical BERs, obtained in a B2B configuration, with null ISI and ASE noise and electrical noise modelled as additive white Gaussian noises.

In the following simulations for both non-optically amplified and optically amplified systems, in order to validate the system equivalent model and the BER method estimation, there are always two distinct simulation environments. Firstly, in the simulation, the transmitter electrical filter is not taken into account, and the receiver electric filter bandwidth, $B_{e,RX}$, is set to $1.2\times R_s$ to avoid signal distortion due to filtering. These two parameters are used in order to avoid introducing ISI in the system. After this validation, the Bessel filter at the transmitter is introduced in the simulation model with a bandwidth of $B_{e,TX}=R_s$. The parameters used in the system validation are presented in Table 3.1, where the optimized system without ICXT was studied and Table A.1. Notice that the selected value for B_o in these validations is considerably larger in comparison with the signal bandwidth, which results in an enhanced ASE noise power in the link.

TABLE A.1: Simulation parameters in a B2B situation for the system validation.

Simulation parameter	Value
RX electrical filter bandwidth	$B_{e,RX} = 1.2 \times R_s$, R_s, $0.75 \times R_s$
Optical filter bandwidth	B_o=320 GHz

A.1 Non-optically amplified link

The BER theoretical expression for a non-amplified link with PAM4 equispaced levels signal transmission in a B2B configuration is given by [53]

$$BER_{theo} = \frac{3}{4} Q\left(\frac{1}{3} \cdot \frac{1-r}{1+r} \cdot \frac{P_{av}}{\sigma_c}\right) \tag{A.1}$$

where P_{av} corresponds to the received signal average power at the optical preamplifier input in a B2B configuration, which is given by Eq. (3.2).

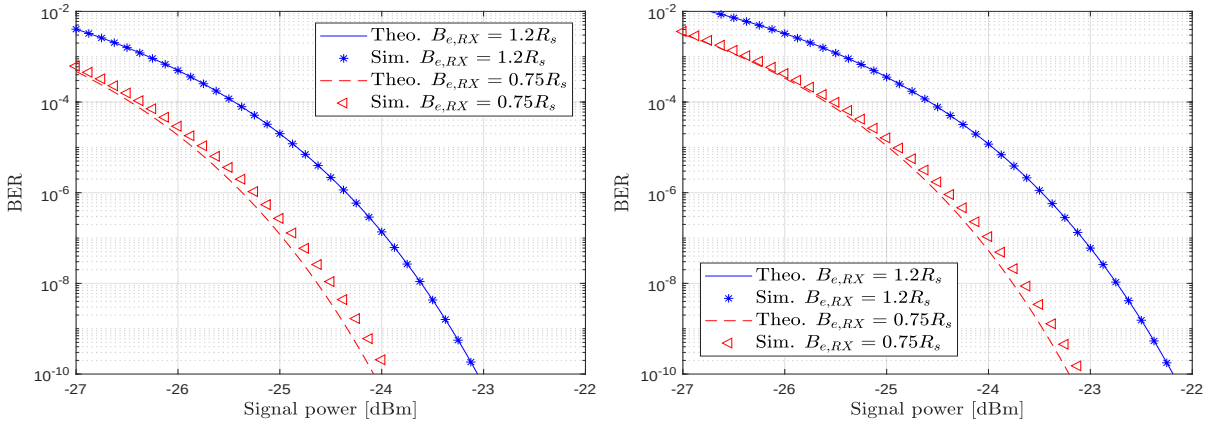

(a) $r = 0$ (b) $r = 0.1$

FIGURE A.1: Dependence of the BER on the receiver sensitivity, in a B2B configuration, for $B_{e,RX}$=1.2×R_s and $B_{e,RX}$=0.75×R_s for a non-amplified link with equispaced PAM 4 power levels. The theoretical BERs obtained from Eq. A.1 are also shown.

Fig. A.1 shows the theoretical and simulated BERs dependence on the receiver sensitivity and extinction ratio, for a non-amplified link with equispaced levels on the PAM4 signal, respectively, for L=0 km (B2B configuration), for $B_{e,RX}$=1.2×R_s and $B_{e,RX}$=0.75×R_s. It can

be observed that the simulated BERs for a B2B configuration and $B_{e,RX}$=1.2×R_s are in total agreement with the theoretical BER, given by (A.1), which validates the implementation of the simulator without ISI and in presence of electrical noise. Due to the ISI introduced by the electrical filtering, for $B_{e,RX}$=0.75×R_s, the simulation results deviate slightly from the theoretical BERs. For a reference BER of 3.8×10^{-5}, the BER estimates differences are 0.9 dB and 1 dB, for $r = 0$ and $r = 0.1$, respectively.

The explanation for this reference BER to analyze the results in Fig. A.1 is as follows. In the absence of ICXT, we consider a certain margin for BER degradation due to ICXT, defining the average BER as two orders of magnitude below the target BER [47]. Thus, the BER without ICXT considered in this work is 3.8×10^{-5}. For a B2B configuration and $B_{e,RX}$=0.75×R_s, the simulation results show that the receiver sensitivity to reach the BER of 3.8×10^{-5} is -26.1 dBm and -25.2 dBm for $r = 0$ and $r = 0.1$, respectively. The observed difference of about 1 dB on the receiver sensitivity, denotes the power penalty degradation due to the extinction ratio, which is in agreement with the theoretical power penalty of 1.1 dB, obtained from Eq. (A.1). Also, regardless the extinction ratio, it is possible to observe a receiver sensitivity improvement of about 1 dB due to the narrowing of electrical filter bandwidth from 1.2×R_s to 0.75×R_s, which results in less electrical noise power in the decision circuit input.

A.2 System equivalent model considering considering only signal-ASE beat noise

The theoretical expression of the BER for the optically amplified link considering only signal-ASE beat noise, and without signal distortion, is given by [53]

$$BER_{theo_{Signal-ASE}} = \frac{1}{4}\left[Q\left(\sqrt{\frac{2}{K}\left(\sqrt{C}-\sqrt{r}\right)\sqrt{\frac{4GR_\lambda P_{av}}{1+A+C+r}}}\right)+ Q\left(\sqrt{\frac{2}{K}\left(\sqrt{A}-\sqrt{C}\right)\sqrt{\frac{4GR_\lambda P_{av}}{1+A+C+r}}}\right)+Q\left(\sqrt{\frac{2}{K}\left(1-\sqrt{A}\right)\sqrt{\frac{4GR_\lambda P_{av}}{1+A+C+r}}}\right)\right] \quad \text{(A.2)}$$

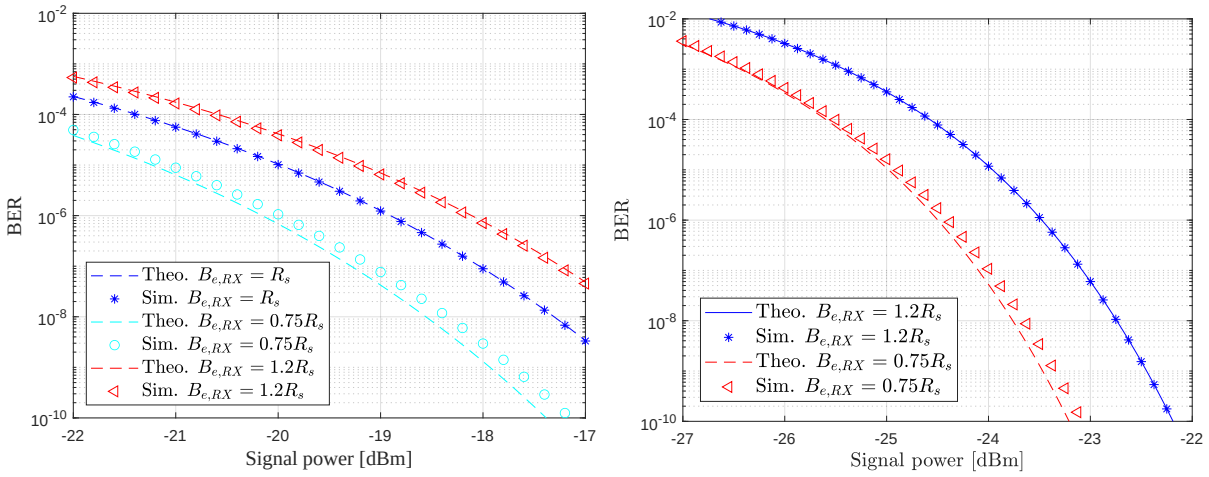

(a) $r = 0$ (b) $r = 0.1$

FIGURE A.2: Dependence of the BER on the receiver sensitivity, for a B2B configuration, for $B_{e,RX}$=1.2×R_s; $B_{e,RX}$=R_s;$B_{e,RX}$=0.75×R_s for an optically amplified link with equispaced PAM4 power levels. The theoretical BER obtained from Eq. A.2 is also shown.

Fig. A.2 shows the theoretical and simulated BERs dependence on the receiver sensitivity and extinction ratio, for a PAM4 signal with equispaced power levels, for a B2B configuration. For this configuration, with negligible ISI, i.e. for $B_{e,RX}$=1.2×R_s and $B_{e,RX}$=R_s, the simulation results are in good agreement with the theoretical results for both extinction ratios. With an electrical filter bandwidth of 0.75×R_s, the receiver sensitivity obtained through simulation, required to achieve the reference target BER is about −21.8 dBm for $r = 0$ and about −20.3 dBm for $r = 0.1$. The small disagreement between the theoretical and simulation results, observed for $B_{e,RX}$=0.75×R_s is partially caused by the ISI introduced after narrowing the electrical filter -3 dB bandwidth. In comparison with the results presented in Fig. A.1, where the link is only affected by electrical noise, there is a sensitivity improvement around 3.9 dB, for the reference BER.

Fig. A.3 shows the theoretical and simulated BERs dependence on the receiver sensitivity and extinction ratio, regarding PAM4 signals with optimized levels considering only the signal-ASE beat noise, for a B2B configuration. In Fig. A.3, the simulated results for an electrical filter bandwidth of 0.75×R_s show that to achieve the reference target BER, the receiver sensitivity is about −24.2 dBm, for $r = 0$, and about −23.0 dBm, for $r = 0.1$. It is possible to observe that, to reach the same reference BER, there is a difference of about 1.2 dB on the receiver sensitivity

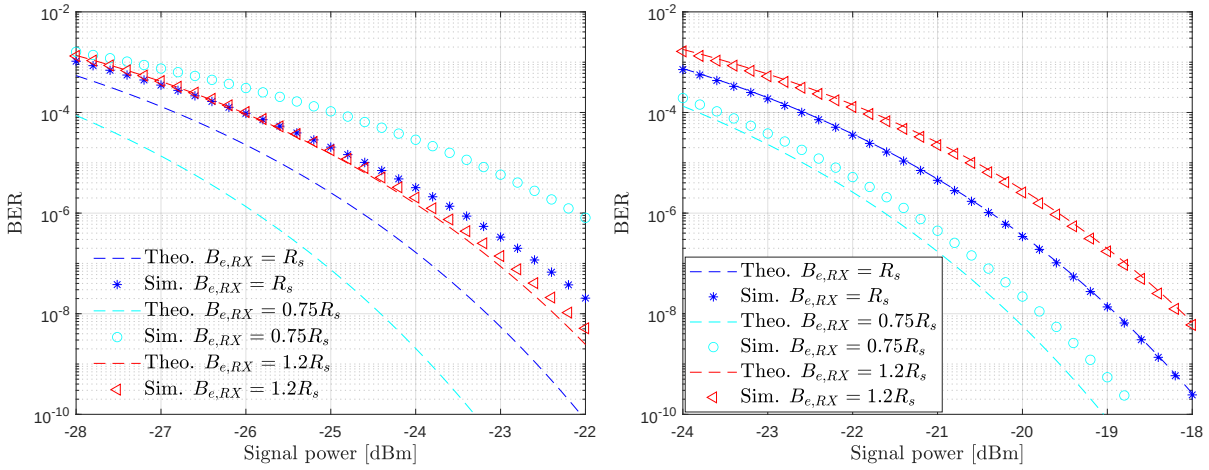

(a) $r = 0$ (b) $r = 0.1$

FIGURE A.3: Dependence of the BER on the receiver sensitivity, for a B2B configuration, for $B_{e,RX}$=1.2×R_s;$B_{e,RX}$=R_s; $B_{e,RX}$=0.75×R_s for an optically amplified link with optimized PAM4 power levels, considering only the signal-ASE beat noises. The theoretical BER obtained from Eq. A.2 is also shown.

from $r = 0$ to $r = 0.1$. Moreover, it is possible to identify an improvement of around 2.4 dB and 2.7 dB on the receiver sensitivity for the target BER, for, respectively, $r = 0$ and $r = 0.1$, in comparison to the results shown in Fig. A.2 for equispaced PAM4 power levels for $r = 0$ and $r = 0.1$, respectively.

It is also possible to observe a remarkable difference between the theoretical and simulated BERs, especially, for $B_{e,RX}$=0.75×R_s and $B_{e,RX}$=R_s and $r = 0$, where for $B_{e,RX}$=0.75×R_s and for the target BER of 3.8×10^{-5} reaches around 3.2 dB. This difference is partially caused by the ISI introduced after narrowing the electrical filter -3 dB bandwidth. However, for $r = 0$, the observed disagreement between the theoretical and simulated BERs is much more pronounced in comparison with the one observed with $r = 0.1$. There are two main reasons for this behavior, firstly, for $r = 0$, the symbol '0' has theoretically a null power level, which leads to a null signal-ASE beat noise for this symbol, which results in having lower BERs in comparison to the simulated BERs, which have the symbol '0' affected by noise resulting from non-negligible signal power levels due to ISI. Secondly, after analysing Fig. A.4, which depicts the eye-diagrams at the receiver input, it is possible to identify that this disagreement is attributed to the higher dependence on ISI in the lower eye of the PAM4 signal with optimized levels, for $r = 0$. Since the lower eye has the smallest opening, in presence of ISI, the error probability relative to

symbols '0' and '1' increases considerably in comparison to the behavior observed for $r = 0.1$. This ISI dependence is the reason why, in simulated results for $r = 0$, $B_{e,RX}$=0.75×R_s has higher BERs in comparison to $B_{e,RX}$=1, 2×R_s and $B_{e,RX}$=R_s.

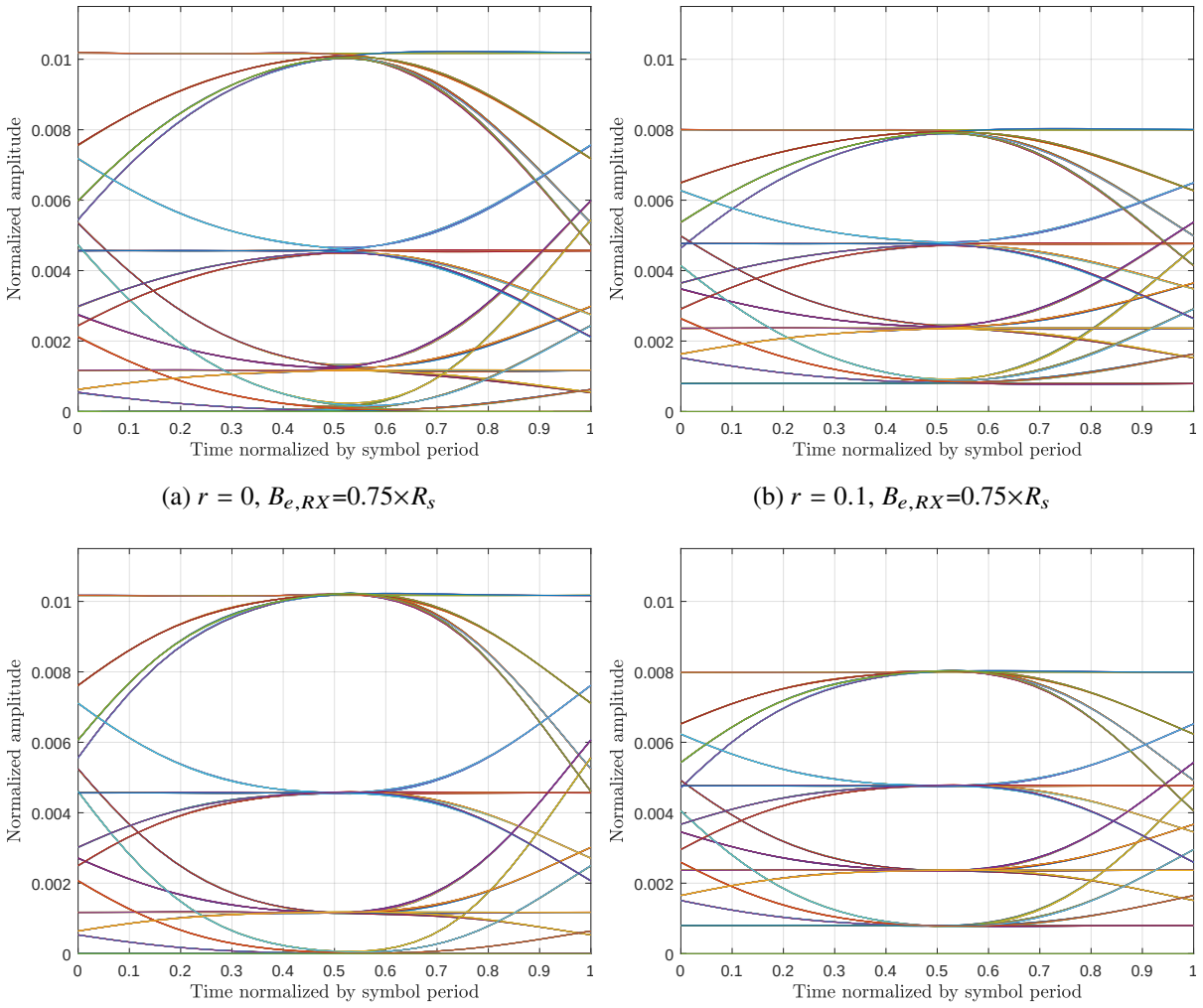

(a) $r = 0$, $B_{e,RX}$=0.75×R_s

(b) $r = 0.1$, $B_{e,RX}$=0.75×R_s

(c) $r = 0$, $B_{e,RX}$=R_s

(d) $r = 0.1$, $B_{e,RX}$=R_s

FIGURE A.4: Eye diagrams of the PAM4 signal on the receiver, for $P_{av} = -24$ dBm, $B_{e,RX}$=0.75×R_s; $B_{e,RX}$=R_s, for an amplified link with optimized PAM4 power levels, considering both signal-ASE and ASE-ASE beat noises.

A.3 System equivalent model considering ASE-ASE beat noise

The BER theoretical expression for the optically amplified link considering both signal-ASE and ASE-ASE beat noises, is given by [53]

$$
\begin{aligned}
BER_{theo_{ASE-ASE}} = \\
&\frac{1}{4}\left\{Q\left[\sqrt{\frac{2}{K}}\left(\sqrt{\frac{4GR_\lambda CP_{av}}{1+A+C+r}+I_{ASE}}-\sqrt{\frac{4GR_\lambda rP_{av}}{1+A+C+r}+I_{ASE}}\right)\right]+\right. \\
&Q\left[\sqrt{\frac{2}{K}}\left(\sqrt{\frac{4GR_\lambda AP_{av}}{1+A+C+r}+I_{ASE}}-\sqrt{\frac{4GR_\lambda CP_{av}}{1+A+C+r}+I_{ASE}}\right)\right]+ \\
&\left.Q\left[\sqrt{\frac{2}{K}}\left(\sqrt{\frac{4GR_\lambda P_{av}}{1+A+C+r}+I_{ASE}}-\sqrt{\frac{4GR_\lambda AP_{av}}{1+A+C+r}+I_{ASE}}\right)\right]\right\}
\end{aligned}
\tag{A.3}
$$

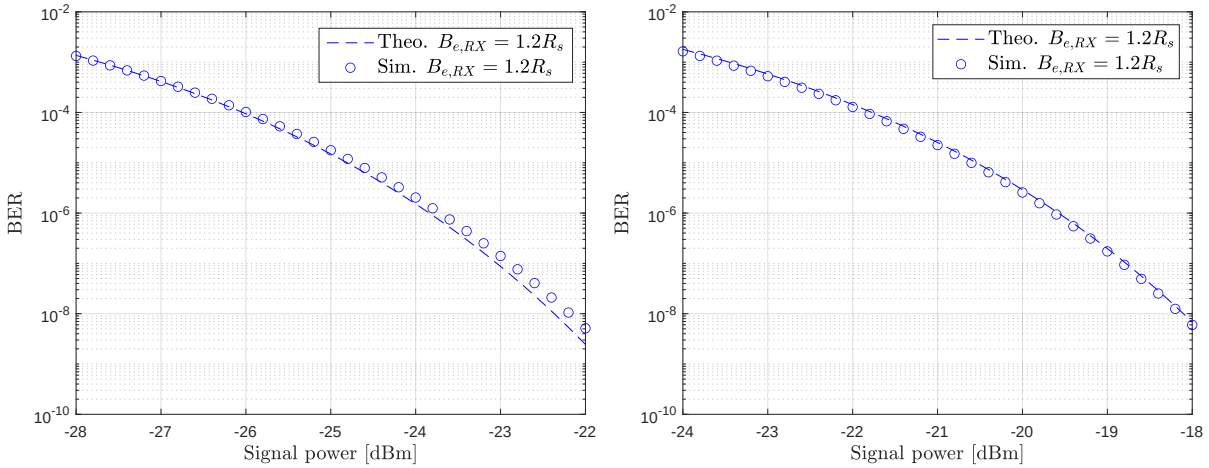

(a) $r = 0$ (b) $r = 0.1$

FIGURE A.5: Dependence of the BER on the receiver sensitivity and extinction ratio, for a B2B configuration and $B_{e,RX}$=1.2R_s, for an optically amplified link with optimized PAM 4 power levels, considering both signal-ASE and ASE-ASE beat noises.

Fig. A.5 shows the theoretical and simulated BERs dependence on the receiver sensitivity and extinction ratio, regarding PAM4 signals with optimized levels considering both signal-ASE and ASE-ASE beat noises, for a B2B configuration. It can be verified that the simulated BERs

for a B2B configuration and $B_{e,RX}$=1.2×R_s are similar with the theoretical BERs, given by Eq. (A.3), which validates the implementation of the simulator without ISI.

The values of A and C, were not optimized taking ASE-ASE beat noise into account. This optimization was neglected in order to evaluate the impact of introducing ASE-ASE noise in the system while having the same simulation environment. Moreover, the optimization of A and C considering also the ASE-ASE beat noise would result in a maximum improvement of 0.5 dB on the receiver sensitivity [53]. Fig. A.6 shows the simulated BERs as a function of the receiver sensitivity for a B2B configuration in the optically amplified link with optimized PAM4 levels.

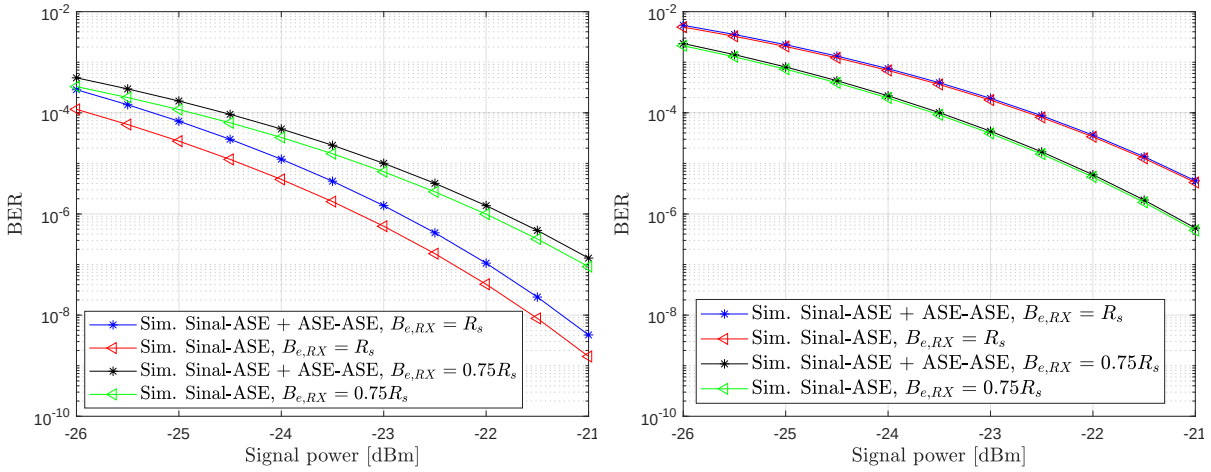

(a) $r = 0$ (b) $r = 0.1$

FIGURE A.6: Dependence of the BER on the receiver sensitivity and extinction ratio, for a B2B configuration, $B_{e,RX}$=R_s and $B_{e,RX}$=0.75×R_s for an optically amplified link with optimized PAM4 power levels, considering only signal-ASE, and both signal-ASE and ASE-ASE beat noises.

Fig. A.6 shows the simulated BERs dependence on the receiver sensitivity and extinction ratio, regarding PAM4 signals with optimized levels considering both signal-ASE and ASE-ASE beat noises, for a B2B configuration. Firstly, the ASE-ASE beat noise is not taken into account, and afterwards it is added to the simulation in order to evaluate the induced degradation of the receiver sensitivity. After analysing the results obtained from the simulation considering both signal-ASE and ASE-ASE beat noises, it is possible to identify a slight degradation of the receiver sensitivity of about 0.4 dB and 0.6 dB, for 0.75×R_s and R_s, for $r = 0$, respectively, in

comparison to the results obtained from the optically amplified link considering only the signal-ASE noise. Negligible differences between the sensitivities obtained with and without ASE-ASE beating noise are observed for $r = 0.1$. The differences between the results considering only signal-ASE, and both signal-ASE and ASE-ASE beat noises are not negligible for $r = 0$ due to a higher ISI dependence, as discussed in A.2, by studying the eye-diagrams at the decision circuit input.

Appendix B

Assessment of the number of BER occurrences above the BER limit to achieve a stabilized OP estimate

This appendix assesses the acceptable number of BER occurrences above the BER limit to achieve an outage probability with very small fluctuations, for an optically amplified PAM4 DD link with full loss and dispersion compensation, emulating an inter-datacenter connection, using the system model described in Chapter 3.

Fig. B.1 shows the OP dependence on the ICXT level, SSRP and extinction ratio, for 50, 100, 150 and 200 BER occurrences above the BER limit. The dashed lines represent a cubic interpolation of $\log_{10}$(OP).

The simulated OPs for a given ICXT level, for each inter-core skew and extinction ratio combination, for a single interfering core, for L =10 km, extracted from Fig. B.1, for N_o=50, N_o=100, N_o=150 and N_o=200, are presented in Table B.1. Table B.1 shows that, as the number of occurrences increases from 50 to 150, the fluctuations get smaller, taking the OP from N_o=200 as the reference value. This values suggest that, for N_o=100, the fluctuations are already considerably small and, hence, the OP estimates have stabilized. However, similarly to the assessment made for an OOK system [47], [48], Fig. B.1 shows that 200 occurrences are a more conservative choice to achieve OP with very small fluctuations.

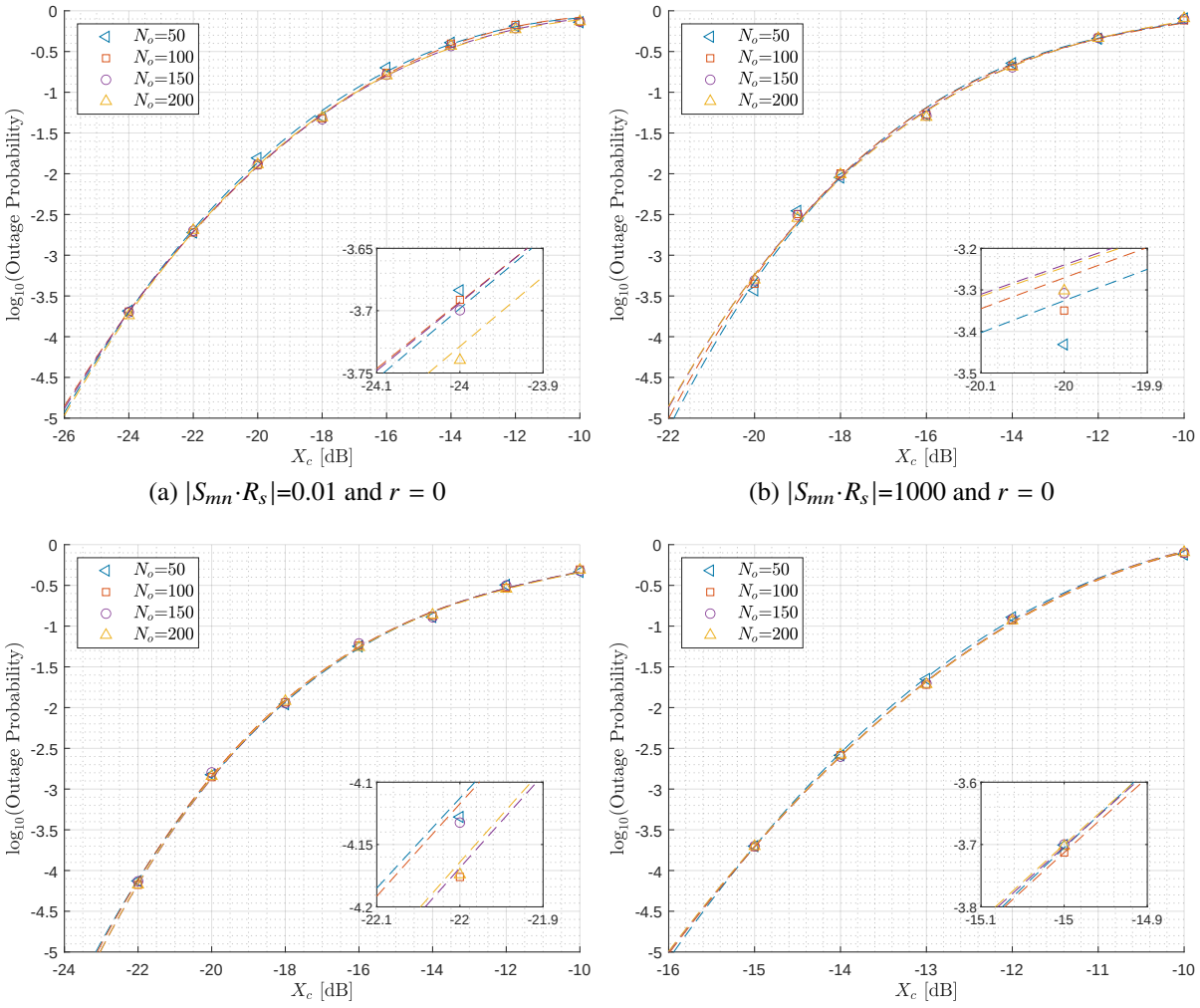

(a) $|S_{mn} \cdot R_s|$=0.01 and $r = 0$

(b) $|S_{mn} \cdot R_s|$=1000 and $r = 0$

(c) $|S_{mn} \cdot R_s|$=0.01 and $r = 0.1$

(d) $|S_{mn} \cdot R_s|$=1000 and $r = 0.1$

FIGURE B.1: Dependence of the OP on the ICXT level, SSRP and extinction ratio, for 50, 100, 150 and 200 BER occurrences above the BER limit. The dashed lines represent a cubic interpolation of $\log_{10}$(OP).

TABLE B.1: Simulated OPs for several ICXT levels, with L=10 km.

			$\log_{10}$(OP)			
X_c [dB]	$\|S_{mn}R_s\|$	r	N_o=50	N_o=100	N_o=150	N_o=200
-24	0.01	0	-3.64	-3.691	-3.7	-3.74
-20	1000	0	-3.431	-3.35	-3.308	-3.302
-22	0.01	0.1	-4.128	-4.176	-4.132	-4.174
-15	1000	0.1	-3.701	-3.713	-3.7	-3.703

References

[1] Cisco, "Cisco global cloud index: forecast and methodology, 2016–2021," *White paper*, pp. 1–46, Feb. 2018.

[2] W. Klaus et al., "Advanced space division multiplexing technologies for optical networks," *IEEE/OSA Journal of Optical Communications and Networking*, vol. 9, no. 4, pp. 1–11, Apr. 2017.

[3] M. Noormohammadpour and C. S. Raghavendra, "Datacenter traffic control: understanding techniques and tradeoffs," *IEEE Communications Surveys Tutorials*, vol. 20, no. 2, pp. 1492–1525, Jun. 2018.

[4] X. Zhou, R. Urata, and H. Liu, "Beyond 1 Tb/s datacenter interconnect technology: challenges and solutions," *Optical Fiber Communications Conference and Exhibition (OFC)*, San Diego, CA, USA, Mar. 2019, paper Tu2F.5.

[5] J. Perin, A. Shastri, and J. Kahn, "Data center links beyond 100 Gbit/s per wavelength," *Optical Fiber Technology*, vol. 44, no. 1, pp. 69–85, Aug. 2018.

[6] K. Saitoh and S. Matsuo, "Multicore fiber technology," *Journal of Lightwave Technology*, vol. 34, no. 1, pp. 55–66, Jan. 1 2016.

[7] R. M. Kingsta and R. S. Selvakumari, "A review on coupled and uncoupled multicore fibers for future ultra-high capacity optical communication," *Optik*, vol. 199, no. 1, pp. 163341–163351, Dec. 2019.

[8] D. L. Butler et al., "Space division multiplexing in short reach optical interconnects," *Journal of Lightwave Technology*, vol. 35, no. 4, pp. 677–682, Feb. 15 2017.

[9] E. Virgillito, "Limitations of PM-QAM based multicore fiber transmission systems due to intercore crosstalk," Master's thesis, Telecommunications engineering, Instituto Superior Técnico, 2016.

[10] J. Rebola, A. V. T. Cartaxo, T. M. F. Alves, and A. Marques, "Outage probability due to intercore crosstalk in dual-core fiber links with direct-detection," *IEEE Photonics Technology Letters*, vol. 31, no. 14, pp. 1195–1198, Jul. 15 2019.

[11] I. Jorge, J. Rebola, and A. V. T. Cartaxo, "Transmission of PAM4 signals in ICXT-impaired intra-datacenter connections with PAM2 signal interference," in *International Conference of Photonics, Optics and Laser Technology (Photooptics)*, pp. 122–130, Valletta, Malta, Feb. 2020.

[12] T. M. F. Alves, J. Rebola, and A. V. T. Cartaxo, "Outage probability due to intercore crosstalk in weakly-coupled MCF systems with OOK signaling," *Optical Fiber Communications Conference and Exhibition (OFC)*, San Diego, CA, USA, Mar. 2019, paper M2I.1.

[13] T. Hayashi, T. Taru, O. Shimakawa, T. Sasaki, and E. Sasaoka, "Design and fabrication of ultra-low crosstalk and low-loss multi-core fiber," *Optics Express*, vol. 19, no. 17, pp. 16576–16592, Aug. 2011.

[14] C. Kachris and I. Tomkos, "A survey on optical interconnects for data centers," *IEEE Communications Surveys Tutorials*, vol. 14, no. 4, pp. 1021–1036, Apr. 2012.

[15] X. Zhou, H. Liu, R. Urata, and S. Zebian, "Scaling large data center interconnects: challenges and solutions," *Optical Fiber Technology*, vol. 44, no. 1, pp. 61–68, Aug. 2018.

[16] E. El-Fiky et al., "168 Gb/s single carrier PAM4 transmission for intra-data center optical interconnects," *IEEE Photonics Technology Letters*, vol. 29, no. 3, pp. 314–317, Feb. 2017.

[17] G. Agrawal, *Fiber-optic communications systems*. John Wiley & Sons, 4^{th} ed., 2010.

[18] M.-J. Li, "MMF for high data rate and short length applications," in *Optical Fiber Communication Conference*, San Francisco, CA, USA, Mar. 2014, paper M3F.1.

[19] H. Venghaus and N. Grote, *Fiber optic communication: key services*. Springer-Verlag, 2nd ed., Berlin, Germany, 2012.

[20] S. P. Singh, R. Gangwar, and N. Singh, *Progress In Electromagnetics Research*. EMW Publishing, 1^{st} ed., 2007.

[21] K. Nakajima, T. Matsui, K. Saito, T. Sakamoto, and N. Araki, "Multi-core fiber technology: next generation optical communication strategy," *IEEE Communications Standards Magazine*, vol. 1, no. 3, pp. 38–45, Sep. 2017.

[22] Y. Sasaki, K. Takenaga, K. Aikawa, Y. Miyamoto, and T. Morioka, "Single-mode 37-core fiber with a cladding diameter of 248 μm," in *Optical Fiber Communications Conference and Exhibition (OFC)*, Los Angeles, CA, USA, Mar. 2017, paper Th1H.2.

[23] J. Sakaguchi et al., "228-spatial-channel bi-directional data communication system enabled by 39-core 3-mode fiber," *Journal of Lightwave Technology*, vol. 37, no. 8, pp. 1756–1763, Apr. 15 2019.

[24] K. Takenaga et al., "Reduction of crosstalk by quasi-homogeneous solid multi-core fiber," in *Conference on Optical Fiber Communication (OFC/NFOEC), collocated National Fiber Optic Engineers Conference*, San Diego, CA, USA, Mar. 2010, paper OWK7.

[25] B. J. Puttnam et al., "Inter-core skew measurements in temperature controlled multi-core fiber," in *Optical Fiber Communications Conference and Exposition (OFC)*, San Diego, CA, USA, Mar. 2018, paper Tu3B.3.

[26] G. Rademacher, R. S. Luís, B. J. Puttnam, Y. Awaji, and N. Wada, "Crosstalk dynamics in multi-core fibers," *Optics Express*, vol. 25, no. 10, pp. 12020–12028, May 2017.

[27] R. S. Luís et al., "Time and modulation frequency dependence of crosstalk in homogeneous multi-core fibers," *Journal of Lightwave Technology*, vol. 34, no. 2, pp. 441–447, Jan. 15 2016.

[28] A. V. T. Cartaxo et al., "Dispersion impact on the crosstalk amplitude response of homogeneous multi-core fibers," *IEEE Photonics Technology Letters*, vol. 28, no. 17, pp. 1858–1861, Sep. 1 2016.

[29] T. M. F. Alves and A. V. T. Cartaxo, "Decorrelation bandwidth of intercore crosstalk in weakly coupled multicore fibers with multiple interfering cores," *Journal of Lightwave Technology*, vol. 37, no. 3, pp. 744–754, Feb. 1 2019.

[30] T. M. F. Alves and A. V. T. Cartaxo, "Intercore crosstalk in homogeneous multicore fibers: theoretical characterization of stochastic time evolution," *Journal of Lightwave Technology*, vol. 35, no. 21, pp. 4613–4623, Nov. 1 2017.

[31] S. Beppu et al., "56-Gbaud PAM4 transmission over 2-km 125-μm-cladding 4-core multi-core fibre for data centre communications," in *European Conference on Optical Communication (ECOC)*, Gothenburg, Sweden, Sep. 2017.

[32] R. O. J. Soeiro, T. M. F. Alves, and A. V. T. Cartaxo, "Dual polarization discrete changes model of inter-core crosstalk in multi-core fibers," *IEEE Photonics Technology Letters*, vol. 29, no. 16, pp. 1395–1398, Aug. 15 2017.

[33] H. Takahashi, K. Igarashi, K. Takeshima, T. Tsuritani, and I. Morita, "Ultra-long-haul transmission using multicore fiber repeatered by multicore EDFA," in *18th OptoElectronics and Communications Conference held jointly with 2013 International Conference on Photonics in Switching (OECC/PS)*, Kyoto, Japan, Jun. 2013, paper TuR1-5.

[34] T. Kobayashi et al., "2 x 344 Tb/s propagation-direction interleaved transmission over 1500-km MCF enhanced by multicarrier full electric-field digital back-propagation," in *European Conference and Exhibition on Optical Communication (ECOC)*, London, United Kingdom, Sep. 2013.

[35] H. Takahashi et al., "First demonstration of MC-EDFA-repeatered SDM transmission of 40 x 128-Gbit/s PDM-QPSK signals per core over 6.160-km 7-core MCF," in *European Conference and Exhibition on Optical Communication (ECOC)*, Amsterdam, Netherlands, Sep. 2012, paper Th.3.C.3.

[36] H. Ono, Y. Miyamoto, T. Mizuno, and M. Yamada, "Gain control in multi-core erbium-doped fiber amplifier with cladding and core hybrid pumping," *Journal of Lightwave Technology*, vol. 37, no. 13, pp. 3365–3372, Jul. 1 2019.

[37] J. Sakaguchi et al., "19-core MCF transmission system using EDFA with shared core pumping coupled in free-space optics," in *European Conference and Exhibition on Optical Communication (ECOC)*, London, UK, Sep. 2013.

[38] K. Takeshima et al., "51.1-Tbit/s MCF transmission over 2520 km using cladding-pumped seven-core EDFAs," *Journal of Lightwave Technology*, vol. 34, no. 2, pp. 761–767, Jan. 15 2016.

[39] A. B. Dar and R. K. Jha, "Chromatic dispersion compensation techniques and characterization of fiber Bragg grating for dispersion compensation," *Optical and Quantum Electronics*, vol. 49, no. 3, pp. 108–143, Feb. 2017.

[40] M. Sumetsky and B. Eggleton, "Fiber Bragg gratings for dispersion compensation in optical communication systems," *Journal of Optical and Fiber Communications Reports*, vol. 2, no. 3, pp. 256–278, Sep. 2005.

[41] W. Lv, J. Li, and K. Xu, "Direct detection of PAM4 signals with receiver-side digital signal processing for bandwidth-efficient short-reach optical transmissions," in *IEEE Optoelectronics Global Conference (OGC)*, pp. 1511–1514, Shenzhen, China, Sep. 2016.

[42] N. Eiselt et al., "Experimental demonstration of 84 Gb/s PAM-4 over up to 1.6 km SSMF using a 20-GHz VCSEL at 1525 nm," *Journal of Lightwave Technology*, vol. 35, no. 8, pp. 1342–1349, Apr. 15 2017.

[43] H. Xin, K. Zhang, L. Li, H. He, and W. Hu, "50 Gbps PAM-4 Over Up to 80-km Transmission With C-Band DML Enabled by Post-Equalizer," *IEEE Photonics Technology Letters*, vol. 32, no. 11, pp. 643–646, Jun. 1 2020.

[44] S. M. Ranzini, S. M. Rossi, R. C. Figueiredo, M. M. Rodrigues, and A. Chiuchiarelli, "1-Tb/s WDM PAM-4 transmission over 80 km of uncompensated SSMF link with direct detection and reduced complexity DSP," *SBMO/IEEE MTT-S International Microwave and Optoelectronics Conference (IMOC)*, Águas de Lindoia, Brazil, Aug. 2017.

[45] R. Rath, D. Clausen, S. Ohlendorf, S. Pachnicke, and W. Rosenkranz, "Tomlinson–Harashima precoding for dispersion uncompensated PAM-4 transmission with direct-detection," *Journal of Lightwave Technology*, vol. 35, no. 18, pp. 3909–3917, Sep. 15 2017.

[46] Zhenping Xing et al., "100 Gb/s PAM4 transmission system for datacenter interconnects using a SiP ME-MZM based DAC-less transmitter and a VSB self-coherent receiver," *Optics Express*, vol. 26, no. 18, pp. 23969–23979, Sep. 2018.

[47] J. Rebola, A. V. T. Cartaxo, and A. Marques, "10 Gbps CPRI signals transmission impaired by intercore crosstalk in 5G network fronthauls with multicore fibers," *Photonic Network Communications*, vol. 37, no. 3, pp. 409–420, Jun. 2019.

[48] A. Marques, "Transmission of 5G signals in multicore fibers impaired by inter-core crosstalk," Master's thesis, Telecommunications and Computer Engineering, ISCTE - Instituto Universitário de Lisboa, Oct. 2018.

[49] A. Udalcovs et al., "Inter-core crosstalk in multicore fibers: impact on 56-Gbaud/λ/core PAM-4 transmission," *European Conference on Optical Communication (ECOC)*, Rome, Italy, Sep. 2017.

[50] Y. Shen et al., "Generation of PAM4 signal over 10-km multi core fiber using DMLs and photodiode," in *9th International Conference on Advanced Infocomm Technology (ICAIT)*, Chengdu, China, Nov. 2017.

[51] X. Pang et al., "7x100 Gbps PAM-4 transmission over 1-km and 10-km single Mode 7-core fiber using 1.5-μm SM-VCSEL," in *Optical Fiber Communications Conference and Exposition (OFC)*, San Diego, CA, USA, Mar. 2018, paper M1I.4.

[52] J. Rebola, C. Lourenço, and J. Oliveira, "Projecto e simulação de um sistema de comunicação óptica de muita alta velocidade," Final year project of degree in Electrical Engineering and Computers, Instituto Superior Técnico, Sep. 1999.

[53] J. Rebola and A. V. T. Cartaxo, "On the quaternary level spacing signalling optimisation for increasing the transmission distance in optical communication systems," *Third Nacional Conferece of Telecommunications(ConfTele)*, Jun. 2001.

[54] C. Pulikkaseril et al., "Spectral modeling of channel band shapes in wavelength selective switches," *Optics Express*, vol. 19, no. 9, pp. 8458–8470, Apr. 2011.

[55] H. Baher, *Analog & digital signal processing*. John Wiley & Sons, 1st ed., England, 1990.

[56] A. Carlson and P. Crilly, *Communication Systems - An introduction to signals and noise in electrical communication*. McGraw-Hill International Editions, 5^{th} ed., New York, USA, 2010.

[57] B. V. Liengme, *SMath for Physics*. 2053-2571, Morgan & Claypool Publishers, 2015.

[58] J. L. Rebola and A. V. T. Cartaxo, "Gaussian approach for performance evaluation of optically preamplified receivers with arbitrary optical and electrical filters," *IEE Proceedings - Optoelectronics*, vol. 148, pp. 135–142, June 2001.

[59] Telecommunications Standardization Sector of IT, "Series G: Transmission Systems and Media, Digital Systems and Networks", Recommendation ITU-T G694.1," 2012.

[60] J. Rebola, T. M. F. Alves, and A. V. T. Cartaxo, "Assessment of the combined effect of laser phase noise and intercore crosstalk on the outage probability of DD OOK systems," *International Conference on Transparent Optical Networks (ICTON)*, Angers, France, Jul. 2019, paper We.D1.4.

[61] I. Jorge, "Transmission of PAM4 signal in intra-datacenters connections with direct-detection and multicore fibers limited by inter-core crosstalk," Master's thesis, Telecommunications and Computer Engineering, ISCTE - Instituto Universitário de Lisboa, Sep. 2019.

[62] P. Winzer and G. Foschini, "MIMO capacities and outage probabilities in spatially multiplexed optical transport systems," *Optics Express*, vol. 19, no. 17, pp. 16680–16696, Aug. 15 2011.

[63] N. Cvijetic, S. Wilson, and D. Qian, "System outage probability due to PMD in high-speed optical OFDM transmission," *Journal of Lightwave Technology*, vol. 26, no. 14, pp. 2118–2127, Jul. 15 2008.

[64] R. S. Luís et al., "On the spectral efficiency limits of crosstalk-limited homogeneous single-mode multi-core fiber systems," *Proceedings Advanced Photonics*, New Orleans, Louisiana, USA, Jul. 2017, paper NeTu2B.2.

[65] T. M. F. Alves and A. V. T. Cartaxo, "Characterization of the stochastic time evolution of short-term average intercore crosstalk in multicore fibers with multiple interfering cores," *Opt. Express*, vol. 26, pp. 4605–4620, February 2018.

[66] S. Gaiarin et al., "High speed PAM-8 optical interconnects with digital equalization based on neural network," *Asia Communications and Photonics Conference (ACP)*, Wuhan, China, Nov. 2016, paper AS1C.1.